Comprehensive Assessment of Plasma Thiol Redox Status for Metabolomics

Comprehensive Assessment of Plasma Thiol Redox Status for Metabolomics

By

Lisa Anne D'Agostino, BSc

A Thesis

Submitted to the School of Graduate Studies

In Partial Fulfillment of the Requirements

For the Degree

Master of Science

McMaster University

MASTER OF SCIENCE
McMaster University
(Chemistry)
Hamilton, Ontario

TITLE: Comprehensive Assessment of Plasma Thiol Redox Status for Metabolomics

AUTHOR: Lisa Anne D'Agostino, BSc (University of Alberta)

SUPERVISOR: Dr. Philip Britz-McKibbin

NUMBER OF PAGES: 121

Abstract

Biological thiols are a class of labile and redox-active metabolite with significant interest to biomedical research due to their involvement in redox mechanisms of cell signaling and physiological control. As a result of oxidative stress, levels of various reduced thiols and oxidized disulfides are altered, which disrupts major cellular regulation pathways modulating protein function and gene expression. Thus, analysis of thiols in biological fluids is essential for understanding the role of oxidative stress and thiol dysregulation in aging and human diseases. However, reliable ex-vivo thiol determination is challenging due to their low abundance and susceptibility to auto-oxidation and thiol-disulfide exchange reactions. In this thesis, capillary electrophoresis-electrospray ionization-mass spectrometry (CE-ESI-MS) in conjunction with maleimide labeling is developed as an integrative strategy for comprehensive plasma thiol redox status analysis for metabolomics. Maleimide labeling helps to address both major constraints in thiol analysis by stabilizing free sulfhydryl groups as their thioether adducts while improving ionization efficiency and analytical sensitivity. This enhancement in ionization efficiency can be quantitatively predicted based on relative changes in fundamental physicochemical properties of thiols that occur upon covalent derivatization when using multivariate calibration. On-line sample preconcentration together with thiol-selective labeling using a cationic quaternary ammonium maleimide analog allowed for simultaneous analysis of reduced thiols and intact oxidized disulfides by CE-ESI-MS with low nanomolar detection limits of 8-30 nM. Improved identification of unknown low abundance thiols and other classes of polar metabolites is also demonstrated by

prediction of relative migration times in CE that is complementary to ESI-MS. Comprehensive plasma thiol speciation together with untargeted profiling of polar metabolites provides a novel platform for holistic understanding of complex changes in metabolic networks associated with thiol dysregulation and/or nutritional intervention for the prevention or treatment of human disorders.

Statement of Contribution

Chapter 2:

-Reprinted from: submitted work under review, *Journal of Proteome Research*, D'Agostino, L. A., Lee, R., Britz-McKibbin, P. *Comprehensive Plasma Thiol Redox Status Determination for Metabolomics.*

R. Lee is credited with assisting with blood sample collection. The author contributed all other experimental procedures and data analysis. The author assisted P. Britz-McKibbin in preparation of the manuscript.

Acknowledgements

I would like to thank the people who have helped me in my journey through graduate school. First, I would like to thank my supervisor Dr. Philip Britz-McKibbin for his guidance and support during my time in his research group, without which I would never have reached this point. I would also like to thank Dr. Alex Adronov and Dr. Murray Potter for their input and assistance as members of my committee. In addition, I would like to share my appreciation for all the support and friendship that my labmates—Jennilee Gavina, Richard Lee, Naomi Janson, Meera Shanmuganathan, Karen Lam, and James Harskamp—have given me.

On a personal level, I would also like to thank my friends and family who have helped me through the trials and tribulations of graduate school. The friends whose companionship and support I appreciate are too numerous to list. I will always remember softball, Frisbee, talking over lunch, participating in MCGSS, and various social gatherings. I would also like to thank my family who have stood by me from near and far throughout my time here and always. In particular, I would like to thank my parents and my sister, Leslie. You were never more than a phone call away and I would not be where I am today without you. I would also like to thank my aunts, uncles, and cousins in this region for helping me to feel at home.

Table of Contents

List of Figures

List of Tables

List of Abbreviations

ADMA	Asymmetric Dimethylarginine
Ala-Ala	*L*-Alanyl-*L*-Alanine or dialanine
APCI	Atmospheric Pressure Chemical Ionization
APPI	Atmospheric Pressure Photoionization
Arg	Arginine
Asp	Aspartate
Bet	Betaine
BGE	Background Electrolyte
C0	*L*-Carnitine
C2	*O*-Acetyl-*L*-Carnitine
CE	Capillary Electrophoresis
CE-LIF	Capillary Electrophoresis with Laser-Induced Fluorescence
CE-MS	Capillary Electrophoresis-Mass Spectrometry
CE-UV	Capillary Electrophoresis with Ultraviolet Absorbance Detection
CE-ESI-MS	Capillary Electrophoresis-Electrospray Ionization-Mass Spectrometry
CID	Collision-Induced Dissociation
Cys	Cysteine
CysGly	Cysteinylglycine
CysOEt	Cysteine Ethyl Ester
CysSS	Cystine
CysSSCysGly	Cysteinyl-Cysteinylglycine Disulfide
CysSSG	Cysteinyl-Glutathione Disulfide
CysSSGluCys	Cysteinyl-γ-Glutamylcysteine Disulfide
CysSSHcy	Cysteinyl-Homocysteine Disulfide
Cyst	Cysteamine
CysT	Cystathionine
CZE	Capillary Zone Electrophoresis
DMG	Dimethyl Glycine
DNA	Deoxyribose Nucleic Acid
E	Electric Field Strength
E_h	Redox Potential Relative to Standard Hydrogen Electrode
E_0	Standard Redox Potential
EIE	Extracted Ion Electropherogram
EMA	Eosin-5-Maleimide
EOF	Electroosmotic Flow
ESI	Electrospray Ionization
ESI-MS	Electrospray Ionization-Mass Spectrometry
ε	Dielectric Constant
F	Faraday's Constant
FL	Fluorescence
FT-ICR-MS	Fourier Transform Ion Cyclotron Resonance Mass Spectrometry

GC-MS	Gas Chromatography-Mass Spectrometry
GluCys	γ-glutamylcysteine
Glu	Glutamic acid
Gly	Glycine
GSH	Reduced Glutathione
GSSCysGly	Glutathione-cysteinylglycine Disulfide
GSSG	Oxidized Glutathione/Glutathione Disulfide
η	Viscosity
Hcy	Homocysteine
HcySS	Homocystine
His	Histidine
Ile	Isoleucine
IS	Internal Standard
IT-MS	Ion trap mass spectrometry
k_A	Rate Constant for Ion Desorption
K_A	Equilibrium Constant for Ion Partitioning
LC	Liquid Chromatography
LC-ESI-MS	Liquid Chromatography-Electrospray Ionization-Mass Spectrometry
LC-FL	Liquid Chromatography with Fluorescence Detection
LC-MS	Liquid Chromatography-Mass Spectrometry
LC-MS/MS	Liquid Chromatography-Tandem Mass Spectrometry
LC-UV	Liquid Chromatography with Ultraviolet Absorbance Detection
L_d	Capillary Length to Detector
Leu	Leucine
LIF	Laser-Induced Fluorescence
LOD	Limit of Detection
logD	Octanol-Water Distribution Coefficient
logP	Octanol-Water Partition Coefficient
LOQ	Limit of Quantitation
L_t	Total Capillary Length
Lys	Lysine
μ_{ep}^{A}	Apparent Electrophoretic Mobility
μ_{ep}	Electrophoretic Mobility
μ_{EOF}	Electroosmotic Mobility
MeHis	3-Methylhistidine
MEKC	Micellar Electrokinetic Chromatography
MESNA	2-Mercaptoethanesulfonic Acid
Met	Methionine
MHA	6-Maleimidohexanoic Acid
MLR	Multiple Linear Regression
MMA	Monomethylarginine
MS	Mass Spectrometry
MSEC	Mean Squared Error of Correlation
MSEP	Mean Squared Error of Prediction

MS^n	Multi-stage Mass Spectrometry
MV	Molecular Volume
m/z	Mass to Charge Ratio
v	Ion Velocity
N	Number of Theoretical Plates
NAC	N-Acetylcysteine
NADH	Reduced Nicotinamide Adenine Dinucleotide
NAEM	*N*-(2-Aminoethyl)maleimide
NAM	*N*-(9-Acridinyl)maleimide
NEM	*N*-Ethylmaleimide
NMBA	*N*-Maleoyl-β-alanine
NMM	*N*-Methylmaleimide
NO	Nitric Oxide
NPEM	*N*-(1-Phenylethyl)maleimide
NTAM	*N*-[2-(Trimethylammonium)ethyl]maleimide
oxoBA	2-Oxobutyric Acid
pK_a	Acid Dissociation Constant
Phe	Phenylalanine
Pna	Penicillamine
PSSCys	Protein-Bound Cysteine
PSSG	Protein-Bound Glutathione
PSSHcy	Protein-Bound Homocysteine
Q^2	Predictive Correlation Coefficient
R	Ideal Gas Constant or Ionic Radius
R^2	Correlation Coefficient
RF	Radio Frequency
RMT	Relative Migration Time
RNA	Ribose Nucleic Acid
RONS	Reactive Oxygen and Nitrogen Species
RPA	Relative Peak Area
RRF	Relative Response Factor
SAH	S-Adenosylhomocysteine
SAM	S-Adenosylmethionine
SDMA	Symmetric Dimethylarginine
Ser	Serine
SF	Sheath Flow
S/N	Signal-to-Noise Ratio
T	Temperature in Kelvin
T_3	Triiodothyronine
T_4	Thyroxine
t_A	Analyte Migration Time
t_{EOF}	Electroosmotic Flow Marker Migration Time
TCEP	*Tris*-(2-Carboxyethyl)phosphine
Thr	Threonine

Trp	Tryptophan
Tyr	Tyrosine
UV	Ultraviolet
V	Voltage
Val	Valine
ζ	Zeta Potential
z_{eff}	Effective Charge

Chapter 1

Background to Oxidative Stress, Thiol Metabolism, Thiol Analysis, and Capillary Electrophoresis-Electrospray Ionization-Mass Spectrometry

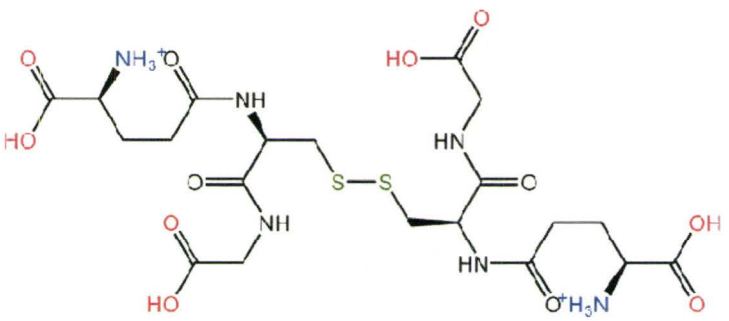

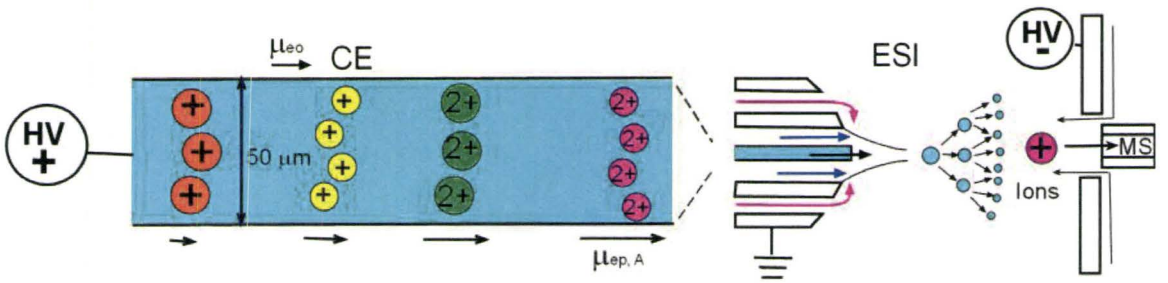

1: Background to Oxidative Stress, Thiol Metabolism, Thiol Analysis, and Capillary Electrophoresis-Electrospray Ionization-Mass Spectrometry

1.1 Oxidative Stress, Aging, and Disease

Biological aging or senescence is the physiological decline that occurs over time after an organism has reached maturity. This universal phenomenon of life is difficult to precisely define and measure as various physiological processes of aging exist, including hormonal changes, graying of hair, wrinkling of skin, loss of muscle mass, reduced cellular turnover and many others.[1] In this thesis, references to aging pertain to senescence or biological aging, which is associated with increased susceptibility to disease, eroding quality of life, and ultimately death. Understanding the fundamental mechanisms underlying age-related physiological decline is a fascinating problem essential to deeper insight into human health and longevity. Over the years, a number of theories of aging have been proposed beginning with naïve comparisons of human aging to mechanical wear and tear.[2] In the 1950s, Harman proposed the free radical theory of aging, which hypothesizes that aging is caused at a molecular level by chemical reactions of free radicals with susceptible biomolecules such as proteins, lipids, and DNA.[3] These oxidative reactions irreversibly alter biomolecules causing progressive declines in their function and consequently the deleterious physiological effects of aging. Free radicals and other reactive oxygen and nitrogen species (RONS) are generated continuously in normal metabolic processes, such as cell respiration. Major intrinsic RONS produced include hydroxyl radical ($HO^{\bullet}$), nitric oxide ($NO^{\bullet}$), and superoxide anion ($O_2^{\bullet -}$).[4]

Therefore, according to Harman's theory, free radicals produced by normal metabolism can cause aging without exposure to extrinsic stressors, such as ionizing radiation.[3]

Over time, increasing knowledge of biological mechanisms involving free radicals and two electron oxidants, such as hydrogen peroxide (H_2O_2), disulfides (RSSR), and peroxynitrite (ONO_2^-), has led to more sophisticated theories of aging. The generation of $O_2^{\bullet-}$ by mitochondria during cell respiration has been established[5] and direct detection of free radicals has been reported *in vivo*.[6] Enzymes that catalyze reactions of free radicals to prevent macromolecular damage have also been discovered, including superoxide dismutase, which catalyzes the dismutation of highly reactive $O_2^{\bullet-}$ and water to H_2O_2 and O_2.[4] The body's defenses against oxidants have also been found to include the tripeptide glutathione (GSH) and ubiquitous proteins called thioredoxins, both of which contain thiols that can undergo reversible oxidation to disulfides.[4] The free radical theory evolved into an oxidative stress hypothesis for aging, postulating that oxidative stress, which causes oxidative damage to biological macromolecules is primarily responsible for the deleterious effects of aging.[7] In general, oxidative stress refers to a pro-oxidant-antioxidant imbalance favoring pro-oxidants or the overwhelming of anti-oxidant defenses by free radical production.[8, 9] The antioxidant defense system has a number of components to inactivate RONS. It includes low molecular weight metabolites, such as GSH, and proteins, such as thioredoxins and superoxide dismutase. Cells also have regenerative mechanisms to repair oxidative damage, such as proteolysis of oxidatively damaged protein and DNA repair for oxidized DNA. However, during acute oxidative insult, these antioxidant defenses are overcome and irreversible damage

occurs. Oxidative stress can be triggered by extrinsic stressors, such as exposure to toxins, nutritional deficiencies, ischemia and reperfusion, or ionizing radiation.[10, 11]

It has also been discovered that RONS also play central functions in physiological regulation and cell signaling. For example, $NO^{\bullet}$ is a signaling molecule with several roles, which is enzymatically produced by nitric oxide synthase from L-arginine. A key role of $NO^{\bullet}$ is in relaxing the endothelium to produce vasodilation.[12, 13] With increasing evidence of the signaling and regulatory functions of redox modification of thiol-containing species and the preponderance of two-electron oxidants over free radicals, Jones has proposed a modified theory of oxidative stress and aging.[4] One important difference between the free radical theory of aging and this contemporary redox hypothesis of aging is the diminished emphasis on free radicals as causal agents of aging.[4] Non-radical oxidants, such as peroxides, are oxidizing species of primary importance because they are produced in greater numbers than free radicals by normal metabolism and those free radicals that are generated are rapidly converted to two-electron oxidants.[4] These conversions include the formation of H_2O_2 from $O_2^{\bullet-}$ by superoxide dismutase and the reaction of $O_2^{\bullet-}$ and $NO^{\bullet}$ forming ONO_2^-. Non-radical oxidants have a significant impact because they are able to oxidize or otherwise modify biological thiol species, which function in physiological regulation and cell signaling as will be discussed in **Section 1.4.3.**[4] In light of the key regulatory role of thiol redox status, oxidative stress can be redefined as a disruption of thiol redox regulation and cell signaling leading to the adverse physiological effects of aging and increased susceptibility to disease.[4]

In accordance with the redox hypothesis of aging, a number of studies have correlated changing thiol levels and increasingly oxidized thiol redox status in biological samples with increasing chronological age.[14, 15] Various diseases have also been associated with changes in thiol levels and redox status likely reflecting the role of oxidative stress in disease pathogenesis. Diseases that are associated with altered thiol levels and redox status include cardiovascular disease,[13, 16, 17] cancer,[18] HIV,[19] Alzheimer's disease,[20] and preeclampsia.[16]

In order to investigate the role of thiol metabolism in human health, it is necessary to develop sensitive and accurate tools for the quantitative analysis of labile thiols in biological samples that preserve their *in vivo* redox state. Capillary electrophoresis-electrospray ionization-mass spectrometry (CE-ESI-MS) was used as an analytical platform for the development of a sensitive and selective method for plasma thiol redox status assessment. This method will enable comprehensive speciation of both reduced thiols and intact oxidized disulfides in conjunction with untargeted analysis of other polar metabolites in plasma. It will take advantage of the ability of CE to desalt, preconcentrate, and separate polar thiols and oxidized disulfides. In addition, MS detection will provide sensitive and selective detection as well as qualitative information to aid in the identification of unknown metabolites. Maleimide derivatization will be used to prevent artifactual oxidation of reduced thiols while enhancing ionization efficiency in ESI-MS, contributing to both method robustness and sensitivity. This work will provide a more holistic picture of thiol dysregulation in the context of global metabolism applicable to investigations of oxidative stress, aging, and disease.

1.2 Capillary Electrophoresis Separations

Capillary electrophoresis (CE) is an exceptionally versatile and efficient micro-separation technique. The unique separation mechanisms operative in CE allow for the resolution of complex sample mixtures ranging from metal ions and metabolites to proteins and intact cells.[21] High voltages allow for high efficiency separations with theoretical plates (N) often exceeding 10^5. In contrast to the parabolic flow profile generated by high pressure pumps in liquid chromatography (LC), the electroosmotic flow (EOF) generated in narrow bore fused-silica capillaries has a laminar or flat flow profile. This flow profile minimizes band broadening due to axial diffusion of solutes during separation. Unlike chromatography, CE lacks a stationary phase. Thus, it is not subject to band broadening due to mass transfer kinetics between the mobile phase and the stationary phase. This leaves only longitudinal diffusion as a significant source of band broadening during separation in CE. Longitudinal diffusion is reduced by minimizing residence times through the application of high voltages up to 30 kV. This is made possible by the use of fused-silica capillaries with narrow internal diameters (25-75 μm), which have a high surface area to volume ratio allowing for efficient heat dissipation, especially with active cooling of the capillary. Joule heating due to ion conduction is thus minimized allowing the application of high voltages without band broadening. Diverse applications of CE are possible due to the ability to readily tune selectivity through modification of the background electrolyte (BGE). CE is also increasingly useful as a biophysical tool to investigate interactions of biomolecules by determining parameters such as dissociation constants (K_d), maximum enzyme velocities

(V_{max}), and standard free energy of unfolding (ΔG_U^o) for proteins, as well as for measurement of fundamental physicochemical properties (pK_a and $logD$).[22, 23]

1.2.1 Electrokinetic Phenomena in CE

The separation in CE is driven by a combination of two distinct electrokinetic processes. The first is the electrophoretic mobility of an ion (μ_{ep}), which is dependent on the physicochemical properties of a solute under an electric field in solution. The second is the electroosmotic flow (EOF), which is an intrinsic electrokinetic pumping mechanism generated by the capillary surface and the electrolyte solution upon the application of an electric potential.

1.2.2 Electrophoretic Mobility (μ_{ep})

The ion velocity (v) per unit of electric field strength (E) in a given electrolyte solution is defined as μ_{ep}. As the shape of most low molecular weight solutes can be approximated by a sphere, μ_{ep} depends on the ratio of effective charge (z_{eff}) to ionic radius (R) of an ion, as well as the viscosity of the BGE (η) as expressed in the Hückel equation:[24]

$$\mu_{ep} = \frac{v}{E} = \frac{z_{eff}}{6 \cdot \pi \cdot \eta \cdot R} \qquad (1)$$

From the above equation, μ_{ep} for an analyte is dependent on its z_{eff} and its R. For weakly ionic analytes, an ion's z_{eff} is determined by the pK_a values of its ionizable functional groups (*e.g.*, amines, carboxylic acids) and the pH of the BGE. R is proportional to the cube root of the hydrated molecular volume (MV) of an ion. Thus, z_{eff} and MV are thermodynamic and molecular parameters that allow for prediction of μ_{ep} and thus

migration times for solutes in CE. Such predictions are presented in **Chapters 2 and 3** as an approach to qualitatively identify unknown low abundance metabolites, such as mixed disulfides. The model in **Equation 1** does not account for hydration effects resulting from solvation of ions in an aqueous solution. Dielectric friction further reduces μ_{ep} and is proportional to z_{eff}^2/MV.[25] Selectivity in CE separations is based on differences in μ_{ep} between solutes. Since μ_{ep} varies depending on the electrolyte properties of the BGE and the chemical properties of the solute, modification of the BGE is the primary way to tune selectivity in CE separations. Adjusting the BGE pH to optimize separations of weakly ionic solutes by altering z_{eff} is a simple yet important example of this. For example, CE was used to experimentally determine two pK_a values for each of thyroxine (T_4) and triiodothyronine (T_3) and to obtain optimum resolution by maximizing differences in μ_{ep} (*i.e.*, pH = 7.6) as shown in **Figure 1.1**.

Additional properties of the BGE may also be adjusted to improve resolution through modification of the apparent μ_{ep} including ionic strength, buffer type, organic solvent content, and the use of additives. Ionic strength impacts solute μ_{ep} through the shielding effects of solvated counter-ions. Increasing ionic strength decreases μ_{ep} by decreasing z_{eff} due to the formation of an electric double layer by counter-ions. Additives in CE can include surfactants, cyclodextrins, and other molecules added to the BGE that are involved in differential covalent or non-covalent interactions with solutes during electromigration. Although conventional CE separates intrinsically charged species only, micellar electrokinetic chromatography (MEKC) incorporates an ionic surfactant above

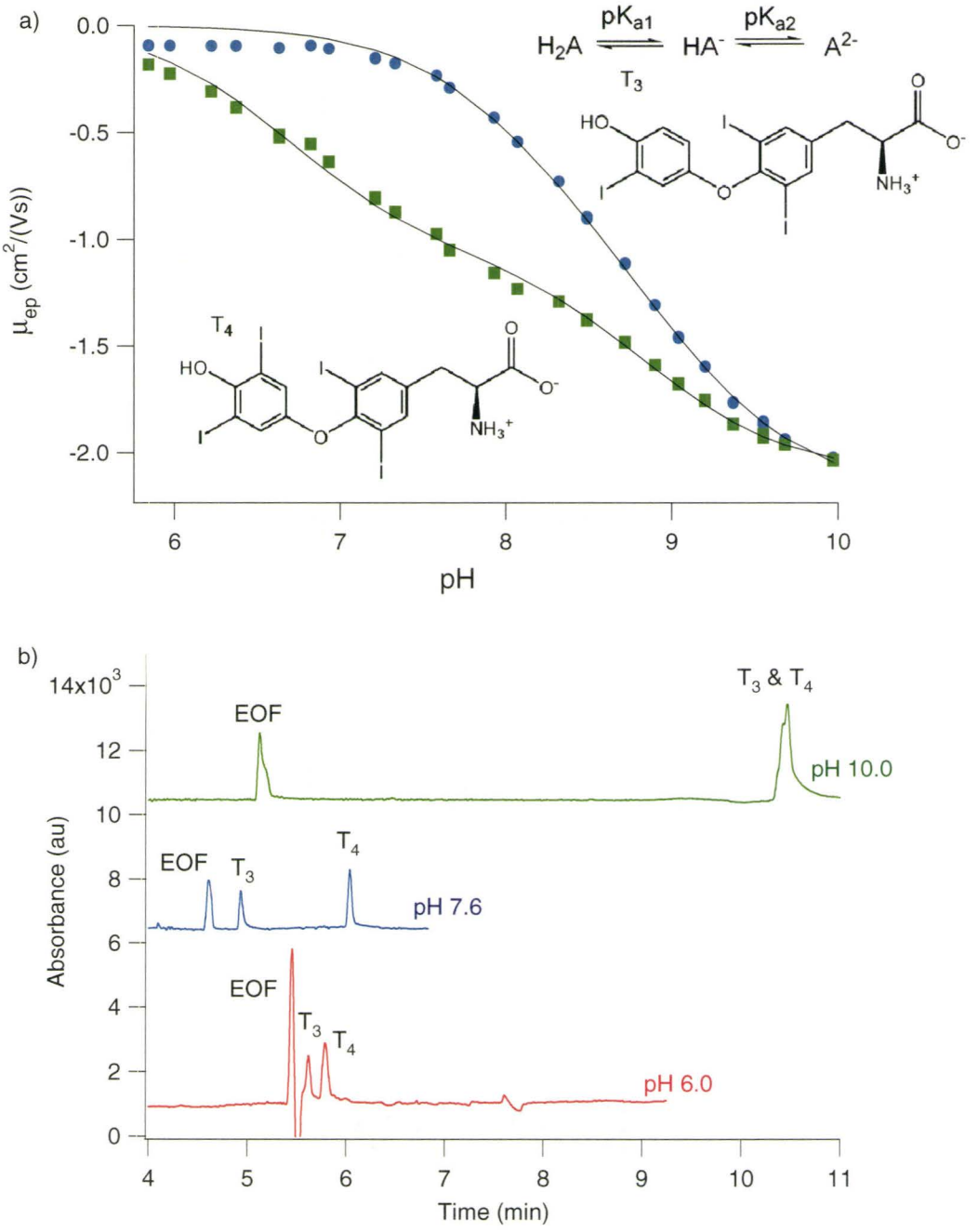

Figure 1.1: **(a)** Plot of μ_{ep} versus BGE pH for determination of pK_a values for T_3 (blue circles) and T_4 (green squares) by CE. The associated changes in protonation states are shown. For T_3, pK_{a1} was 8.05 ± 0.05 and pK_{a2} was 9.05 ± 0.05. For T_4, pK_{a1} was 6.69 ± 0.03 and pK_{a2} was 8.85 ± 0.04. **(b)** Electropherograms for a separation of 30 μM T_3 and 40 μM T_4 with different BGE pHs and UV absorbance detection at 254 nm. Resolution is greatest in pH 7.6, 30 mM phosphate buffer and least in pH 10.0, 90 mM borate buffer. T_3 and T_4 migrate near the 100 μM caffeine EOF marker in pH 6.0, 18 mM citrate buffer. Separations were conducted with a 5 sec. injection and a 17.5 kV separation for pH 6.0 and a 15 kV separation for pH 10.0 and pH 7.6.

its critical micelle concentration in the background electrolyte (BGE) facilitating separation of neutral molecules on the basis of partitioning into the micellar pseudo-stationary phase.[26] In addition, the use of cyclodextrins as additives in CE allows for chiral separations based on the differential stability of inclusion complexes of different enantiomers in free solution. The ability to use multiple additives and modify their concentrations in the BGE in free solution makes CE an exceptionally versatile technique compared to LC, which is limited by covalently immobilized stationary phases. Use of several additives in the BGE solution permits optimization of complex mixture separations by CE[27] with resolution controlled by multiple yet complementary electrokinetic and thermodynamic parameters.

1.2.3 Electroosmotic Flow (EOF)

The electrokinetically-driven bulk flow of solution in a narrow-bore capillary upon application of a voltage is the EOF. Generation of the EOF occurs according to the Debye-Hückel-Stern model with formation of an electric double layer near the capillary surface. Fused-silica capillaries have weakly acidic silanol groups ($pK_a \approx 6.5$) at the surface.[28] Ionization of these groups on the surface leads to the formation of an electric double layer with a Stern layer of immobilized cations nearest the surface followed by a diffuse layer of mobile cations and anions as illustrated in **Figure 1.2 (a)**. An applied electric field attracts the cations in the diffuse layer toward the cathode and the anions in the diffuse layer toward the anode. However, the diffuse layer is disproportionately rich in cations due to their attraction to the negatively charged capillary wall. This leads to a net flow toward the cathode, the EOF, as the excess cations in the diffuse layer are

solvated and drag their solvation spheres with them. The magnitude of the EOF is dependent on the zeta potential (ζ), which is the electric potential between the rigid layer boundary (Stern plane) and the bulk solution. The magnitude and direction of the EOF is determined by the properties of the capillary surface and the BGE as described in the Smoluchowski equation:[29]

$$\mu_{EOF} = \frac{\varepsilon \cdot \zeta}{4 \cdot \pi \cdot \eta} \qquad (2)$$

where ε is the dielectric constant, ζ is the zeta potential, and η is the solution viscosity. Under highly acidic BGE conditions (pH < 2), ζ approaches zero due to protonation of the capillary wall silanols and the EOF is suppressed.[24] As a pumping mechanism, the EOF differs from pressure-driven flow in that it creates a flat flow profile in capillaries with a diameter under 120 μm as shown in **Figure 1.2 (b)**.[24] In contrast, the pressure-driven flow in LC has a parabolic flow profile due to different levels of resistance to the flow of liquid at varying distances from column walls and particle surfaces in a packed column. A flat flow profile via the EOF is limited to narrow-bore capillaries because in capillaries over 120 μm heat dissipation is inefficient and Joule heating distorts the flow profile due to temperature and viscosity gradients across the capillary.[24] Axial diffusion due to a parabolic flow profile typically increases band broadening in LC relative to CE.

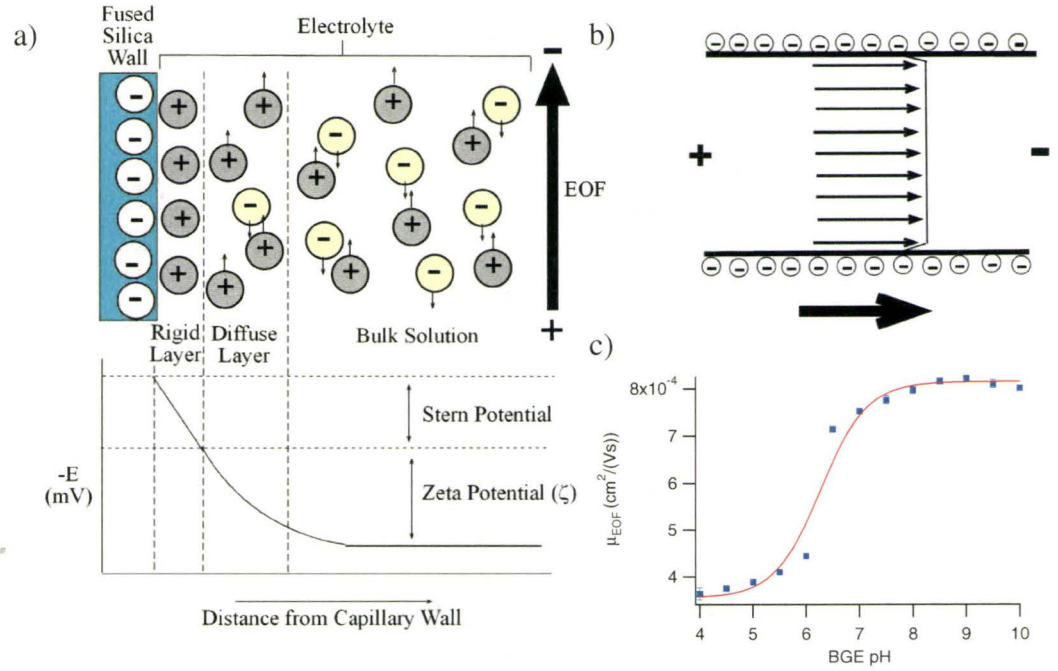

Figure 1.2: (**a**) Schematic of the Debye-Huckle-Stern model of the electric double layer showing the rigid and diffuse layers and the zeta potential (ζ) that generates the EOF near the capillary wall under an external voltage. (**b**) Flat flow profile generated by the EOF in normal polarity CE with a BGE pH > 2. (**c**) Graph of μ_{EOF} as a function of BGE pH. The pK_a of the silanol groups in the fused silica capillary is evident as an inflection point at approximately pH 6.3.

1.2.4 Apparent Mobility

The apparent electrophoretic mobility of an ion ($\mu_{ep}{}^{A}$) is determined by the two electrokinetic forces in CE as the vector sum of μ_{ep} and the electroosmotic mobility (μ_{EOF}):

$$\mu_{ep}^{A} = \mu_{ep} + \mu_{EOF} \qquad (3)$$

Experimentally, μ_{ep} can be determined by measuring the migration times of an analyte and a neutral EOF marker (*e.g.*, caffeine) in a capillary of known dimensions under a defined potential using:

$$\mu_{ep} = \frac{L_t \cdot L_d}{V}\left(\frac{1}{t_A} - \frac{1}{t_{EOF}}\right) \quad (4)$$

where L_t is the total capillary length, L_d is the capillary length to the detector, V is the applied voltage, t_A is the migration time for the analyte, and t_{EOF} is the migration time for an EOF marker. Determining μ_{ep} is important because it is an intrinsic property of a solute under particular BGE conditions that can be measured with high precision relative to t_A. This is because t_A is affected by μ_{EOF}, which varies due to slight alterations to the surface of the capillary wall. Alternatively, relative migration time (RMT), which is migration time relative to an internal standard (IS), can also provide greater reproducibility than t_A when determining μ_{ep} is inconvenient due to a slow EOF under acidic BGE conditions.

The vector superposition of μ_{ep} and μ_{EOF} determines the migration time in normal polarity CE as illustrated in **Figure 1.3** for neutral or alkaline buffer conditions with a strong EOF and for highly acidic conditions with a weak EOF. Neutral or alkaline conditions transport all cationic, anionic, and neutral species towards the detector with the EOF, whereas acidic conditions effectively resolve only cationic species because the EOF is not fast enough to move anions towards the capillary outlet. The superposition of μ_{ep} with a weak EOF in CE-ESI-MS with pH 1.8 BGE allows for desalting of biological samples. Removal of small inorganic anions, such as Cl^-, occurs because they have a large negative μ_{ep}, which is greater than μ_{EOF}, resulting in migration out of the capillary inlet. In contrast, small inorganic cations, such as Na^+, have a large positive μ_{ep} and

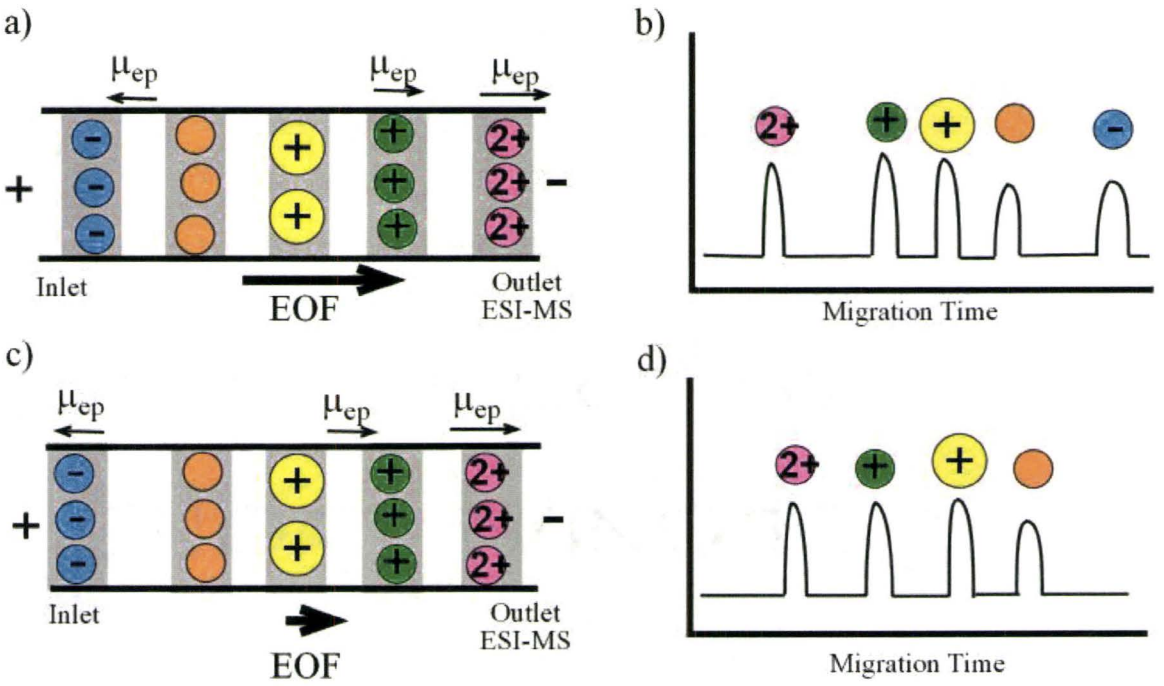

Figure 1.3: Illustration of the separation of a mixture of ions in CE based on their μ_{ep} showing **(a)** CZE separation at pH > 6 with a strong EOF, **(b)** typical electropherogram for neutral/alkaline conditions, **(c)** CZE separation at pH < 2 with a suppressed EOF, and **(d)** typical electropherogram for strongly acidic conditions.

migrate ahead of most metabolites of interest and do not interfere with their detection by ESI-MS due to ionization suppression.[25]

1.2.5 On-Line Sample Preconcentration in CE

In CE, small sample injection volumes often pose a challenge since detectors must be sensitive enough to detect low solute concentrations. However, in most cases injecting a larger sample plug in CE is not effective in improving sensitivity because sample overloading results in broad analyte peaks and poor resolution. Fortunately, a number of methods exist that allow for on-line preconcentration of extended sample injections during electrophoretic separation prior to detection, including field-enhanced sample stacking, transient isotachophoresis, dynamic pH junction and sweeping.[30] In this

thesis, on-line preconcentration combining dynamic pH junction with transient isotachophoresis is utilized for sample preconcentration to improve sensitivity for low abundance metabolites, such as thiols and disulfides. The preconcentration occurs via a discontinuous electrolyte system where samples are prepared at pH 5 and the BGE pH is 1.8. Mobility differs for analytes on either side of the discontinuous electrolyte system. The weakly acidic analytes are positively charged and have positive μ_{ep} in the acidic BGE and are neutral in the sample zone and have zero μ_{ep}. **Figure 1.4** illustrates the key developments occurring during preconcentration of an extended sample plug upon application of a separation voltage. First, the analyte focuses at the sample-BGE boundary nearest the inlet due to its greater positive mobility in the acidic BGE than in the sample as shown in **Figure 1.4 (a)**. Second, the analyte is partially focused with some peak fronting remaining as shown in **Figure 1.4 (b)**. Finally, the analyte is fully focused as shown in **Figure 1.4 (c)** and normal CE separation proceeds over the remaining capillary length. During the preconcentration process, ammonium ions act as leading co-ions and H^+ ions act as terminating co-ions in transient isotachophoresis, which causes solutes of intermediate mobility to be preconcentrated at the boundary between the leading and terminating co-ions. When preconcentration is complete, the pH discontinuity between sample and BGE has been dissipated.[25] This preconcentration is compatible with the on-line sample desalting described previously, since Na^+ ions migrate ahead of analyte ions.

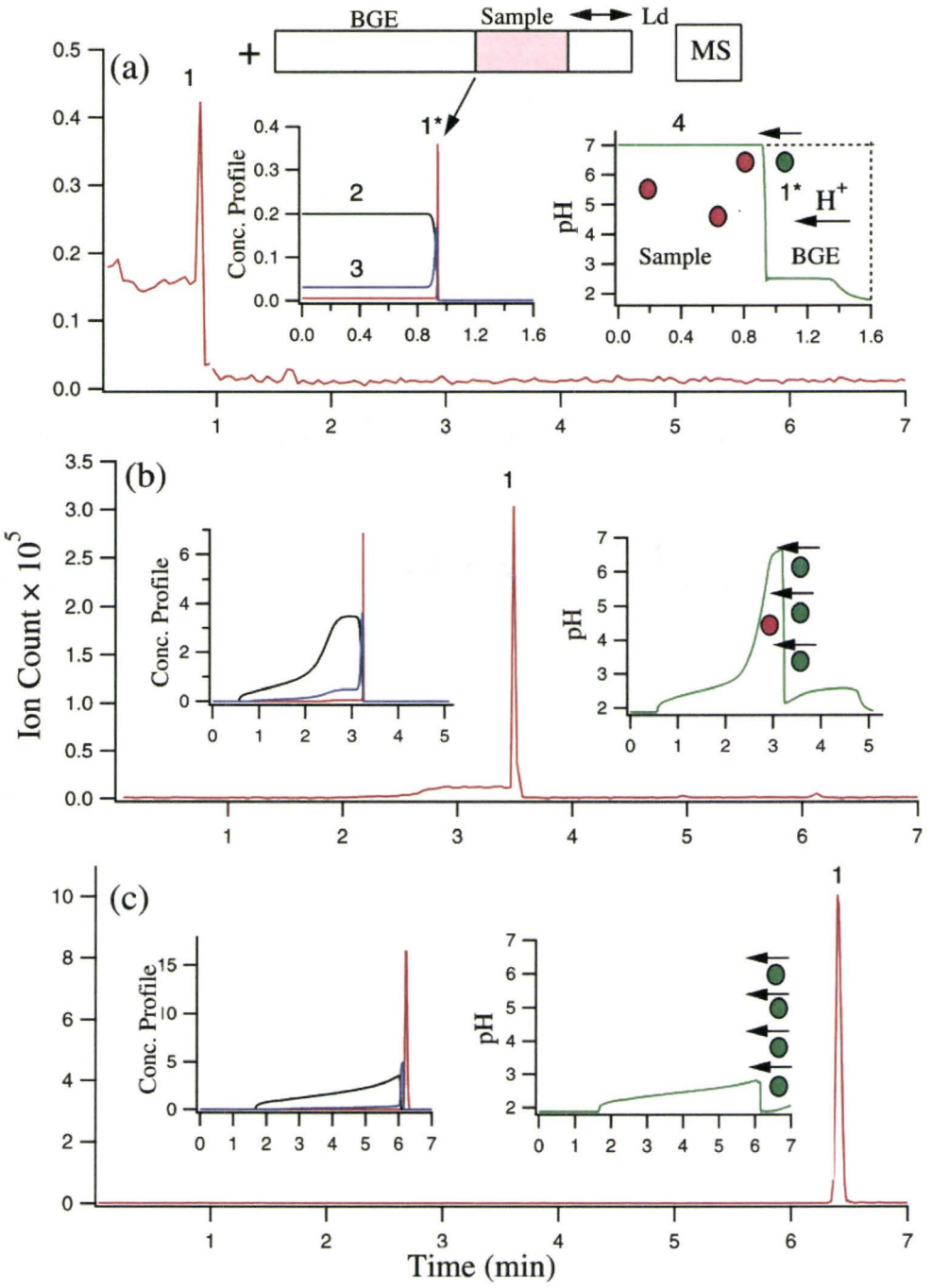

Figure 1.4: Time-resolved electropherograms showing the dynamics of in-capillary tryptophan (Trp) focusing by transient isotachophoresis and dynamic pH junction from experimental data and computer simulations using Simul 5.0 (insets). A sample plug of 12.5 cm was placed at distances of (a) 7.5 cm, (b) 25 cm, and (c) 40 cm from the distal end of the capillary. The BGE is 1 M formic acid, pH 1.8 and the sample is in 200 mM ammonium acetate, pH 7.0 with 15 mM NaCl. Concentration profiles are numbered as follows: (1) Trp, (2) NH_4^+, (3) Na^+, and (4) pH.[25]

1.3 Capillary Electrophoresis-Mass Spectrometry and Electrospray Ionization Efficiency

The most common detector in CE is UV absorbance, which offers moderate concentration sensitivity (μM-mM), low cost and high reliability. It requires the presence of a chromophore on the analyte. Otherwise, derivatization may be required for non-absorbing species. Alternatively, a BGE additive that can serve as an electrokinetic probe enables the detection of UV transparent analytes, such as polyols, via dynamic complexation in CE.[31] However, UV absorbance lacks selectivity for the analysis of complex mixtures, even when using a diode array detector to acquire full absorbance spectra. Therefore, high separation efficiency and peak capacity are required to avoid co-migration of analytes causing spectral interferences. Excellent sensitivity (nM-pM) can be achieved with laser-induced fluorescence (LIF) detection in CE.[32] However, most analytes are not intrinsically fluorescent. Therefore, derivatization with a fluorophore is frequently required, but this can add complexity to analyses due to possible multiple labeling of analyte molecules, incomplete derivatization, or time-consuming sample preparation. Electrochemical detection is also available for CE analysis of electrochemically-active analytes with limited selectivity. Mass spectrometric (MS) detection in CE is applicable to a wider range analytes with enhanced selectivity even with co-migrating analytes due to mass-selective detection. Several modes of ionization are available for capillary electrophoresis-mass spectrometry (CE-MS), including electrospray ionization (ESI), atmospheric pressure chemical ionization (APCI) and atmospheric pressure photoionization (APPI).[33] ESI is the most common ionization mode in CE-MS.[34] Capillary electrophoresis-electrospray ionization-mass spectrometry

(CE-ESI-MS) is suitable for direct analysis of most polar analytes, while APCI and APPI are compatible with increasingly non-polar analytes.[33]

1.3.1 Mass Spectrometric Detection

A CE-MS ion source interfaces CE with one of several types of mass spectrometer such as a quadrupole, a triple quadrupole, a time-of-flight mass spectrometer (TOF-MS), or an ion trap. As a detector, MS can provide qualitative as well as quantitative information about analytes. Quantitative analysis in MS is based on the number of ions of a specific *m/z* detected. The qualitative data provided by MS can include the molecular ion mass, isotope patterns, and fragmentation patterns in tandem mass spectrometry (MS/MS) or multistage mass spectrometry (MS^n), all of which can aid in identifying unknown analytes. Accurate mass of the molecular ion and isotope pattern analysis combine to aid in the assignment of a molecular formula to an unknown analyte, when using high resolution MS. With low resolution MS, such as quadrupole ion traps and quadrupole mass filters, a number of possible molecular formulas may be consistent with the measured mass, since it is often only determined with unit mass precision. However, high resolution MS, including TOF-MS, orbitrap MS, or Fourier transform-ion cyclotron resonance MS (FT-ICR-MS) can determine the mass of the molecular ion with greater precision allowing for the assignment of a unique molecular formula to analytes of sufficiently low molecular mass.[35] Isotope patterns result from the natural distribution of isotopes of particular elements and can be diagnostic of the presence of particular combinations of elements in an analyte. For example, there are two isotopes of sulfur with greater than one percent abundance—^{32}S and ^{34}S—with ^{34}S having 4.4% of the

abundance of ^{32}S. Therefore, for compounds containing one sulfur atom, such as reduced thiols, there is an isotopomer ion 2 *m/z* higher than the most abundant isotopomer ion (MH^+) with 4.4% of abundance of the main isotopomer ion. For compounds with two sulfur atoms, such as disulfides, the isotopomer ion 2 *m/z* higher has 8.8% of the abundance of the main isotopomer ion and an isotopomer 4 *m/z* higher has 0.2% relative abundance. Isotope patterns, such as these, can be interpreted and are diagnostic of various molecular formulas.[36] However, this reveals nothing about the molecular structure. Fragmentation patterns from MS/MS and MS^n provide information about the structure of unknown analytes aiding in their identification. However, all forms of qualitative information from MS are of poorer quality for low abundance analytes making their characterization by MS difficult. In this thesis, quadrupole ion trap MS (IT-MS), is used. It can perform full-scan MS with high sensitivity as well as MS^n for structural elucidation of unknown metabolites with unit mass resolution and full width at half maximum of ≤ 0.6 *m/z* units.

IT-MS operation is based on selective stabilization and destabilization of ion orbits within a quadrupolar electric field. The ion trap consists of a hyperbolic ring electrode across which RF voltage is applied and grounded end-cap electrodes. Ions of a range of *m/z* are trapped in the ion trap by applying an RF voltage that places these ions within a stable region of the stability diagram defined by the solutions to the Mathieu equations shown in **Figure 1.5**. In such a region, the ions have stable orbits within the ion trap and do not collide with the electrodes, which would neutralize them. Full-scan MS is accomplished by scanning the RF potential to sequentially destabilize the orbits of

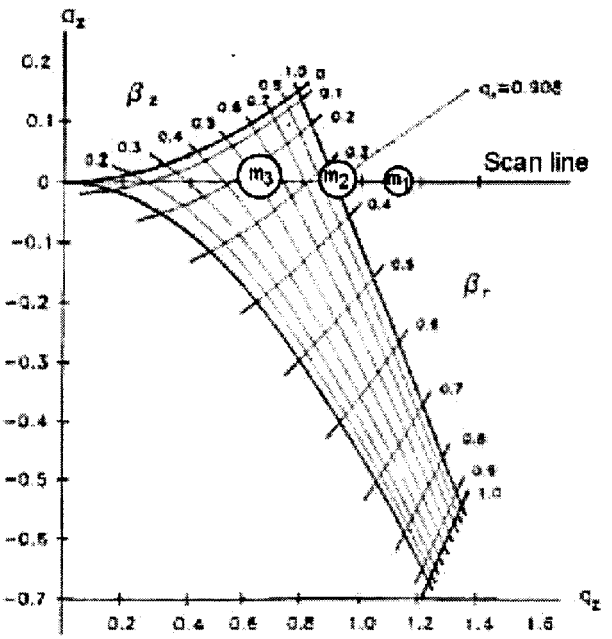

Figure 1.5: Stability diagram showing regions of stable ion trajectories within an ion trap as determined by the solutions to the Mathieu equations. A scan line for mass-selective axial ejection is shown that ejects the singly charged ions in the order m_1 then m_2 then m_3 where the mass of $m_1<m_2<m_3$. [37]

all the *m/z* within the trap in the axial direction such that one *m/z* at a time is ejected from the trap to the detector, with low *m/z* ions ejected first and high *m/z* ions ejected last. For fragmentation experiments, a selected *m/z* can be isolated within the trap and fragmented by collision-induced dissociation (CID) prior to mass-selective ejection to detect the fragment ions. Isolation of a particular *m/z* of ions for fragmentation occurs via the application of RF potentials that destabilize the orbits of all other *m/z* ions in the trap, ejecting them. The RF potential can then be adjusted to excite the trapped ions to larger, higher energy orbits where they undergo CID with helium damper gas. Following CID, mass selective detection of the fragments can occur as for full-scan MS or fragment ions of a specific *m/z* can be isolated for another round of CID. If too many ions are trapped,

Coulombic repulsions result in space-charge effects that perturb ion trajectories and cause a loss of mass resolution.[38] For the ion trap used in this thesis, the *m/z* of the ions with the most stable orbits in the trap can be adjusted using a parameter called the target mass, which was adjusted to avoid trapping efficiency bias in studies of ionization efficiency.

1.3.2 Electrospray Interfaces for Capillary-Electrophoresis

CE-ESI-MS requires specialized ESI interfaces to generate a stable and robust electrospray due to the low flow rate emitted from a CE capillary (~10-100 nL/min) in contrast to high flow rates in LC (μL/min). CE-ESI-MS interfaces may be either sheath-flow interfaces or sheathless interfaces. Sheath-flow interfaces employ a make-up flow. This flow forms an electrical contact between the BGE in the capillary and the electrode that drives both the CE and the ESI processes. The sheath flow also alters the solvent composition of the CE-ESI-MS output improving ESI compatibility and increases the flow rate to that required by commercial ESI sources. The coaxial sheath-flow interface is the most robust and reliable CE-ESI-MS interface to date and is commercially available.[34] However, the sheath flow dilutes the CE effluent reducing concentration sensitivity compared to sheathless interfaces. The dilution factor in sheath-flow interfaces may be less than half with a specialized coaxial sheath-flow nanospray interface.[34] However, commercial sheath-flow interfaces do not offer ideal sensitivity since a novel sheath-flow interface incorporating low flows of a modifier solution with a beveled emitter tip can improve sensitivity for amino acid analysis by five-fold over a commercial interface.[39] The beveled tip lowers the optimal flow rate because a small Taylor cone can form at its sharpest point.[34] This reduces the sheath flow required

thereby reducing dilution. Sheathless interfaces do not employ a make-up sheath flow and are the more sensitive CE-ESI-MS interface. However, sheathless interfaces are especially delicate and are not yet commercially available due to a lack of robustness.[34]

For CE-ESI-MS in this thesis, the coaxial sheath-flow interface illustrated schematically in **Figure 1.6** was utilized. In addition to the sheath liquid, this interface supplies a nitrogen nebulizer gas to assist in robust and stable electrospray formation. This nebulizer gas and to a lesser extent the sheath liquid flow, can induce suction effects at high flow rates introducing a parabolic distortion to the flat CE flow profile causing band broadening.[40] Therefore, sheath flow and nebulizer gas flow rates should be optimized to minimum values for the formation of a stable electrospray to minimize suction and dilution effects. The ion source is also heated to facilitate faster evaporation from droplets in the electrospray improving the efficiency of the ionization process. This interface establishes an electrical contact with the BGE by grounding the sprayer that is in contact with the sheath liquid, which is in contact with the BGE at the sprayer tip. This electrical contact drives the CE and ESI processes. Ions formed in the ESI source are extracted orthogonally into the IT-MS and focused by several ion lenses as they move from the atmospheric pressure ESI source to the ion trap, which is under high vacuum.

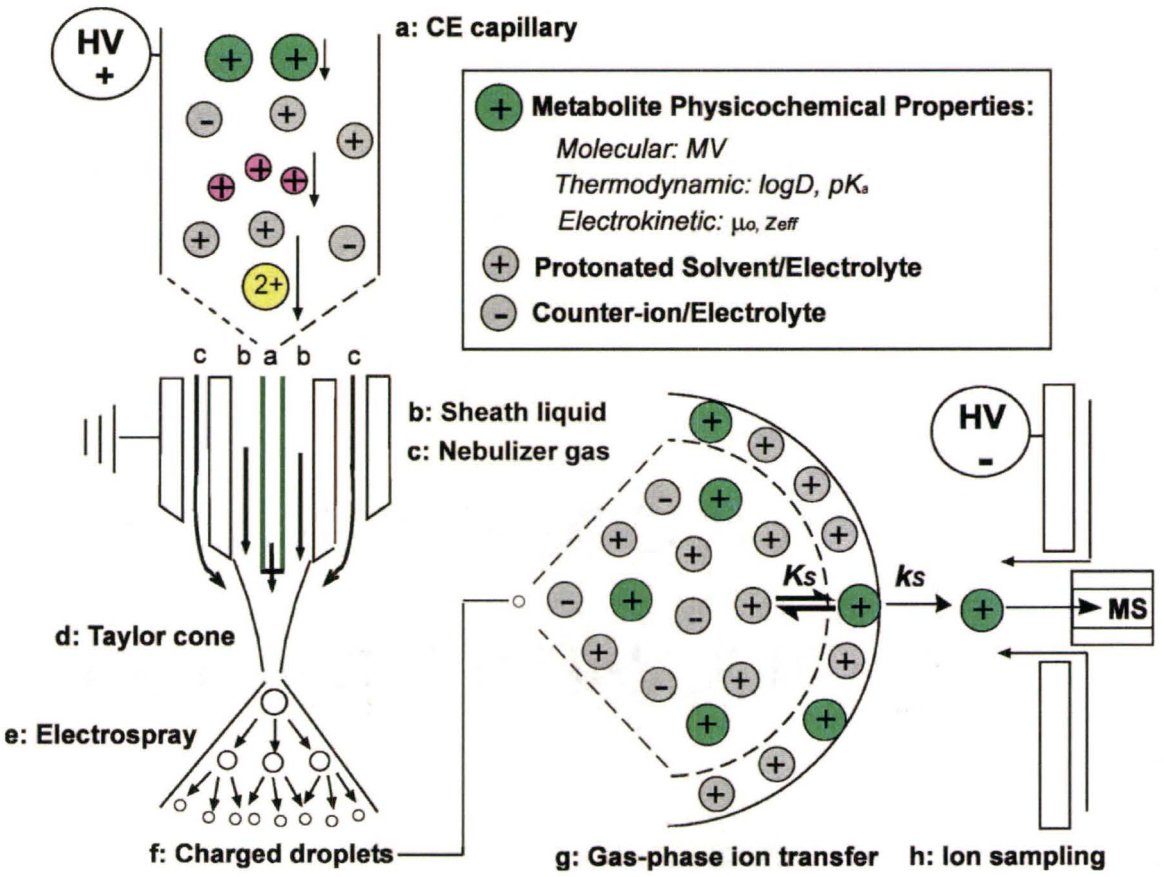

Figure 1.6: Diagram of coaxial sheath-flow interface for CE-ESI-MS and ion evaporation from a charged droplet according to the equilibrium partitioning model showing partitioning to the droplet surface with equilibrium constant, K_s, and ion evaporation from the droplet surface with rate constant, k_s.[23]

1.3.3 Mechanism of Electrospray Ionization

Electrospray ionization (ESI) is a process producing an emission of gas phase ions from a capillary filled with a flowing electrolyte solution and held under a 2-5 kV electric potential.[41] When the potential is applied, ions in the fluid in the capillary move under the influence of the electric field. A capillary outlet held at a positive relative potential emits positive ions and this arrangement is called positive ion mode ESI. In positive ion mode, cations in the capillary accelerate toward the capillary exit and electrostatic

repulsion builds between them. This repulsion exceeds the surface tension of the electrolyte solution and solvent containing positive charges moves toward the negative electrode, which is often the inlet to a mass spectrometer, forming a Taylor cone. Under a sufficient electric field, a fine liquid filament emerges from the tip of the Taylor cone and divides into small, charged droplets. Evaporation of solvent from the charged droplets in a heated ion source (100-300°C) increases charge density and leads to droplet fission due to electrostatic repulsions.[41] There is some controversy as to the exact mechanism in which gas phase ions are produced from these charged droplets. Dole proposed the initial charged residue model whereby repeated fission leads to tiny droplets that contain a single ion that becomes a gas phase ion upon evaporation of the solvent.[42] Recent evidence[43] supports an alternative mechanism for formation of ions from small molecules, the ion evaporation model first proposed by Iribarne and Thompson.[44] In this model, ions solvated by several solvent molecules evaporate from the droplet surface when charge repulsion at the surface overcomes surface tension. In either case, the counter electrode in an ESI-MS source is the inlet to a mass spectrometer, which samples ions into a mass analyzer for subsequent resolution based on their *m/z*.

1.3.4 Ionization Efficiency in ESI-MS

In ESI-MS, equimolar solutions of different analytes can have responses varying over three orders of magnitude.[23] This is due to variations in ionization efficiency, which is the fraction of a solute converted from the solution phase to gas phase ions during the ESI process. These differential responses may be reduced by low flow rates in nanospray sources.[45] The intrinsic physicochemical properties of solutes that determine

ESI ionization efficiency are not entirely understood and no broadly applicable method for predicting solute ionization efficiency exists to date. Models have been proposed to describe the mechanisms determining ionization efficiency and several studies have correlated solute molecular or thermodynamic properties to ESI ionization efficiency. Enke first introduced an equilibrium partitioning model to explain ionization efficiency based on the extent to which solutes partition towards the surface of the charged droplets formed in ESI. Ions that are surface active and partition near the droplet surface can best participate in ion evaporation and have greater ionization efficiency.[46] Alternative theories about ESI ionization efficiency indicate that mass transport mechanisms are involved in ionization efficiency. In addition to surface activity, diffusion and electrophoretic migration of ions in droplets with axial charge gradients may influence ion desorption rates with higher μ_{ep} associated with increased ionization efficiency.[47, 48] A number of studies have demonstrated that one or two physicochemical properties can influence ionization efficiency, including the difference between hydration free energy and the gas phase proton binding energy of amino acids,[49] the solvation energy of alkali metal ions,[50] and the nonpolar surface area of tripeptides.[51] More recently, multivariate methods have been utilized to relate multiple physicochemical properties to the ESI ionization efficiency of singly charged metabolites,[23] tripeptides,[52] and singly charged organic compounds.[53] For instance, positive correlations with ESI ionization efficiency were found for *MV*, pK_a, octanol-water distribution coefficient (*logD*), and/or total area,[23, 52, 53] whereas polar surface area was negatively correlated with ionization

efficiency.[52] Ion formation by ion evaporation from a charged droplet in accordance with Enke's equilibrium partitioning model is shown in **Figure 1.6.**

In general, small hydrophilic ions have weak ionization efficiency in ESI-MS due to their low surface activity. Also, solutes that lack acidic or basic functional groups that facilitate their ionization, such as carbohydrates and steroids, have weak ion response in ESI-MS often requiring ion pair formation with another ion in solution such as Na^+ or NH_4^+ to facilitate ionization. Some researchers have noted improved ESI response with derivatization of biomolecules. Hydrophobic derivatization that significantly increases surface activity[54] or introducing a charge to a neutral molecule[55] have both been reported as effective strategies to improve ionization efficiency and therefore sensitivity in ESI-MS. However, no systematic study of multiple physicochemical properties altered by chemical derivatization and their effect on ESI ionization efficiency has yet been undertaken. The first such study is described in **Chapter 2** of this thesis using maleimide derivatization of free sulfhydryl groups on biological thiols. Many biological thiols have low endogenous concentrations and maleimide derivatization is a means to improve their ionization efficiency in order to improve analytical sensitivity. The derivatization also stabilizes the reactive sulfhydryl groups improving assay robustness and can modulate the μ_{ep} of biological thiols in CE to shorten analysis times and reduce band broadening.

1.4 Thiol Metabolism, Redox Status, and Redox Regulation

CE-ESI-MS is well suited to the analysis of polar metabolites with weakly ionic functional groups such as amino acids and small peptides.[56, 57] This makes it a promising platform for the direct analysis of biological thiols, including both reduced thiols and

oxidized disulfides. These species are of significant interest because they can serve as sensitive biomarkers associated with oxidative stress, aging, and disease.[14, 58]

1.4.1 Metabolism of Thiols

The five major biological thiols that can be metabolically interconverted are cysteine (Cys), homocysteine (Hcy), cysteinylglycine (CysGly), γ-glutamylcysteine (GluCys), and reduced glutathione (GSH). The structures and metabolic pathways involving these thiols are depicted in **Figure 1.7**. GSH is the predominant intracellular thiol and plays an important role in the antioxidant defenses of the cell. Oxidized glutathione disulfide (GSSG) is produced from reduced GSH in reactions that scavenge for RONS. This process can be reversed by glutathione reductase to replenish the antioxidant reduced GSH pool.[59] Normally, Cys is the limiting reagent in GSH biosynthesis. Thus, production of GluCys by γ-glutamylcysteine synthetase is the rate limiting step.[59] Cys is the predominant extracellular thiol and adequate levels of it, as well as glutamic acid (Glu) and glycine (Gly), are essential for normal GSH biosynthesis.[59] *N*-acetylcysteine (NAC) shows promise in treating GSH deficiency as a source of Cys that can be administered orally.[19] Methionine (Met) is an essential amino acid that can be metabolized in the liver into Cys with Hcy as an intermediate, while Cys is considered a conditionally essential amino acid.[60] Both Met and Cys are utilized in protein biosynthesis. Cys residues in proteins are involved in redox regulation of protein activity that will be discussed in **Section 1.4.3**. Despite its importance in GSH biosynthesis, excess reduced Cys in cell culture media is cytotoxic[61] and Cys is excitotoxic to neurons through its activity on *N*-methyl-*D*-aspartate receptors.[62]

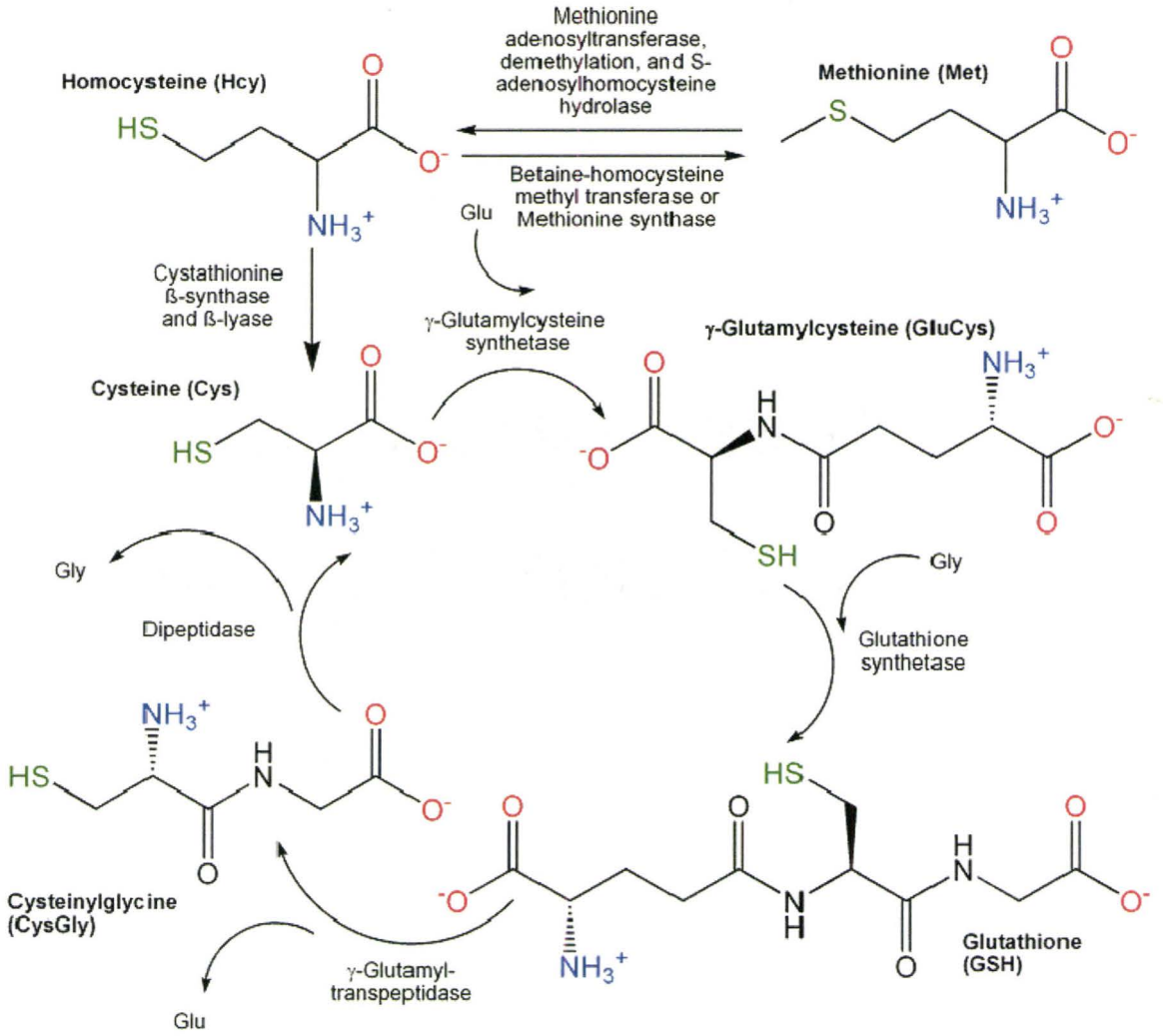

Figure 1.7: Metabolic relationships of various biological thiols in human metabolism including Hcy, Cys, GluCys, GSH and CysGly.

Hcy metabolism is of significant medical interest because elevated Hcy levels have been identified as a cardiovascular disease risk factor.[63] Met is converted into Hcy via a two step trans-methylation process. First, methionine adenosyltransferase converts

Met to *S*-adenosylmethionine (SAM). Demethylation of SAM occurs via the methylation of an acceptor biomolecule, such as DNA or a protein resulting in *S*-adenosylhomocysteine (SAH). The final conversion to Hcy occurs when *S*-adenosylhomocysteine hydrolase hydrolyzes SAH.[64] Methylation of proteins by SAM can occur at arginine (Arg) residues forming monomethylarginine (MMA), symmetric dimethylarginine (SDMA), or asymmetric dimethylarginine (ADMA). ADMA is a competitive inhibitor of NO synthase, which links thiol metabolism to NO biosynthesis.[65] Hcy may be remethylated to Met either with a methyl group from betaine (Bet) by betaine-homocysteine methyltransferase or with a methyl group from 5-methyltetrahydrofolate by methionine synthase.[66] In the former reaction, Bet is converted to dimethylglycine (DMG). Conversion of Hcy into Cys occurs in a two step process. First, cystathionine β-synthase produces cystathionine from Hcy and serine (Ser). Next, cystathionine β-lyase cleaves cystathionine into Cys, ammonia, and α-ketobutyrate.[67]

In biological samples, thiols exist in several fractions due to their redox-active nature. Reduced thiols are those in the free sulfhydryl form shown in **Figure 1.7**. Oxidized thiols are those that have been oxidized to form a disulfide bond. These disulfide bonds can form with another low molecular weight thiol forming a symmetric disulfide (homodimer) or a mixed disulfide (heterodimer), or with a Cys residue in a protein forming a protein-bound thiol. Free thiol levels include both free reduced thiols and symmetric/mixed disulfides, free oxidized thiol levels include only low molecular weight disulfides, and total thiol levels include all free thiols and protein-bound thiols.

To obtain a deeper understanding of thiol metabolism and the role of different fractions of reduced and oxidized thiols in human health, assays that allow for comprehensive thiol speciation are required for accurate assessment of various thiol metabolites. Interconversion between the different thiol fractions, such as oxidation of free thiols to disulfides, occurs reversibly *in vivo*. Therefore, it is of interest to develop methods that can provide a snapshot of the state of thiols in a biological sample without oxidation artifacts or thiol-disulfide exchange reactions during sample handling. Various thiols have different propensities for oxidation with for example NAC being less quickly oxidized than Cys.[19] The reduction potential of thiols is pH dependent and is influenced by the pK_a of the thiol group. Thiolate ions with greater sulfhydryl pK_a values are better reducing agents but the concentration of thiolate ions with high pK_a values is lower resulting in a complex dependence of reducing potential that is influenced by steric factors, solution pH, and sulfhydryl pK_a.[68] Besides oxidation, thiols can react *in vivo* in thiol-disulfide exchange reactions in which one thiol in a low-molecular weight or protein-bound disulfide is replaced by a free thiol. Thiol-disulfide exchange is favored when the free thiol involved has a higher pK_a than the thiol in the disulfide.[69] For example, Cys has a sulfhydryl pK_a of 8.2 to 8.5, while Hcy has a sulfhydryl pK_a of 8.7 to 10.0.[69] A greater percentage of plasma Hcy is bound to protein than plasma Cys because Hcy is less stable than Cys as a thiolate anion and when Hcy encounters protein-bound Cys, thiol exchange is favored.[69] In general, the rate of thiol-disulfide exchange is determined by a rate law that involves the product of a rate constant and the concentration of thiolate anion. The rate constant is positively correlated with the pK_a of

the free sulfhydryl and negatively correlated with the pK_a of the constituent thiols of the disulfide.[70] Since the concentration of thiolate anion is lower for thiols with higher pK_a values, observed reaction rates are usually lower for higher pK_a free sulfhydryls.[70] Rates of thiol-disulfide exchange can also be influenced by steric and electrostatic factors. For example, high pK_a peptide thiols react more slowly with GSSG than would expected based on pK_a alone. This occurs because high pK_a thiols in peptides are usually adjacent to negatively charged groups that repel negatively charged GSSG.[70] Because a variety of mixed and symmetric disulfides can form dynamically through oxidation of thiols and thiol-exchange, it is important to be able analyze the content of specific disulfides in biological samples in order to assess their role in oxidative stress and disease pathogenesis.

1.4.2 Thiol Redox Potentials

The reduced to oxidized ratio of a thiol, such as the GSH/GSSG ratio, in a biological sample can serve as a biomarker of oxidative stress.[10] However, due to the stoichiometry of thiol oxidation, in which two reduced thiols form one disulfide, it does not completely describe the redox status of the thiol pool. The redox potential (E_h) of a thiol/disulfide couple is a measure of the tendency of a particular thiol pool to donate or accept electrons from other redox active species.[71] E_h is calculated using the Nernst equation, which for a general thiol redox couple is:

$$E_h = E^\circ + \left(\frac{RT}{2F}\right)\ln\left(\frac{[ThSS]}{[Th]^2}\right) \qquad (5)$$

where E_h is the potential of the thiol redox couple relative to a standard hydrogen electrode, E^o is the standard potential for the thiol redox couple, R is the ideal gas constant, T is the temperature in Kelvin, F is Faraday's constant, *[ThSS]* is the concentration of the disulfide form of the thiol, and *[Th]* is the concentration of the reduced thiol. At the physiological pH of 7.4, E^o is -264 mV for the GSH/GSSG redox couple and -250 mV for the cysteine/cystine (Cys/CysSS) redox couple.[71] **Equation 5** may be simplified as follows using units of mV for E_h:

$$E_h = E_0 + 29.55mV \cdot \log\left(\frac{[ThSS]}{[Th]^2}\right) \qquad (6)$$

The physiological importance of thiol redox potential is apparent in the correlation of E_h with the cell cycle. Both the intracellular GSH/GSSG and the extracellular Cys/CysSS redox couples become increasingly oxidized as cells move from proliferation to growth arrest and/or differentiation to apoptosis.[72] Proliferation of cells occurs at an intracellular GSH/GSSG E_h of -260 to -230 mV and an extracellular Cys/CysSS E_h below -80 mV. Growth arrest and/or differentiation occurs at an intracellular E_h of -220 to -190 mV and an extracellular E_h of about -80 mV, while apoptosis occurs at an intracellular E_h of -170 to -150 mV and an extracellular E_h of 0 to -80 mV.[72] The mechanism for the effect of redox on the cell cycle has not been fully elucidated but it likely involves redox modification of Cys residues on proteins,[72] which alters protein function and activity and is involved in cell signaling as will be discussed in **Section 1.4.3**. During periods of acute oxidative stress, such as during strenuous aerobic exercise, the GSH/GSSG redox couple in erythrocytes may become temporarily oxidized

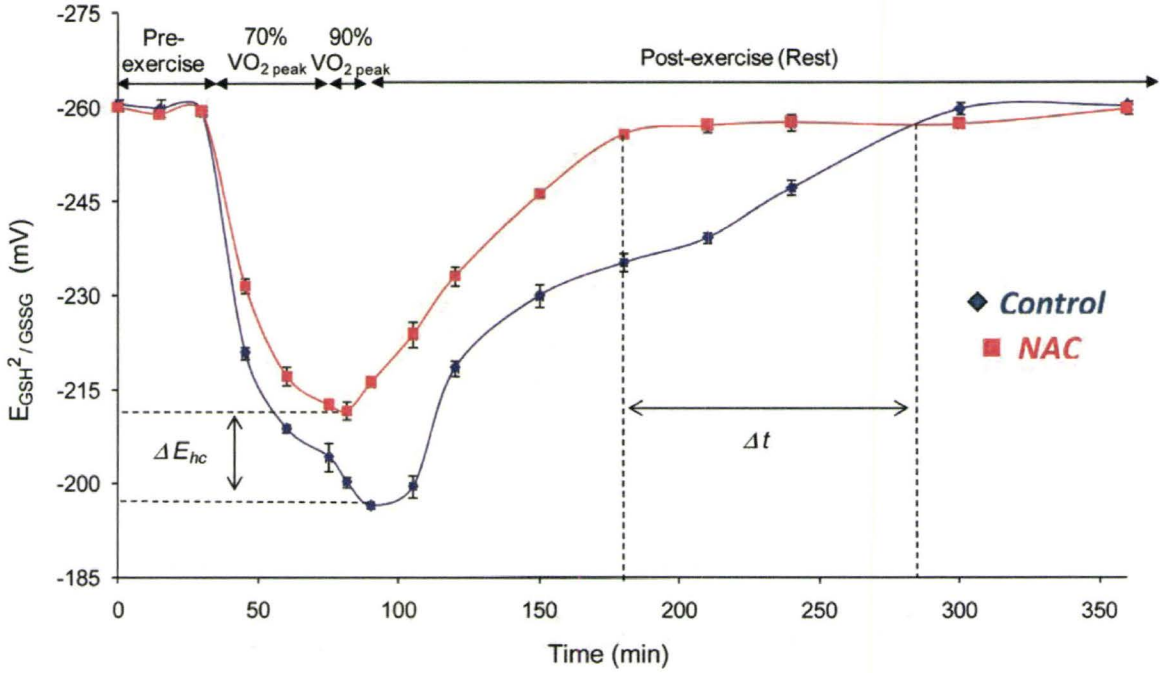

Figure 1.8: Overlay traces of E_h for the GSSG/GSH redox couple in erythrocytes ($E_{GSH}^2/_{GSSG}$) as a function of time before, during, and after a standardized strenuous exercise protocol for control and NAC trials. A more reduced $E_{GSH}^2/_{GSSG}$ at peak oxidation ($\Delta E_{hc} \approx +15$ mV) and a shorter recovery time to redox homeostasis ($\Delta t \approx 100$ min) was measured with NAC pretreatment relative to the control for the same subject.[73]

before returning to homeostasis with a highly reduced redox potential (~-260 mV).[73] The duration and magnitude of the oxidation of the GSH/GSSG redox couple may be attenuated by high dose oral NAC pretreatment, as illustrated in **Figure 1.8**.[73] Anecdotally, this result was accompanied by reduced fatigue and NAC may thus be useful in improving recovery time and reducing symptoms of fatigue in humans during episodes of acute oxidative stress.

The redox potentials defined for specific thiol/symmetric disulfide couples may represent an oversimplification of the redox status of thiol systems because oxidized forms of a thiol also include low-molecular weight mixed disulfides and protein-bound

thiols. Thus, a more thorough assessment of the redox state of a thiol in a biological sample may be obtained by considering concentrations of all forms of that thiol in the expression for E_h. Thorough assessment of thiol redox potentials can only be accomplished by analytical methods that accurately measure reduced thiols, intact disulfide species, and protein-bound thiols.

1.4.3 Redox Signaling

The redox hypothesis of oxidative stress postulates that disruptions in redox signaling and control cause the physiological decline associated with aging.[4] Thus, it is important to consider the mechanisms of redox signaling and physiological regulation. Redox signaling is involved in regulation of proteins including transcription factors, metabolic enzymes, and membrane transport channels as well as in calcium- and phosphorylation-dependent signaling mechanisms.[74]

The primary mechanism of redox signaling and control is through reversible covalent modification of accessible protein Cys residues. The redox modifications that are possible for protein thiols include disulfide formation, *S*-gluathionylation, *S*-nitrosylation, acylation, DNA binding, and the formation of thiohemiacetals.[4] With active site Cys residues, redox modifications such as intra-protein disulfide formation, *S*-glutathionylation, or S-nitrosylation will either activate or inactivate the protein, functioning as an "on-off" switch that is influenced by the cellular redox environment. For example, *S*-glutathionylation of an active site Cys in capase-3 regulates its activity.[4] For Cys residues in allosteric sites, the same redox modifications can exert nuanced control on protein activity acting in a similar fashion to a rheostat.[4] For example, *S*-

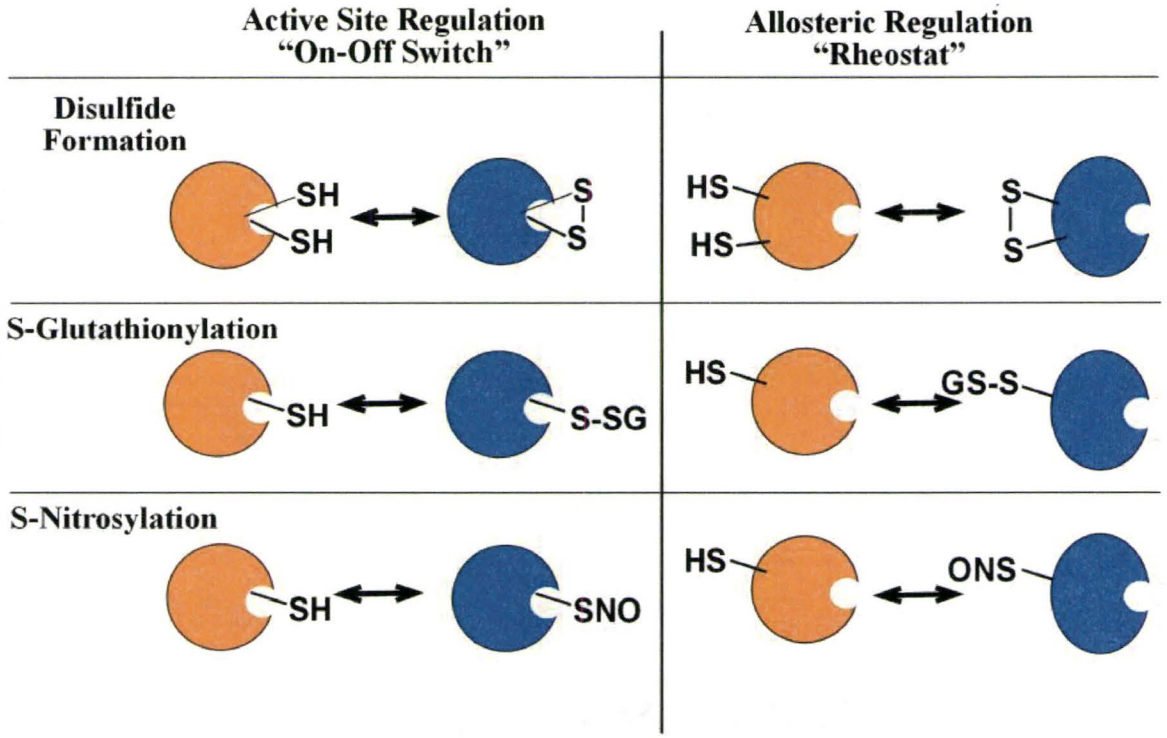

Figure 1.9: Illustration of protein redox regulation by disulfide formation, *S*-glutathionylation, or *S*-nitrosylation either in the active site or at an allosteric site. Active site modifications function as an "on-off switch," while allosteric modifications function as a "rheostat."

glutathionylation of mitochondrial complex I allosterically regulates its activity with superoxide production increased above basal levels upon *S*-glutathionylation.[75] Macromolecular interactions of proteins are also subject to redox control because disulfide bonds can join two proteins together. This can influence movement of proteins from one subcellular location to another, can tether of proteins to the cytoskeleton, or can form activated multimeric protein complexes.[4] For example, glucocorticoid receptor translocation into nuclei is influenced by oxidation.[4] Six different possibilities for allosteric and active site protein regulation by disulfide bond formation, *S*-glutathionylation, and *S*-nitrosylation are illustrated in **Figure 1.9**.

Elucidating specific mechanisms of redox signaling and control is the subject of on-going research. Hydrogen peroxide may function as a second messenger in redox regulatory systems, as it is produced by and degraded by enzymes and acts as an oxidant in a particular place at a specific time.[76] In addition, the general mechanism of redox regulation is still not fully understood. There is evidence that thiol/disulfide couples are not in equilibrium *in vivo*, so thermodynamic equilibrium is an unlikely mechanism for redox regulation. It appears that oxidants act on a set of specific protein targets that are sensitive to oxidation and can then transmit the redox signal. There may also be a few very redox sensitive sensor proteins that are oxidized first and proceed to selectively oxidize other target proteins that are involved in signal transmission.[74] Investigating redox signaling is important because there is accumulating evidence that thiol redox status and disruption of redox regulation are involved in aging and disease progression.

1.4.4 Redox Status, Oxidative Stress, Aging, and Disease

A number of studies have examined the associations between thiol metabolite levels and/or thiol redox status and aging and disease. The results of these studies suggest that changes in thiol levels and redox status are correlated with disease, although their causative role in disease remains unclear.

A number of correlations between age and plasma thiol levels and thiol redox status have been documented. Reduced CysGly levels decrease with age while total and oxidized levels of this thiol remain unchanged,[15] whereas reduced GSH levels decrease and GSSG levels increase with age.[14] Oxidized and total levels of Hcy and Cys increase with age, while reduced levels of these thiols are unaffected[15] or may decrease slightly

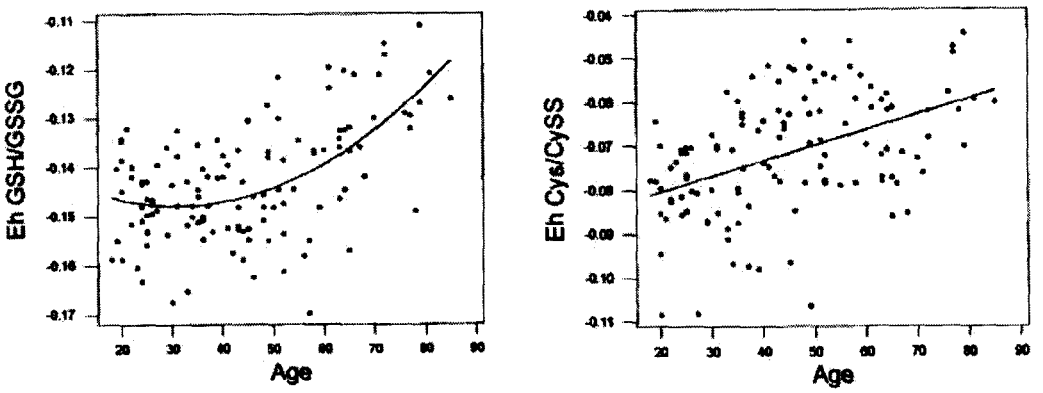

Figure 1.10: E_h for GSH/GSSG and Cys/CysSS in plasma as a function of age. GSH/GSSG has a quadratic line of best fit, while Cys/CysSS has a linear line of best fit.[14]

for Cys.[14] In addition, thiol groups on plasma proteins are increasingly oxidized with age.[15] Thiol redox potentials tend to become increasingly oxidized with age with the plasma Cys/CysSS couple becoming linearly oxidized throughout the lifespan. In contrast, the plasma GSH/GSSG couple becomes progressively more oxidized after the fourth decade of life as illustrated in **Figure 1.10.**[14, 15] These changes are indicative of increases in oxidative stress with age with reduced antioxidant capacity for the elderly. This raises the possibility that oxidative stress has a causative role in age-related disease and physiological decline.

A wide range of diseases have been correlated with thiol dysregulation and/or oxidative stress as indicated by altered levels of thiol metabolites and/or oxidized thiol redox potentials. A selection of these correlations is summarized in **Table 1.1.** Elevated total plasma Hcy (> 15 μM), which is an independent, graded risk factor for cardiovascular disease, has been found to increase with age, male gender, folate and

Table 1.1: Selected reports of associations between disease and thiol metabolite levels and redox status

Disorder	Thiol Marker	Biological Sample Type	Reference
Alzheimer's disease	Decreased GSH with familial Alzheimer's disease	Human lymphoblasts	Cecchi *et al.*, 1999[20]
Brain ischemia and reperfusion	Decreased total GSH	Rat brain	Namba *et al.*, 2001[77]
	Oxidized GSH/GSSG ratio, decreased total GSH	Gerbil hippocampus	Park *et al.*, 2000[78]
Cancer	Oxidized GSH/GSSG ratio, Increased GSSG	Human whole blood	Navarro *et al.*, 1999[18]
Cardiovascular disease	Increased CysSS, total Cys, and protein-bound Cys	Human plasma	Mills *et al.*, 2000[79]
	Increased total Hcy	Human plasma	Refsum et al., 2006[16]
Complications in pregnancy	Increased total Hcy	Human plasma	Refsum *et al.*, 2006[16]
Diabetes mellitus	Increased GSH bound to hemoglobin	Human erythrocytes	Niwa *et al.*,2000[80]
	Decreased reduced and total GSH, oxidized GSH/GSSG E_h Decreased reduced GSH	Human plasma Human whole blood	Samiec *et al.*,1998[81]
Early-stage atherosclerosis	Oxidized GSH/GSSG E_h, Decreased GSH, Increased CysSS	Human plasma	Ashfaq *et al.*, 2006[63]
Endothelial dysfunction	Increased CysSS, Increased CysSSG	Human plasma	Ashfaq *et al.*, 2008[13]
HIV	Decreased GSH	Human erythrocytes and CD4 T cells	Atkuri *et al.*, 2007[19]
Ischemic stroke	All Hcy species increased; Increased total, free, reduced, and oxidized Cys; Decreased total, protein-bound, and reduced CysGly; Decreased total, protein-bound, and oxidized GSH	Human plasma	Williams *et al.*, 2001[17]
Liver disease	Increased total GSH, Increased GSSG	Human plasma and erythrocytes	Loguercio *et al.*, 1996[82]
	Decreased GSH	Human liver biopsy	Altomare *et al.*, 1988[83]
Parkinson's disease	Decreased reduced GSH	Human brain tissue (substantia nigra)	Sofic *et al.*, 1992[84]
Preeclampsia	Oxidized GSH/GSSG Ratio	Human erythrocytes	Spickett *et al.*, 1998[85]

vitamin B_{12} deficiency, smoking, sedentary lifestyle, high blood pressure, and high cholesterol.[16]

1.5 Methods and Challenges in Thiol Redox Status Analysis

In developing analytical methods to measure thiols and their redox status, two primary challenges must be confronted. First, reduced thiols are labile and are easily oxidized to disulfides during sample handling prior to analysis. This can occur with common sample preparation steps such as acid precipitation of proteins.[56] Secondly, adequate sensitivity is required to measure reduced thiols, many of which have sub-micromolar concentrations in complex biological matrices, such as plasma.

1.5.1 Total Thiol Analysis

Clinically, total thiol analysis is most commonly performed, which disregards the redox status of the thiols. This is the case when total Hcy is measured as a cardiovascular risk factor. Such analyses do not provide any biological context regarding thiol redox status and cannot differentiate between free sulfhydryls, disulfides, and protein-bound thiols. However, total thiol analysis is convenient to perform with greater analytical robustness than thiol redox status analysis since artifactual oxidation is eliminated.

Total thiol analysis can be performed on a number of analytical platforms including gas chromatography-mass spectrometry (GC-MS)[86]; LC with UV[87], fluorescence (FL)[88] or tandem mass spectrometric (MS/MS) detection[89]; and CE with UV, LIF, or amperometric detection.[32] Total thiol analysis begins with addition of a reducing agent, such as tris-(2-carboxyethyl)phosphine (TCEP), to reduce all the

disulfides in the sample to the free sulfhydryl.[88] In order to perform the most common UV and fluorescence detection based methods, the reduced sample is then derivatized with a thiol-selective reagent that contains a chromophore or fluorophore as required.[88] Adequate separations are required with optical detection methods to avoid spectral interferences.[87] GC-MS requires a more complex derivatization procedure to enhance volatility as well as extensive sample clean-up.[86] LC-MS/MS offers greater selectivity but is more expensive than LC-FL. Both radioimmunoassays and enzymatic immunoassays have also been developed for total thiol analyses, such as total Hcy analysis.[90] Immunoassays may suffer from bias due to cross-reactivity of the antibodies utilized.

1.5.2 Thiol Redox Status Analysis

Analysis of thiol redox status is a considerably more complex problem than total thiol analysis due to the need to avoid oxidation artifacts or thiol-disulfide exchange and to obtain measurements of multiple thiol species simultaneously. A variety of analytical platforms have been used for thiol redox status analysis, including LC-UV,[91] LC-FL[88], CE-UV,[92] CE-LIF[32], LC-MS/MS[89], LC-FT-ICR-MS[93], and CE-MS.[73] To prevent artifactual oxidation of free sulfhydryls, thiol redox status analysis methods involve either cold[56] and/or acidic[91] sample preparation or a thiol-selective derivatization step.[94, 95] Derivatization can also improve the analytical properties of thiols by adding a fluorophore or a chromophore and/or improving their retention properties in LC. A variety of derivatization chemistries have been reported for thiols including, bimanes, maleimides, halogeno-benzofurans, and ortho-pthalaldehyde.[87] Effective prevention of

oxidation artifacts is an important characteristic of a thiol redox analysis method. Sample preparation methods that are known to cause oxidation artifacts should be avoided. These include acid deproteinization, which can cause artifactual oxidation through the denaturation of redox-active proteins releasing metal ions.[56] Derivatization can make samples stable to oxidation for a period of time, removing the need for immediate analysis.[58] The timing of derivatization is an important consideration. While it prevents thiol oxidation, derivatization of whole blood upon collection[58, 93-97] will also label protein thiols. Modification of protein thiols alters their metabolic activity,[4] which is undesirable for untargeted metabolomics approaches. Freezing, thawing and acid deproteinizing a plasma sample prior to derivatization[98, 99] may take too long to prevent artifactual oxidation, which acid deproteinization can cause.[56] To avoid alkylation of proteins and oxidation artifacts, derivatization of plasma should take place immediately after deproteinization by ultrafiltration performed at 4°C.

In order to assess multiple thiol pools, many redox status analysis methods require a number of separate sample preparations and analytical runs. This can range from a single sample preparation for simultaneous analysis of reduced thiols and intact disulfides[56, 94] to as many as four separate sample preparation procedures for analysis of total thiols, reduced thiols, protein-bound thiols, and free oxidized thiols.[95] Performing simultaneous analysis of multiple thiol fractions should improve analytical throughput. In addition, methods that analyze free thiols or free oxidized thiols after chemical reduction[17, 95, 96, 98-101] fail to provide information on the identities and concentrations of the specific symmetric and mixed disulfides present in biological samples. A few

methods are available that maintain intact disulfides for redox analysis and can quantify multiple disulfides present in biological samples simultaneously.[93, 94, 97, 102, 103] These methods often suffer from complex sample pretreatment and/or long analysis time.

Another important consideration with thiol redox status analysis is adequate sensitivity because some reduced thiols and oxidized disulfides are present at sub-micromolar concentrations in plasma.[94] While derivatization can improve sensitivity and lower detection limits,[92] the choice of detection method is particularly important in achieving biologically relevant detection limits. Mass spectrometry[97] and fluoresence[98] have achieved the lowest detection limits for thiol analysis with detection limits in the nanomolar range or lower. Mass spectrometry has advantages over fluorescence in terms of the specificity of mass selective detection, particularly with MS/MS. Due to a lack of selectivity, optical methods require adequate separation efficiency to eliminate spectral interferences.[87] UV absorbance is intrinsically less sensitive than fluorescence and has inadequate sensitivity for many thiol analyses in biological samples, particularly without derivatization.[92, 104] Negative ion mode ESI-MS[105] may also provide poor sensitivity compared to positive ion mode.[97, 106] Sensitivity can also be improved using preconcentration. On-line preconcentration in CE[56] is a faster and more convenient method for preconcentration than off-line solid-phase extraction.[97]

For complex biological samples, the total analysis time of assays should also be considered. Some methods require lengthy overnight derivatizations combined with LC runs of over 50 minutes to fully resolve a fluorescently labeled sample.[107] Polar compounds such as thiol-containing amino acids are poorly retained in reverse-phase LC,

whereas ion exchange LC can result in electrostatic adsorption that compromises separation performance. However, CE is readily amenable to polar, ionizable analytes, such as biological thiols. As a result, CE methods often involve simpler sample preparations because LC methods may require additional derivatizations to improve retention properties.[94, 97] CE-MS is an attractive platform for thiol redox status analysis combining the suitability of CE for separation of polar thiol metabolites with the specificity of mass-selective detection. Unlike MS/MS, CE-MS is suitable for untargeted polar metabolite profiling providing greater insight into thiol metabolism using full-scan IT-MS. Key characteristics of reported methods for thiol redox status analysis by MS, LC with optical detection, and CE with optical detection are summarized in **Table 1.2**, **Table 1.3**, and **Table 1.4**, respectively.

Abbreviations used in **Table 1.1**, **Table 1.2**, and **Table 1.3**: 2MPA: 2-mercaptopropionic acid; 4,4'-DTP: 4,4'-dithiodipyridine, ABD-F: 4-fluoro-7-sulfamoylbenzofuran; Abs.: absorbance wavelength; ACN: acetonitrile; BGE: background electrolyte; bTh: protein-bound thiols; CE: capillary electrophoresis; CMQT: 2-chloro-1-methylquinolinium tetrafluoroborate; CysSSNAC: cysteinyl *N*-acetylcysteine disulfide; DAD: diode array detector; deriv.: derivatization; DPZ: deproteinization; DTT: dithiothrietol; ELM: Ellman's reagent; Em.: emission wavelength; Ex.: excitation wavelength; FEM: *N*-(2-ferroceneethyl)maleimide; GSNO: *S*-nitrosoglutathione; FL: fluorescence; FMEA: ferrocenecarboxylic acid (2-maleimidoyl)ethylamide; froxTh: free oxidized thiols; frTh: free thiols; FT-ICR-MS: Fourier transform ion cyclotron resonance mass spectrometry; GSSNAC: glutathione-N-acetylcysteine disulfide; hGSH: homoglutathione; HGZ: homogenization; HILIC: hydrophilic interaction chromatography; IAA: iodoacetic acid; IAM: iodoacetamide; IPFC: isopropylchloroformate; IS: internal standard; IT-MS: ion trap mass spectrometry; LC: liquid chromatography; mBrB: monobromobimane; MPA: metaphosphoric acid MRM: multiple reaction monitoring; MS/MS: tandem mass spectrometry; N/A: not available; NACSS: *N*-acetylcysteine disulfide; neg.: negative; NEM: *N*-ethylmaleimide; PnaSS: penicillamine disulfide; preconcent.: preconcentration; oxTh: oxidized thiols; red.: chemical reduction; RP: reverse phase; rTh: reduced thiols; SBD-F: 4-fluoro-7-sulfobenzofuran; SIM: selected ion monitoring; SPE: solid-phase extraction; TBP: tri-*n*-butylphosphine TCEP: triscarboxyethylphosphine; TOF-MS: time-of-flight mass spectrometry; tTh: total thiols; UF: ultrafiltration; UV: ultraviolet

Table 1.2: Summary of methods reported for simultaneous reduced thiol and oxidized disulfide analysis in biological samples using MS.

Reference	*Thiols*	*Specimen & collection*	*Sample pretreatment*	*Separation conditions*	*MS mode*	*Calibration*	*LOD (nM)*	*Comments*
Lee *et al.*, 2010, 2009[56, 73]	GSH, GSSG, NAC, CysSSNAC, NACSS, GSSNAC	Erythrocytes, EDTA tubes at 4°C	Cells lysed; UF; on-line preconcent.	CE, 1 M formic acid BGE, pH 1.8	Full-scan (+/-); IT-MS	Non-isotopic IS	25-4000	Disulfides intact; Untargeted metabolite profiling; Simple workup; Poor NAC sensitivity
Suh *et al.*, 2009[97]	Cys, CysSS, CysGly, CysGlySS, GSH, GSSG, Hcy, HcySS	Plasma, erythrocytes; EDTA-tubes with IAM	IAM deriv. in tube, acid-DPZ; SPE; IPFC deriv.	RP LC; isocratic elution	MRM (+), MS/MS	Isotopic and Non-isotopic IS	0.25-0.50	Disulfides intact; Total Thiols; Excellent sensitivity; Complex sample workup
Johnson *et al.*, 2008[93]	Cys, CysSS, GSH, GSSG, CysSSG	Plasma; heparin buffer, pH 8.3 with IAA	IAA deriv. in tube; 2:1 ACN-DPZ	Anion exchange LC; gradient elution	Full-scan (-), FT-ICR-MS	Isotopic IS	N/A	Direct free thiol analysis < 10 min; Sample artifacts; Poor GSSG sensitivity
Zhu *et al.*, 2008[106]	GSH/GSSG	Macrophage culture; acid-lysis with ABD-F	ABD-F deriv. during lysis; acid-DPZ	RP (C18) LC; gradient elution	MRM (+), MS/MS	Isotopic IS	10-500	Intact GSH/GSSG; Excellent sensitivity and robustness; Thiol IS labeled first to avoid bias
Seiwert *et al.*, 2007[101]	Cys, Hcy, CysGly, GSH, NAC: rTh and oxTh	Urine; acid/EDTA-treated at 4°C with dilution	FEM deriv., quench, TCEP red., FMEA deriv.	RP (C8) LC; gradient elution	MRM (+), MS/MS	Non-isotopic IS	30-110	Differential labeling for rTh & oxTh; < 20 min; Disulfides not intact

Reference	*Thiols*	*Specimen & collection*	*Sample pretreatment*	*Separation conditions*	*MS mode*	*Calibration*	*LOD (nM)*	*Comments*
Bouligand *et al.*, 2006[103]	Cys, CysSS, GSH, GSSG, Hcy, HcySS CysGly, GluCys	Mouse liver; -80°C frozen	HGZ at 4°C; IAA deriv.; acid-DPZ	RP (C18) LC; gradient elution	MRM (+), MS/MS	Non-isotopic IS	≈ 100	Intact disulfides; < 15 min; HGZ standardization required; Protein normalization
Soga *et al.*, 2006[108]	GSH, GSSG	Mouse liver; blood -80°C frozen	HGZ at 4°C; extraction and UF	CE, acidic BGE, pH 1.8	Full-scan (+); TOF-MS	Non-isotopic IS	N/A	Untargeted metabolite profiling; Serum ophthalmic acid as biomarker for GSH depletion; Cys not detected
Rellán-Alvarez *et al.*, 2006[105]	GSH, GSSG, hGSH, GSNO	Plant extract; -80°C frozen	HGZ & filtration at 4°C	RP (C18) LC; gradient elution	Full-scan (-), TOF-MS	Isotopic IS	1000-3000	Intact disulfides; No deriv.; Poor sensitivity in neg. ion mode
Iwasaki *et al.*, 2003[109]	GSH, GSSG	Saliva	NEM deriv.; vortex; SPE	HILIC; gradient elution	SIM (+), MS	Non-isotopic IS	30-300	Direct salivary GSH/GSSG; Complex sample workup
Steghens *et al.*, 2003[110]	GSH, GSSG	Whole blood; erythrocytes; EDTA/ Heparin	NEM deriv. and acid-DPZ; centrifug.	Mixed-mode anion exchange LC; isocratic elution	SIM (+), MS	Non-isotopic IS	≈ 500	Rapid analysis < 6 min; Inadequate sensitivity for GSSG; Oxidation artifacts without deriv.
Guan *et al.*, 2003[102]	GSH, GSSG, Cys, Hcy, HcySS	Rat tissues, -80°C frozen, blood, heparin tubes	HGZ, lysis, or fractionation; ELM labeling; acid-DPZ;	RP (C18) LC; gradient elution	MRM (+), MS/MS	Non-isotopic IS	80-1500	Intact disulfides; analysis < 20 min; Interferences for CysSS in tissue extracts

Table 1.3: Summary of methods reported for determination of reduced and oxidized thiols in biological samples using LC with optical detection

Reference	*Thiols*	*Specimen & collection*	*Sample pretreatment*	*LC conditions*	*Detection mode*	*LOD (nM)*	*Comments*
Conlan *et al.*, 2009[111]	Cys, GSH: frTh and rTh	Human muscle cell culture, -80°C frozen,	acid-DPZ then: rTh: mBrB deriv.; frTh: DTT red. then mBrB deriv.	RP monolith (C18); isocratic elution	FL: Ex. 360 nM Em. 455 nM	30-50	Disulfides not intact; 2 sample preparations; Cys, GSH only
Sjoberg *et al.*, 2006[100]	Cys, Hcy, GSH, CysGly: rTh, tTh, and frTh	Human plasma, EDTA tubes, analyzed within 24 hours for frTh/rTh	rTh: acid DPZ, SBD-F deriv.; tTh: TBP red., acid DPZ, SBD-F deriv.; frTh: acid DPZ, TBP red., SBD-F deriv.	RP (C18); isocratic elution	FL: Ex. 385 nM Em. 515 nM	N/A	3 separate sample preparations; Disulfides not intact
Chwatko *et al.*, 2002[96]	Hcy: tTh, bTh, frTh, and rTh	Human plasma, EDTA tube, CMQT deriv. before plasma isolation for rTh, -20°C frozen	rTh: CMQT deriv. plasma, acid DPZ; tTh: $NaBH_4$ red., CMQT deriv., acid DPZ; frTh/bTh: acid DPZ, red. and deriv. of soluble and protein fractions	RP (C18); gradient elution	UV with DAD	100	Hcy only; 4 separate sample preparations; 2MPA internal standard; Disulfides not intact
Williams *et al.*, 2001[17]	Hcy, Cys, CysGly, GSH: rTh, frTh and tTh	Human plasma, citrate tubes, -70°C frozen	rTh: mBrB deriv., acid DPZ; frTh: UF DPZ, $NaBH_4$ red., mBrB deriv.; tTh: $NaBH_4$ red., acid DPZ, mBrB deriv.	RP (C18); gradient elution	FL: Ex. 365 nM Em. 475 nM	~10	3 separate sample preparations; Disulfides not intact

Reference	*Thiols*	*Specimen & collection*	*Sample pretreatment*	*LC conditions*	*Detection mode*	*LOD (nM)*	*Comments*
Jones *et al.*, 2000, 2002, 2007, 2009[14, 58, 94, 107]	Cys, CysSS, GSH, GSSG, CysGly, GluCys, GSSCysGly, GSSG, CysSSG, CysGlySS, CysSSCysGly	Human plasma, IAA tubes, acid DPZ plasma frozen at -80°C	Dansyl chloride deriv.	Weak anion exchange; gradient elution	FL: Ex. 305-395 nm Em. 510-650 nm	10-20 for GSSG	Simultaneous reduced thiol/intact disulfide analysis, IS used, >16 h for dansylation, > 50 min separation
Andersson *et al.*, 1993[91]	Cys, Hcy, GSH, GluCys, CysGly: rTh, frTh, and tTh	Human plasma, EDTA tubes, plasma or acid DPZ plasma frozen at -80°C	rTh: use DPZ plasma; frTh: use DPZ plasma, DTT red.; tTh: use plasma, DTT red., acid DPZ	RP ion pair; isocratic elution; postcolumn 4,4'-DTP deriv.	UV: Abs. 324 nm	50	3 separate sample preparations; Postcolumn derivatization setup required; Disulfides not intact
Mansoor *et al.* 1992[95]	Cys, Hcy, CysGly, GSH: rTh, bTh, tTh, and froxTh	Human plasma, heparin tubes with mBrB or NEM or nothing added	rTh: mBrB plasma, acid DPZ; bTh: untreated plasma, acid DPZ, $NaBH_4$ red. of protein pellet, mBrB deriv.; tTh: untreated plasma, $NaBH_4$ red., acid DPZ, $NaBH_4$ red., mBrB deriv.; froxTh: NEM plasma, acid DPZ, $NaBH_4$ red., mBrB deriv.	RP (C18); gradient elution	FL: Ex. 400 nM Em. 475 nM	80	4 separate sample preparations from 3 blood tubes; Disulfides not intact

Table 1.4: Summary of methods reported for determination of reduced and oxidized thiols in biological samples using CE with optical detection

Reference	*Thiols*	*Specimen & collection*	*Sample pretreatment*	*CE conditions*	*Detection mode*	*LOD (nM)*	*Comments*
Zunic *et al.*, 2008[104]	GSH, GSSG, CysSS, HcySS	Human whole blood	Cold H_2O lysis, UF	CZE, 10 mM phosph. pH 2.8 BGE	UV: Abs. 200 nm	900-37000	No deriv.; Intact disulfides; Sensitivity inadequate for CysSS, HcySS
Zinellu *et al.*, 2004, [98]	Cys, Hcy, CysGly, GluCys, GSH : rTh, frTh, tTh	Human plasma, EDTA tubes, -80°C frozen	rTh: acid DPZ, 5-IAF deriv.; frTh: acid DPZ, TBP red., 5-IAF deriv. tTh: TBP red., acid DPZ, 5-IAF deriv.	CZE; phosph./ borate with N-methyl-D-glucamine, pH 11-11.4 BGE	LIF	0.1-0.2	Disulfides not intact; High sensitivity; 3 sample preparations; Deriv. after freeze/thaw
Chassaing *et al.*, 1999[112]	Hcy, GSH, NAC : rTh, tTh	Human plasma, EDTA tubes, -80°C frozen or acid DPZ and -80°C frozen	rTh: acid DPZ plasma, FM deriv.; tTh: untreated plasma, DTT red., acid DPZ, FM deriv.	MEKC: 10 mM phosph., 50 mM SDS, pH 7.0, 25% ACN BGE	LIF: Ex. 488 nM Em. 520 nM	10	Deriv. after freeze/thaw; Cyst IS, 2 sample preparations; No info. on froxTh
Davey *et al.*, 1997[113]	GSH, GSSG	Plant tissue, flash frozen (LN_2), crushed	HGZ with frozen 3% MPA, 2 mM EDTA, thawed, extracted twice with 3% MPA, 2 mM EDTA, filtration	CZE: 200 mM borate pH 9.0 20% ACN BGE	UV: Abs. 185 nM	6500	No deriv.; Low sensitivity with UV; Intact GSH/GSSG only
Russell *et al.*, 1996[92]	Cys, Hcy, GSH, CysSS, HcySS, GSSG, Pna, PnaSS, captopril	Erythrocytes, heparin tubes,	Underiv.: Cell lysis, acid DPZ, filtration Deriv.: Cell lysis, acid DPZ, filtration, ELM deriv.	CZE: 100 mM phosph. pH 2.3 BGE	UV : Abs. 200, 357 nm	Underiv. : 20000-90000 Deriv.: 5000-59000	Low sensitivity with UV; Only GSH/GSSG detected in erythrocytes; Intact disulfides

1.6 Research Objectives

This thesis is aimed at developing an improved analytical methodology for thiol redox status analysis based on CE-ESI-MS with maleimide derivatization. It explores maleimide derivatization as a strategy to prevent artifactual oxidation of free sulfhydryl groups and to improve ionization efficiency in ESI-MS. This thesis quantitatively investigates the impact of maleimide derivatization on ionization efficiency and analytical sensitivity. It also develops and validates a multivariate model to predict the improvement in ionization efficiency upon maleimide derivatization. This thesis then selects an optimal maleimide to improve sensitivity in thiol redox status analysis and validates a CE-ESI-MS method for plasma redox status analysis using that maleimide. This method simultaneously analyzes reduced thiols and intact disulfides for thiol redox status assessment that is compatible with untargeted metabolite profiling in metabolomics. The specific research objectives that will be addressed in this thesis are:

1. Investigate the magnitude of improvements in the ionization efficiency of thiols upon derivatization with various maleimide analogues in CE-ESI-MS
2. Develop a multivariate model for the prediction of the improvement in ionization efficiency upon maleimide derivatization in CE-ESI-MS
3. Validate a method for simultaneous analysis of reduced thiols and intact disulfides in plasma using an optimal maleimide for derivatization to prevent oxidation artifacts and improve sensitivity

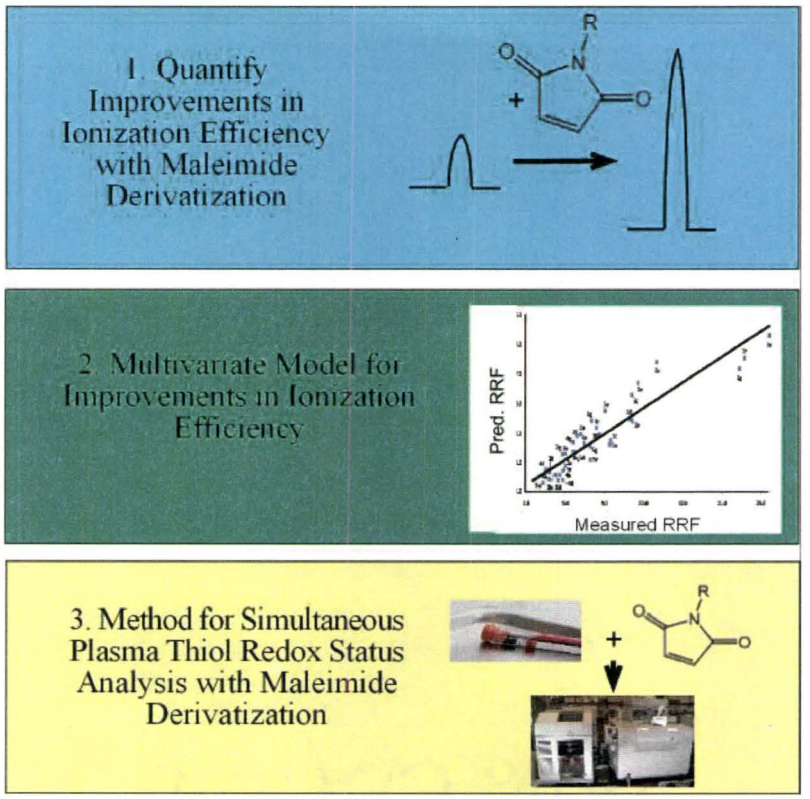

Figure 1.11: Summary of research objectives for this thesis.

1.7 References

(1) Medawar, P. B. *Ciba Foundation Colloquium on Ageing* **1955**, *1*, 4-15.
(2) Williams, G. C. *Evolution* **1957**, *11*, 398-411.
(3) Harman, D. *Biogerontology* **2009**, *10*, 773-781.
(4) Jones, D. P. *Am. J. Physiol.-Cell Physiol.* **2008**, *295*, C849-C868.
(5) Nohl, H.; Hegner, D. *Eur. J. Biochem.* **1978**, *82*, 563-567.
(6) Nilsson, U. A.; Lundgren, O.; Haglind, E.; Bylund-Fellenius, A. C. *Am J Physiol Gastrointest Liver Physiol* **1989**, *257*, G409-414.
(7) Sohal, R. S.; Mockett, R. J.; Orr, W. C. *Free Radic. Biol. Med.* **2002**, *33*, 575-586.
(8) Jones, D. P. *Antioxid. Redox Signal.* **2006**, *8*, 1865-1879.
(9) Steckert, A.; Valvassori, S.; Moretti, M.; Dal-Pizzol, F.; Quevedo, J. *Neurochem. Res.* **2010**, *35*, 1295-1301.
(10) Dalle-Donne, I.; Rossi, R.; Colombo, R.; Giustarini, D.; Milzani, A. *Clin Chem* **2006**, *52*, 601-623.
(11) Masutani, H. *Pharamacogen. J.* **2001**, *1*, 165-166.

(12) Ignarro, L. J.; Buga, G. M.; Wood, K. S.; Byrns, R. E.; Chaudhuri, G. *Proc. Natl. Acad. Sci. U. S. A.* **1987**, *84*, 9265-9269.
(13) Ashfaq, S.; Abramson, J. L.; Jones, D. P.; Rhodes, S. D.; Weintraub, W. S.; Hooper, W. C.; Vaccarino, V.; Alexander, R. W.; Harrison, D. G.; Quyyumi, A. A. *Hypertension* **2008**, *52*, 80-85.
(14) Jones, D. P.; Mody, V. C.; Carlson, J. L.; Lynn, M. J.; Sternberg, P. *Free Radic. Biol. Med.* **2002**, *33*, 1290-1300.
(15) Giustarini, D.; Dalle-Donne, I.; Lorenzini, S.; Milzani, A.; Rossi, R. *J. Gerontol. A Biol. Sci. Med. Sci.* **2006**, *61*, 1030-1038.
(16) Refsum, H.; Nurk, E.; Smith, A. D.; Ueland, P. M.; Gjesdal, C. G.; Bjelland, I.; Tverdal, A.; Tell, G. S.; Nygard, O.; Vollset, S. E. *J. Nutr.* **2006**, *136*, 1731S-1740.
(17) Williams, R. H.; Maggiore, J. A.; Reynolds, R. D.; Helgason, C. M. *Clin. Chem.* **2001**, *47*, 1031-1039.
(18) Navarro, J.; Obrador, E.; Carretero, J.; Petschen, I.; Aviñó, J.; Perez, P.; Estrela, J. M. *Free Radic. Biol. Med.* **1999**, *26*, 410-418.
(19) Atkuri, K. R.; Mantovani, J. J.; Herzenberg, L. A. *Curr. Opin. Pharmacol.* **2007**, *7*, 355-359.
(20) Cecchi, C.; Latorraca, S.; Sorbi, S.; Iantomasi, T.; Favilli, F.; Vincenzini, M. T.; Liguri, G. *Neuroscience Letters* **1999**, *275*, 152-154.
(21) Armstrong, D. W.; Schulte, G.; Schneiderheinze, J. M.; Westenberg, D. J. *Anal. Chem.* **1999**, *71*, 5465-5469.
(22) Gavina, J. M. A.; Mazhab-Jafari, M. T.; Melacini, G.; Britz-McKibbin, P. *Biochemistry* **2009**, *48*, 223-225.
(23) Chalcraft, K. R.; Lee, R.; Mills, C.; Britz-McKibbin, P. *Anal. Chem.* **2009**, *81*, 2506-2515.
(24) Jandik, P.; Bonn, G. *Capillary Electrophoresis of Small Molecules and Ions*; VCH Publishers: New York, 1993.
(25) Lee, R.; Ptolemy, A. S.; Niewczas, L.; Britz-McKibbin, P. *Anal. Chem.* **2006**, *79*, 403-415.
(26) Terabe, S.; Otsuka, K.; Ichikawa, K.; Tsuchiya, A.; Ando, T. *Anal. Chem.* **1984**, *56*, 111-113.
(27) Kranack, A. R.; Bowser, M. T.; Britz-McKibbin, P.; Chen, D. D. Y. *Electrophoresis* **1998**, *19*, 388-396.
(28) Landers, J. P., Ed. *Handbook of Capillary Electrophoresis*, 2nd ed.; CRC Press: Boca Raton, Fl, USA, 1997.
(29) Copper, C. L. *J. Chem. Ed.* **1998**, *75*, 343-3471.
(30) Simpson Jr, S. L.; Quirino, J. P.; Terabe, S. *J. Chromatogr. A* **2008**, *1184*, 504-541.
(31) Kaiser, C.; Segui-Lines, G.; D'Amaral, J. C.; Ptolemy, A. S.; Britz-McKibbin, P. *Chem. Comm.* **2008**, 338-340.
(32) Carlucci, F.; Tabucchi, A. *J. Chromatogr. B* **2009**, *877*, 3347-3357.
(33) Mol, R.; de Jong, G. J.; Somsen, G. W. *Electrophoresis* **2005**, *26*, 146-154.
(34) Maxwell, E. J.; Chen, D. D. Y. *Anal. Chim. Acta* **2008**, *627*, 25-33.

(35) Marshall, A. G. *Int. J. Mass Spectrom.* **2000**, *200*, 331-356.
(36) McLafferty, F. W.; Turecek, F. *Interpretation of Mass Spectra*, 4th ed.; University Science Books: Sausalito, CA, USA, 1993.
(37) March, R. E. *J. Mass Spectrom.* **1997**, *32*, 351-369.
(38) March, R. E.; Todd, J. F. J. *Quadrupole Ion Trap Mass Spectrometry*, Second Edition ed.; John Wiley & Sons: Hoboken, New Jersey, 2005.
(39) Maxwell, E. J.; Zhong, X. F.; Zhang, H.; van Zeijl, N.; Chen, D. D. Y. *Electrophoresis* **2010**, *31*, 1130-1137.
(40) Mokaddem, M.; Gareil, P.; Belgaied, J. E.; Varenne, A. *Electrophoresis* **2008**, *29*, 1957-1964.
(41) Kebarle, P.; Peschke, M. *Anal. Chim. Acta* **2000**, *406*, 11-35.
(42) Dole, M.; Mack, L. L.; Hines, R. L.; Mobley, R. C.; Ferguson, L. D.; Alice, M. B. *J. Chem. Phys.* **1968**, *49*, 2240-2249.
(43) Nguyen, S.; Fenn, J. B. *Proc. Natl. Acad. Sci. U. S. A.* **2007**, *104*, 1111-1117.
(44) Iribarne, J. V.; Thomson, B. A. *J. Chem. Phys.* **1976**, *64*, 2287-2294.
(45) Valaskovic, G. A.; Utley, L.; Lee, M. S.; Wu, J. T. *Rapid Commun. Mass Spectrom.* **2006**, *20*, 1087-1096.
(46) Enke, C. G. *Anal. Chem.* **1997**, *69*, 4885-4893.
(47) Bokman, C. F.; Bylund, D.; Markides, K. E.; Sjoberg, J. R. *J. Am. Soc. Mass Spectrom.* **2006**, *17*, 318-324.
(48) Zhou, S. L.; Cook, K. D. *J. Am. Soc. Mass Spectrom.* **2001**, *12*, 206-214.
(49) Sakairi, M.; Yergey, A. L.; Siu, K. W. M.; Leblanc, J. C. Y.; Guevremont, R.; Berman, S. S. *Anal. Chem.* **1991**, *63*, 1488-1490.
(50) Leize, E.; Jaffrezic, A.; VanDorsselaer, A. *J. Mass Spectrom.* **1996**, *31*, 537-544.
(51) Cech, N. B.; Enke, C. G. *Anal. Chem.* **2000**, *72*, 2717-2723.
(52) Raji, M. A.; Frycak, P.; Temiyasathit, C.; Kim, S. B.; Mavromaras, G.; Ahn, J. M.; Schug, K. A. *Rapid Commun. Mass Spectrom.* **2009**, *23*, 2221-2232.
(53) Oss, M.; Kruve, A.; Herodes, K.; Leito, I. *Anal. Chem.* **2010**, *82*, 2865-2872.
(54) Williams, D. K.; Meadows, C. W.; Bori, I. D.; Hawkridge, A. M.; Comins, D. L.; Muddiman, D. C. *J. Am. Chem. Soc.* **2008**, *130*, 2122-2123.
(55) Yang, W.-C.; Adamec, J.; Regnier, F. E. *Anal. Chem.* **2007**, *79*, 5150-5157.
(56) Lee, R.; Britz-McKibbin, P. *Anal. Chem.* **2009**, *81*, 7047-7056.
(57) Chalcraft, K. R.; Britz-McKibbin, P. *Anal. Chem.* **2009**, *81*, 307-314.
(58) Jones, D. P.; Liang, Y. L. *Free Radic. Biol. Med.* **2009**, *47*, 1329-1338.
(59) Wu, G.; Fang, Y.-Z.; Yang, S.; Lupton, J. R.; Turner, N. D. *J. Nutr.* **2004**, *134*, 489-492.
(60) Reeds, P. J. *J. Nutr.* **2000**, *130*, 1835S-1840.
(61) Nishiuch, Y.; Sasaki, M.; Nakayasu, M.; Oikawa, A. *In Vitro* **1976**, *12*, 635-638.
(62) Mathisen, G.; Fonnum, F.; Paulsen, R. *Neurochem. Res.* **1996**, *21*, 293-298.
(63) Ashfaq, S.; Abramson, J. L.; Jones, D. P.; Rhodes, S. D.; Weintraub, W. S.; Hooper, W. C.; Vaccarino, V.; Harrison, D. G.; Quyyumi, A. A. *J. Am. College Cardiol.* **2006**, *47*, 1005-1011.
(64) Struys, E. A.; Jansen, E. E. W.; de Meer, K.; Jakobs, C. *Clin Chem* **2000**, *46*, 1650-1656.

(65) Desiderio, C.; Rossetti, D. V.; Messana, I.; Giardina, B.; Castagnola, M. *Electrophoresis* **2010**, *31*, 1894-1902.
(66) Steenge, G. R.; Verhoef, P.; Katan, M. B. *J. Nutr.* **2003**, *133*, 1291-1295.
(67) Grillo, M. A.; Colombatto, S. *Amino Acids* **2008**, *34*, 187-193.
(68) Keire, D. A.; Strauss, E.; Guo, W.; Noszal, B.; Rabenstein, D. L. *J. Org. Chem.* **1992**, *57*, 123-127.
(69) Urquhart, B. L.; House, A. A.; Cutler, M. J.; Spence, J. D.; Freeman, D. J. *J. Pharm. Sci.* **2006**, *95*, 1742-1750.
(70) Bulaj, G.; Kortemme, T.; Goldenberg, D. P. *Biochemistry* **1998**, *37*, 8965-8972.
(71) Jones, D. P. In *Protein Sensors and Reactive Oxygen Species, Pt B, Thiol Enzymes and Proteins*; Academic Press Inc: San Diego, 2002; Vol. 348, pp 93-112.
(72) Moriarty-Craige, S. E.; Jones, D. P. *Ann. Rev. Nutr.* **2004**, *24*, 481-509.
(73) Lee, R.; West, D.; Phillips, S. M.; Britz-McKibbin, P. *Anal. Chem.* **2010**, *82*, 2959-2968.
(74) Winterbourn, C. C.; Hampton, M. B. *Free Radic. Biol. Med.* **2008**, *45*, 549-561.
(75) Taylor, E. R.; Hurrell, F.; Shannon, R. J.; Lin, T.-K.; Hirst, J.; Murphy, M. P. *J. Biol. Chem.* **2003**, *278*, 19603-19610.
(76) Forman, H. J.; Maiorino, M.; Ursini, F. *Biochemistry* **2010**, *49*, 835-842.
(77) Namba, K.; Takeda, Y.; Sunami, K.; Hirakawa, M. *Journal of Neurosurgical Anesthesiology* **2001**, *13*, 131-137.
(78) Park, E.-M.; Choi, J.-H.; Park, J.-S.; Han, M.-Y.; Park, Y.-M. *Brain Res. Protoc.* **2000**, *6*, 25-32.
(79) Mills, B. J.; Weiss, M. M.; Lang, C. A.; Liu, M. C.; Ziegler, C. *J. Lab. Clin. Med.* **2000**, *135*, 396-401.
(80) Niwa, T.; Naito, C.; Mawjood, A. H. M.; Imai, K. *Clin Chem* **2000**, *46*, 82-88.
(81) Samiec, P. S.; Drews-Botsch, C.; Flagg, E. W.; Kurtz, J. C.; Sternberg, P.; Reed, R. L.; Jones, D. P. *Free Radic. Biol. Med.* **1998**, *24*, 699-704.
(82) Loguercio, C.; Taranto, D.; Vitale, L. M.; Beneduce, F.; Del Vecchio Blanco, C. *Free Radic. Biol. Med.* **1996**, *20*, 483-488.
(83) Altomare, E.; Vendemiale, G.; Albano, O. *Life Sci.* **1988**, *43*, 991-998.
(84) Sofic, E.; Lange, K. W.; Jellinger, K.; Riederer, P. *Neurosci. Lett.* **1992**, *142*, 128-130.
(85) Spickett, C. M.; Reglinski, J.; Smith, W. E.; Wilson, R.; Walker, J. J.; McKillop, J. *Free Radic. Biol. Med.* **1998**, *24*, 1049-1055.
(86) Stabler, S. P.; Marcell, P. D.; Podell, E. R.; Allen, R. H. *Anal. Biochem.* **1987**, *162*, 185-196.
(87) Toyo'oka, T. *J. Chromatogr. B* **2009**, *877*, 3318-3330.
(88) McMenamin, M. E.; Himmelfarb, J.; Nolin, T. D. *J. Chromatogr. B* **2009**, *877*, 3274-3281.
(89) Rafii, M.; Elango, R.; House, J. D.; Courtney-Martin, G.; Darling, P.; Fisher, L.; Pencharz, P. B. *J. Chromatogr. B* **2009**, *877*, 3282-3291.
(90) Ueland, P. M. *Clin Chem* **2008**, *54*, 1085-1086.

(91) Andersson, A.; Isaksson, A.; Brattstrom, L.; Hultberg, B. *Clin. Chem.* **1993**, *39*, 1590-1597.
(92) Russell, J.; Rabenstein, D. L. *Anal. Biochem.* **1996**, *242*, 136-144.
(93) Johnson, J. M.; Strobel, F. H.; Reed, M.; Pohl, J.; Jones, D. P. *Clin. Chim. Acta* **2008**, *396*, 43-48.
(94) Jones, D. P.; Carlson, J. L.; Mody, V. C.; Cai, J. Y.; Lynn, M. J.; Sternberg, P. *Free Radic. Biol. Med.* **2000**, *28*, 625-635.
(95) Mansoor, M. A.; Svardal, A. M.; Ueland, P. M. *Anal. Biochem.* **1992**, *200*, 218-229.
(96) Chwatko, G.; Bald, E. *J. Chromatogr. A* **2002**, *949*, 141-151.
(97) Suh, J. H.; Kim, R.; Yavuz, B.; Lee, D.; Lal, A.; Ames, B. N.; Shigenaga, M. K. *J. Chromatogr. B* **2009**, *877*, 3418-3427.
(98) Carru, C.; Deiana, L.; Sotgia, S.; Pes, G. M.; Zinellu, A. *Electrophoresis* **2004**, *25*, 882-889.
(99) Zinellu, A.; Pinna, A.; Zinellu, E.; Sotgia, S.; Deiana, L.; Carru, C. *Amino Acids* **2008**, *34*, 69-74.
(100) Sjoberg, B.; Anderstam, B.; Suliman, M.; Alvestrand, A. *Am. J. Kidney Dis.* **2006**, *47*, 60-71.
(101) Seiwert, B.; Karst, U. *Anal. Chem.* **2007**, *79*, 7131-7138.
(102) Guan, X.; Hoffman, B.; Dwivedi, C.; Matthees, D. P. *J. Pharm. Biomed. Anal.* **2003**, *31*, 251-261.
(103) Bouligand, J.; Deroussent, A.; Paci, A.; Morizet, J.; Vassal, G. *J. Chromatogr. B* **2006**, *832*, 67-74.
(104) Zunic, G.; Spasic, S. *J. Chromatogr. B* **2008**, *873*, 70-76.
(105) Rellán-Álvarez, R.; Hernández, L. E.; Abadía, J.; Álvarez-Fernández, A. *Anal. Biochem.* **2006**, *356*, 254-264.
(106) Zhu, P.; Oe, T.; Blair, I. A. *Rapid Commun. Mass Spectrom.* **2008**, *22*, 432-440.
(107) Blanco, R. A.; Ziegler, T. R.; Carlson, B. A.; Cheng, P. Y.; Park, Y.; Cotsonis, G. A.; Accardi, C. J.; Jones, D. P. *Am. J. Clin. Nutr.* **2007**, *86*, 1016-1023.
(108) Soga, T.; Baran, R.; Suematsu, M.; Ueno, Y.; Ikeda, S.; Sakurakawa, T.; Kakazu, Y.; Ishikawa, T.; Robert, M.; Nishioka, T.; Tomita, M. *J. Biol. Chem.* **2006**, *281*, 16768-16776.
(109) Iwasaki, Y.; Hoshi, M.; Ito, R.; Saito, K.; Nakazawa, H. *J. Chromatogr. B* **2006**, *839*, 74-79.
(110) Steghens, J.-P.; Flourié, F.; Arab, K.; Collombel, C. *J. Chromatogr. B* **2003**, *798*, 343-349.
(111) Conlan, X. A.; Stupka, N.; McDermott, G. P.; Francis, P. S.; Barnett, N. W. *Biomed. Chromatogr.* **2009**, *24*, 455-457.
(112) Chassaing, C.; Gonin, J.; Wilcox, C. S.; Wainer, I. W. *J. Chromatogr. B* **1999**, *735*, 219-227.
(113) Davey, M. W.; Bauw, G.; VanMontagu, M. *J. Chromatogr. B* **1997**, *697*, 269-276.

Chapter 2

Comprehensive Plasma Thiol Redox Status Determination for Metabolomics

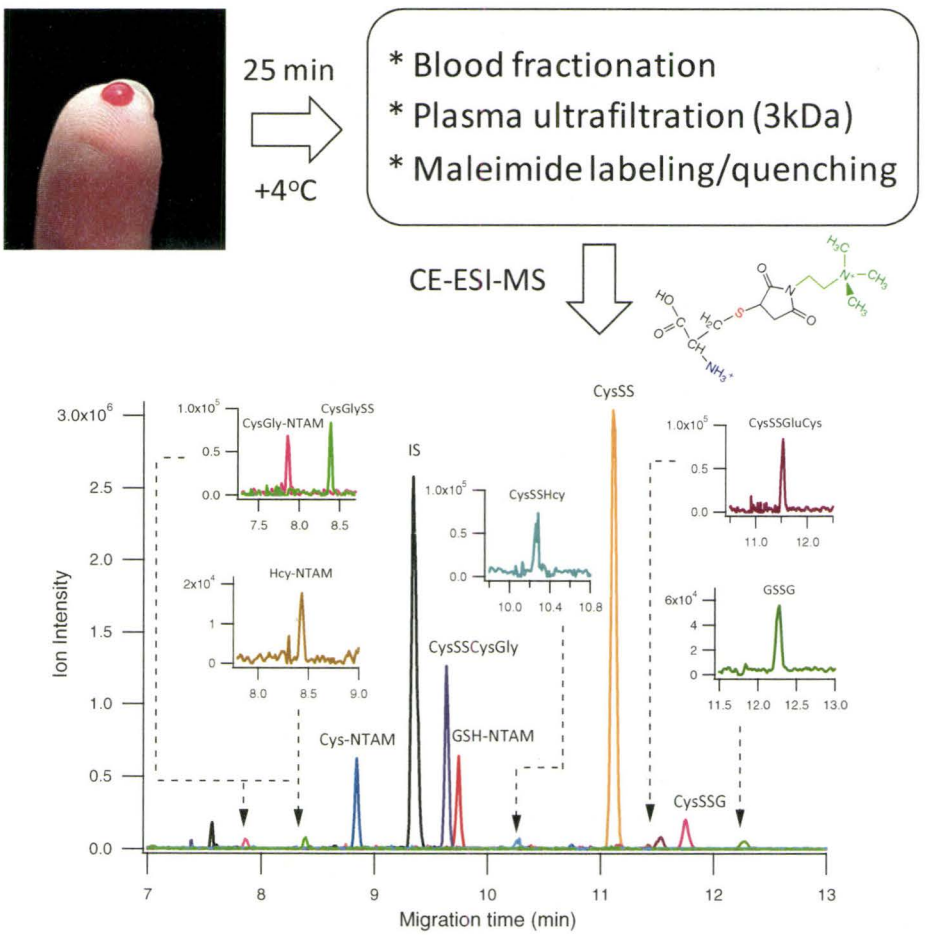

2: Comprehensive Plasma Thiol Redox Status Determination for Metabolomics

2.1: Abstract

Thiol homeostasis plays an important role in human health and aging by regulation of cellular responses to oxidative stress. Due to major constraints that hamper reliable plasma thiol/disulfide redox status assessment in clinical research, we introduce an improved strategy for comprehensive thiol speciation using capillary electrophoresis-electrospray ionization-mass spectrometry (CE-ESI-MS) that overcomes sensitivity, selectivity and dynamic range limitations of conventional techniques. This method integrates both specific and non-specific approaches towards sensitivity enhancement for artifact-free quantification of low abundance thiols using finger-prick blood collection without complicated sample handling. A multivariate model was developed to predict the relative increase in ionization efficiency for reduced thiols when conjugated to various maleimide analogs based on their intrinsic physicochemical properties. Optimization of maleimide labeling in conjunction with on-line sample preconcentration by CE-MS allowed for simultaneous analysis of nanomolar levels of reduced thiols, free oxidized thiols as their intact symmetric or mixed disulfides, as well as various metabolites associated with thiol metabolism. Improved identification of low abundance thiols and other classes of plasma metabolites was also achieved by accurate prediction of their relative migration times *in silico* when using CE as a qualitative tool complementary to MS experiments. Plasma thiol redox status determination together with untargeted

metabolite profiling offers a systemic approach for elucidation of the causal role of dysregulated thiol metabolism in the etiology of human diseases.

2.2 Introduction

Aging and many pathological diseases are associated with oxidative stress,[1] which is a condition characterized by a disruption of redox signaling and physiological control leading to irreversible cellular damage by reactive oxygen/nitrogen species. Cells maintain a highly reducing environment to ensure protein activity during aerobic metabolism, detoxification, immune response and/or oxidative insult due to the presence of high concentrations of endogenous thiols, such as reduced glutathione (GSH).[2] Although GSH functions as a versatile antioxidant and enzyme cofactor (*e.g.*, glutathione peroxidases/transferases) to scavenge for both free radical and non-radical oxidants, reversible protein thiolation represents an important redox regulatory mechanism to prevent irreversible oxidation that can lead to deleterious protein misfolding and aggregation.[3] Biomarkers of oxidative damage are widely used in clinical research,[4] however the plasma thiol redox status offers a sensitive yet convenient parameter for assessing whole-body oxidative stress.[5] Accurate quantification of reduced thiols and free oxidized disulfides in plasma allows for determination of the intra-cellular or extra-cellular redox environment of an organism, such as the reduced glutathione/oxidized glutathione (GSH/GSSG) and cysteine/cystine (Cys/CysSS) redox couples,[6] respectively. Mounting evidence has shown that perturbations in thiol homeostasis and an oxidative shift in the thiol/disulfide redox potential are associated with aging[7-9] and various human disorders, such as atherosclerosis, renal failure and pre-eclampsia.[10-12] However, the

complex dynamics of thiol redox status in regulating protein function and gene expression, as well as the causal role of thiol dysregulation in disease pathogenesis remain unclear.

Reliable assays for plasma thiols are plagued by *ex vivo* artifacts during sample handling.[13] Moreover, accurate quantification of sub-micromolar levels of labile yet low abundance thiols is problematic. For these reasons, current methods often rely on measuring total reduced thiols in plasma after chemical reduction of both free and protein-bound thiol fractions for routine clinical testing.[14] A plethora of assays have been developed for analysis of thiols in biological fluids,[15] however liquid chromatography with fluorescence detection (LC-FL) is most widely used due to its high sensitivity and good robustness.[16] In this case, assessment of free oxidized thiols is often estimated indirectly after chemical reduction and thiol-selective labeling, which prevents differentiation of intact free oxidized thiols as their symmetric or mixed disulfides. Alternatively, thiol alkylation can be performed during blood collection followed by dansylation, which permits analysis of the soluble fraction of both reduced and oxidized aminothiols by LC-FL.[6] However, this method is limited by long elution times (> 50 min) to avoid interferences while not being applicable to acidic thiols without reactive amine moieties. New advances in LC-electrospray ionization-mass spectrometry (LC-ESI-MS) permit quantification of thiols along with their qualitative identification.[17] However, given the poor retenlysis of reduced thiols and intact oxidized disulfides in biological samples by LC-MS is challenging without complicated sample workup.[18-25] Recently, ion-exchange LC-Fourier transform-MS was reported to assess plasma thiol

redox status due to its short analysis times and high mass accuracy.[26] Nevertheless, reliable thiol quantification was complicated by artifacts that required stable isotope internal standards, whereas sensitivity was inadequate for routine GSSG quantification.[26] Since perturbations in thiol homeostasis underlie many human disorders, comprehensive analytical strategies based on metabolomics are required to elucidate specific metabolic pathways modulated during disease progression for early detection and improved therapeutic intervention.[27, 28] However, a reliable platform for plasma thiol redox determination that is compatible with untargeted metabolite profiling has yet to be reported.

Equimolar concentrations of metabolites in solution often generate signals that can vary up to 10^3-fold in electrospray ionization (ESI)-MS with weak responses for small/polar metabolites, such as reduced thiols.[29] Chemical modification offers a novel approach to improve solute ionization efficiency by introducing a charged and/or hydrophobic moiety.[30, 31] To date, chemical labeling of plasma thiols in ESI-MS has been primarily applied for quenching oxidation and/or improving chromatographic performance without insight into its overall impact on ionization efficiency.[20, 21, 26, 32] Herein, we demonstrate that maleimide labeling in conjunction with on-line sample preconcentration in CE-MS provides an integrated strategy for simultaneous analysis of nanomolar levels of reduced thiols, oxidized disulfides and polar metabolites in human plasma without complicated sample handling. Comprehensive plasma thiol redox status assessment was achieved with unprecedented sensitivity and selectivity when using full-scan monitoring in CE-MS, where direct speciation and unambiguous identification of

biologically-active free thiols was realized together with large-scale analysis of global metabolism.

2.3 Experimental Section

2.3.1 Chemicals and Reagents

Buffers and samples were prepared in de-ionized water from a Barnsted EASY-pure II LF ultrapure water system (Dubuque, IA). *L*-cysteine (Cys), *DL*-homocysteine (Hcy), cysteinylglycine (CysGly), γ-glutamyl-cysteine (GluCys), reduced glutathione (GSH), *N*-acetyl-*L*-cysteine (NAC), *L*-cysteine ethyl ester hydrochloride (CysOEt), oxidized glutathione (GSSG), *L*-cystine (CysSS), *L*-homocystine (HcySS), *N*-methylmaleiminde (NMM), *N*-ethylmaleimide (NEM), (*R*)-(+)-*N*-(1-phenylethyl) maleimide (NPEM), *N*-maleoyl-β-alanine (NMBA), 6-maleimido-hexanoic acid (6-MHA), *N*-(2-aminoethyl)maleimide trifluoroacetate salt (NAEM), sodium 2-mercaptoethane-sulfonate (MESNA), *L*-alanyl-*L*-alanine (Ala-Ala), formic acid, and ammonium acetate were obtained from Sigma-Aldrich (St. Louis, USA). N-[2-(trimethylammonium)ethyl]maleimide chloride (NTAM) and *L*-cysteinyl-glutathione disulfide (CySSG) were obtained from Toronto Research Chemicals Inc. (North York, Canada). Other oxidized mixed disulfides were prepared in-house by mixing equimolar solution of reduced thiols together at room temperature over 24 hrs without further purification. In order to prevent auto-oxidation, 10 mM reduced thiol stock solutions were prepared in either 0.05% formic acid with 1 mM ascorbic acid or 0.1% formic acid using degassed de-ionized water. Stock solutions were refrigerated and used within one

week. All stock solutions were kept on ice until less than 5 min prior to maleimide labeling and/or CE-ESI-MS analysis.

2.3.2 Apparatus and Conditions

CE-ESI-MS studies were performed on an Agilent CE system equipped with an XCT 3D ion trap mass spectrometer, an Agilent 1100 series isocratic pump, and a G16107 CE-ESI-MS sprayer kit (Agilent Technologies Inc., Waldbronn, Germany). Separations were performed on 80 cm long uncoated fused-silica capillaries with 50 μM internal diameter. Capillaries were preconditioned by rinsing 15 min with methanol, 15 min with 0.1 M NaOH, 15 min with water, and 75 min with 1 M formic acid. Separations were performed using 30 kV at 25°C with 1 M formic acid, pH 1.8 as the background electrolyte (BGE). Capillaries were rinsed with BGE for 4 min between runs and for 75 min at the end of each day. Sample injections were 5-120 s at 50 mbar followed by 60 s injections of BGE at 50 mbar. The BGE injection prevents oxidation of reduced thiols within the sample plug at the anode (inlet) upon voltage application in CE.[33] On-line preconcentration by CE was performed using a 90 s injection of sample prepared in 200 mM ammonium acetate, pH 5.0, which allowed for sample enrichment of thiol-maleimide adducts and oxidized disulfides simultaneously.[34] The 3D ion trap MS settings included a maximum acquisition time of 200 ms with 4 average scans using a smart target of 250,000 ions. N_2 was used as the nebulizing gas at 5 psi and drying gas at 10.0 L/min using a temperature of 300°C in the ion source, where the cone (ESI) voltage was 4 kV. Sheath liquid flow rate was 10 μL/min containing 60% *v/v* methanol with 0.1% formic acid, which was optimized after experimental design. In order to minimize

trapping efficiency bias for ions with different *m/z* when using a 3D ion trap, the target mass was adjusted to the average *m/z* for model aminothiols or thiol-maleimide adducts to allow for direct comparison of the impact of maleimide labeling on thiol ionization efficiency that is not dependent on selectivity of mass analyzer. The target masses used for assessment of relative response factors (RRFs) for thiols upon maleimide labeling were set using a *m/z* at 199, 256, 289, 310, 324, 368, 400, 410 for reduced thiols, NAEM, NTAM, NMM, NEM, NMBA, NPEM and MHA derivatives, respectively, and *m/z* 282 for plasma analysis with NTAM. Other mass analyzer settings were constant during this investigation, including a trap drive level of 100%, compound stability of 50%, normal width optimization when using a full-scan mass range of 50-700 *m/z*.

2.3.3 Maleimide Derivatization

Thiol-selective maleimide labeling was performed by addition of 50 mM maleimide in a thiol standard solution prepared in 200 mM ammonium acetate, pH 5.0. Weakly acidic electrolyte conditions were important to prevent intra-molecular nucleophilic attack of amine groups for cationic maleimide derivatives, as well as minimize reduced thiol auto-oxidation. Acetonitrile was used to prepare stocks of all maleimides except NAEM and NTAM. Due to their limited solubility in organic solvent, both NAEM and NTAM stock solutions were prepared in 0.1% formic acid and used within 24 hrs to limit hydrolysis of the maleimide label. For ionization efficiency studies, chemical derivatization was performed using 5 mM maleimide which was over a 100-fold excess over the total molarity of reduced thiols. At least 3 min of reaction time at 4°C was allowed for plasma thiols. NAEM or NTAM derivatization was followed by

quenching of excess maleimide with 50 μL of 50 mM MESNA as an acidic thiol. Residual MESNA was then subsequently reacted for 3 min with 16 μL of 50 mM NMM. The first MESNA quench was used to generate a neutral adduct with excess cationic maleimides which co-migrated with the electroosmotic flow (EOF) as a way to avoid interferences for thiol-maleimide adducts in CE-ESI-MS. The second NMM quenching step removes excess MESNA, thereby avoiding potential thiol/disulfide exchange reactions with endogenous oxidized thiols in plasma. This procedure was found to prevent long-term changes in CySS and CySSG levels. For method calibration and plasma analyses with NTAM, the reaction times were 3 min each using 1 mM NTAM, 1.25 mM MESNA, and 0.4 mM NMM. Other neutral maleimide analogs did not require quenching since they co-eluted with EOF by CE-MS.

2.3.4 Prediction and Measurement of Physicochemical Parameters

Molecular volume (*MV*) was calculated using Chem3D Ultra version 8.0 software (CambridgeSoft, Inc., Cambridge, USA) as the Connolly solvent-excluded volume following energy-minimization of structures using an iterative molecular mechanics 2 (MM2) algorithm after molecular dynamics. The apparent electrophoretic mobility (μ_{ep}) for thiols were measured in triplicate using a 5 s sample injection of standards using 1 M formic acid, pH 1.8 as BGE. The effective charge (z_{eff}) at pH 1.8 was determined by the Henderson-Hasselbach equation from predicted pK_a values for metabolites (*e.g.*, α-carboxylic acid) using ACD/pK_a 8.03 (Advanced Chemistry Development Inc., Toronto, Canada). Similarly, the octanol-water distribution coefficient (*logD*) for metabolites at pH 7 was also estimated in silico using ACD/logD 8.02 (Advanced Chemistry

Development Inc.). All experimental or predicted physicochemical data for thiol-maleimide adducts, oxidized disulfides and other plasma metabolites used in multivariate calibration models for prediction of relative response factor (RRF) and relative migration time (RMT) are summarized (**Table S2-3** and **Table S2-4**).

2.3.5 Multivariate Calibration

Relative response factor (RRF > 1) was determined by the ratio of the measured sensitivity (*i.e,* slope of calibration curve) for a reduced thiol relative to its corresponding maleimide thioether adduct, which reflects the apparent increase in ionization efficiency upon chemical derivatization. Correction of measured ion responses performed at different time periods (*e.g.,* NAEM, NTAM) was required using NEM and MHA derivatives due to long-term variations in spray stability without an internal standard, which was not applicable in this case since various target mass settings on the ion trap were selected for different thiol-maleimide derivatives. Multivariate data analysis for modeling RRF and RMT for metabolites in terms of their physicochemical parameters was performed by multiple linear regression (MLR) using Excel (Microsoft, Inc., Redmond, USA). The data matrix for all physicochemical parameters were standardized (*e.g.,* corrected by subtracting mean then dividing by standard deviation) prior to MLR to scale parameters having different absolute values and ranges. *k*-fold cross validation was used for assessing model robustness by random selection of a test set when using the remaining metabolites as the training set. Predictive accuracy was determined by measuring the correlation for determination (R^2) and mean square error for calibration (*MSEC*), as well as correlation for prediction (Q^2) and mean square error for prediction

(*MSEP*) for training and test analytes, respectively. In the case of multivariate model for RRF, it was determined that the ratio of *MV*, μ_{ep} and *logD*, as well as the difference in z_{eff} for thiol-maleimide adduct relative to reduced thiol provided the greatest predictive accuracy for describing increases in RRF for thiols upon maleimide labeling. Thus, the physicochemical parameters considered for the model were MV/MV_{SH}, $logD/logD_{SH}$, $\mu_{ep}/\mu_{ep,SH}$, and z_{eff} -$z_{eff,SH}$. Model refining was assessed by comparing the predictive accuracy for RRF when using fewer variables in MLR (**Table S2-4**). Similarly, a multivariate model for prediction of RMT for NTAM-thiols, oxidized disulfides and other plasma metabolites was performed by MLR with *k*-fold cross validation using several intrinsic physicochemical properties of an ion as described in the text.

2.3.6 Method Validation

Thiol quantification was performed by external calibration where the average integrated peak area of analyte was normalized to an internal standard (20 μM Ala-Ala). Calibration curves for NTAM-thiols and oxidized disulfides were performed over a 50-fold range using 5-7 different concentrations measured in triplicate. The concentration range for calibration curves were selected based on the limit of quantitation (LOQ, $S/N \approx 10$) and average plasma concentration range for a specific thiol. Reproducibility studies were performed within a single day (n=3) over three consecutive days (n=9) after repeated freezing/thawing of filtered plasma sample. Assay precision was assessed in terms of long-term variability in RMTs and average signals (*i.e.*, relative peak area) based on endogenous thiols detected in plasma. A single non-isotopic internal standard was used for normalization of ion responses and their migration times in CE-ESI-MS.

Recovery studies were performed on both thiol and oxidized disulfides spiked at 50% of their calibration range in filtered plasma samples. Recovery was calculated as *(measured concentration-endogenous concentration)* x 100/ *added concentration.*

2.3.7 Plasma Sample Preparation

A disposable "pin-prick" method using a mini-capillary blood collection vial (SAFE-T-FILL, Ram Scientific Inc., Yonkers, USA) coated with K_2EDTA was used to collect a human blood sample from a healthy male volunteer after written informed consent was provided. The blood sample was fractionated by centrifugation for 5 min at 4°C and 200 rpm. Plasma was removed and ultrafiltered using Nanosep 3kDa Omega microfilters (PALL Corporation, Ann Arbor, USA) centrifuged at 14,000 rpm and 4°C for 10 min. 40 µL of plasma was then spiked with 3 µL of 800 µM Ala-Ala (internal standard) and 2.4 µL of 200 µM CysOEt (recovery standard). The sample was then diluted with 60 µL of 400 mM ammonium acetate at pH 5.0 and 6.2 µL of water and derivatized with 3 µL of 40 mM NTAM. After 3 min, 2.7 µL of 56 mM MESNA was added followed 3 min later by 2.7 µL of 18 mM NMM. Overall, plasma samples were diluted 3-fold with 200 mM ammonium acetate, pH 5 and 20 µM Ala-Ala, which required about 25 min to process from blood collection prior to CE-MS analysis.

2.4 Results

2.4.1 Maleimide labeling for improving ionization efficiency of reduced thiols

We first performed a systematic investigation of the impact of chemical derivatization to enhance the relative response factor (RRF) of reduced thiols using seven different maleimide analogs as a model system (**Figure 2.1**). Maleimides were selected

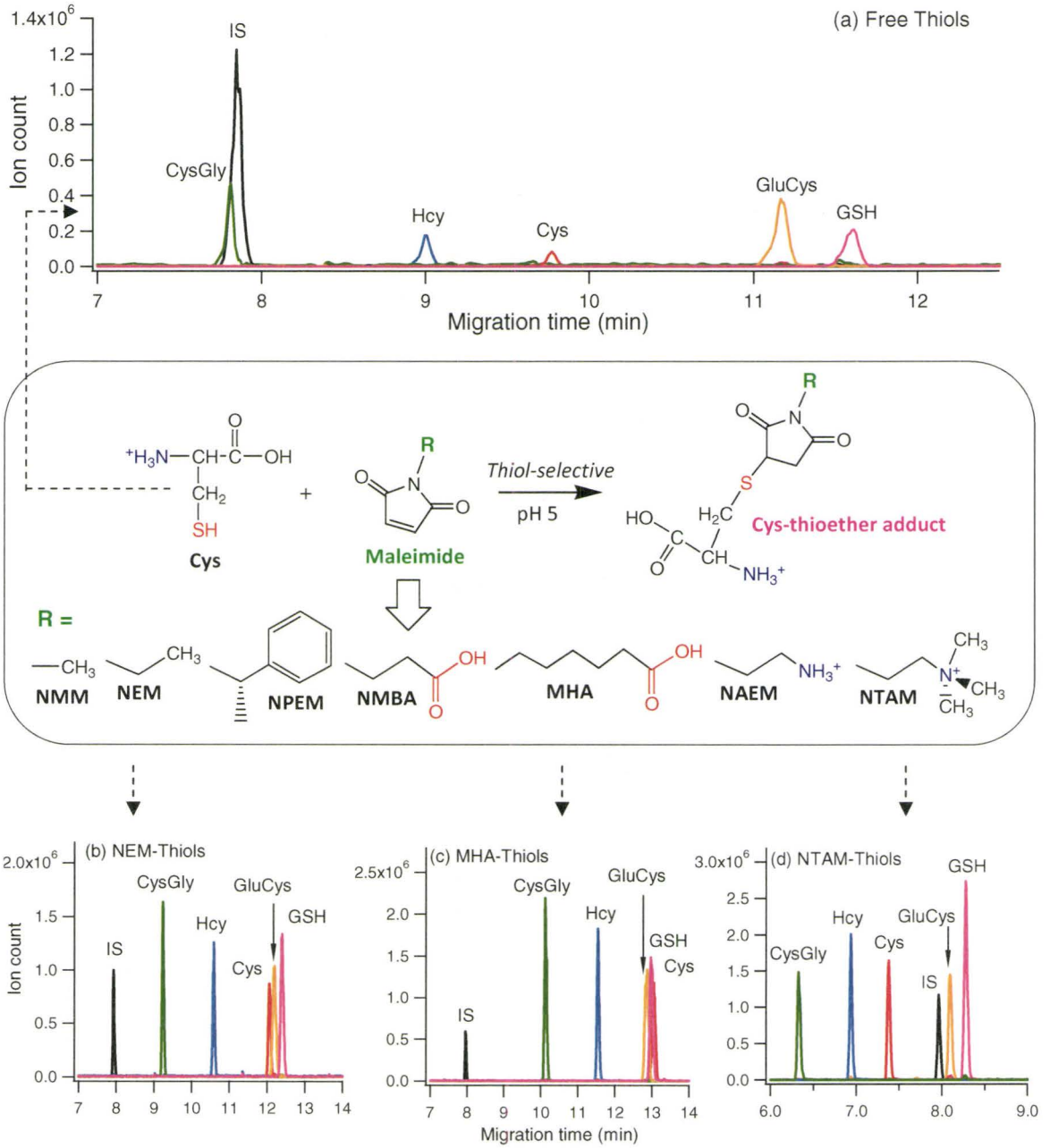

Figure 2.1: Thiol-selective labeling strategy for enhancing ionization efficiency of free reduced thiols in CE-ESI-MS using seven different maleimide analogs as a model system. Formation of a stable thioether adduct also avoids oxidation artifacts for reliable analysis of thiols while modulating their electromigration behavior based on the specific substituent group (*R*). Abbreviations for maleimides refer to *N*-methylmaleimide (NMM), *N*-ethylmaleimide (NEM), *N*-phenylethylmaleimide (NPEM), *N*-maleoyl-β-alanine (NMBA), 6-maleimidohexanoic acid (MHA), *N*-aminoethylmaleimide (NAEM) and *N*-(trimethylammonium)ethylmaleimide (NTAM).

due to their selectivity for sulfhydryls at pH ≈ 5 with fast reaction kinetics at 4°C unlike other labels,[15] which is critical to minimize ex vivo oxidation of thiols. We found that maleimide labeling significantly modulated the ion response, mobility and band diffusion properties of reduced thiols (**Figure 2.1 a**) when using CE-ESI-MS. All experiments were performed using acidic conditions (pH 1.8) with full-scan monitoring under positive-ion mode with a 3D ion trap.[33] Also, a non-sulfhydryl internal standard (IS) was used to improve thiol quantification and normalize migration times for metabolites (*i.e.*, relative migration time, RMT) correcting for long-term variations in spray stability and electroosmotic flow, respectively.[33] In comparison to neutral (**Figure 2.1 b**) and anionic (*i.e.*, protonated at pH 1.8) analogs (**Figure 2.1 c**), cationic maleimides (**Figure 2.1 d**) were promising derivatives since they form divalent thioether adducts that migrate faster with greater ion responses than native thiols.

Next, a quantitative model for describing the apparent increases in RRF for thiols upon maleimide derivatization (**Figure S2.6**) was developed based on several intrinsic physicochemical properties associated with ionization efficiency, such as molecular volume (*MV*), effective charge (*i.e.*, z_{eff} or pK_a) and electrophoretic mobility (μ_{ep}).[29] Remarkably, these same parameters can be used to accurately predict electromigration behavior,[35] which highlights similar electrohydrodynamic ion transport processes in CE and ESI-MS. However, since ion desorption occur at the gas-liquid interface of charged droplets, thermodynamic parameters related to ion desolvation also need to be considered, such as the octanol-water distribution coefficient (*logD*).[29] Multivariate calibration was used to predict the RRF of various thiol-maleimide adducts, as well as

identify underlying factors influencing their ionization efficiency in terms of relative changes in four solute physicochemical properties,[29] which were estimated *in silico* (*MV*, pK_a *logD*) or measured experimentally (μ_{ep}) (**Table S2.3**). RRF was determined by measuring the sensitivity ratio for each thiol-maleimide adduct (n=35) relative to reduced thiol (n=5) derived from the slopes of their calibration curves (**Table S2.3** and **Figure S2.7**). In general, it was found that the magnitude of RRF increased with maleimide labeling, but it was most effective for low molecular weight thiols (*e.g.*, 10 to 25-fold for Cys) relative to larger peptides (*e.g.*, 4 to 10-fold for GSH). As anticipated, bulkier maleimide analogs with hydrophobic/ionic moieties (*e.g.*, NPEM, MHA, NTAM) generated a larger increase in RRF relative to NMM (**Figure 2.2 a**). Although RRF derived from peak heights provide a more reliable indicator of sensitivity enhancement (**Figure S2.8**), RRF from integrated peak areas allow for better predictive accuracy when using multiple linear regression (MLR) with a 7-fold cross-validation (R^2 = 0.8604 for complete model and Q^2 = 0.86 ± 0.10 for average test sets) as it is not confounded by band broadening (**Table S2.4**). Consistent with recent ESI-MS models,[29, 36] a relative increase in *MV* of the thiol-maleimide adduct relative to reduced thiol (*i.e.*, MV/MV_{SH} ratio) was the most important variable ($P = 4.83 \times 10^{-13}$) positively correlated with RRF since it is directly related to an increase in solute surface activity upon derivatization (**Figure 2.2 b**). A decrease in effective charge ($P = 2.67 \times 10^{-4}$) and an increase in apparent mobility ($P = 5.38 \times 10^{-4}$) were two other factors significantly increasing RRF that are likely related to lower desolvation energetics and faster ion desorption rates for

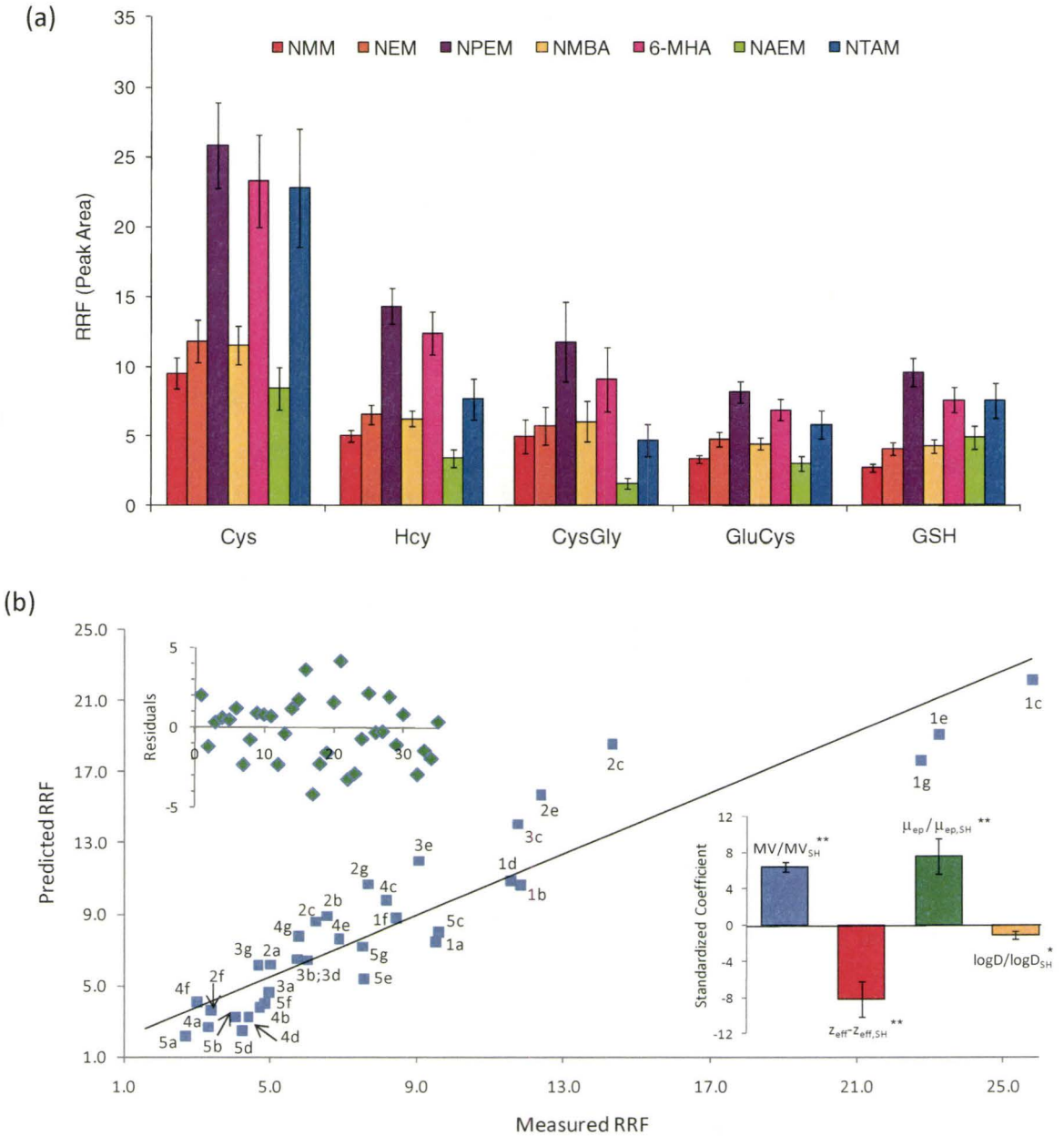

Figure 2.2: Multivariate model for predicting the enhancement in RRF for various thiol-maleimide adducts (n=35) based on four intrinsic physicochemical parameters (bottom inset, **Table S2-3**) associated with solute ionization efficiency. Multiple linear regression of standardized variables was performed for model thiols in order to predict their RRF (y) based on the equation: y = (8.27 ± 0.39) + (6.40 ± 0.53) MV/MV_{SH} - (8.2 ± 2.0)z_{eff}-$z_{eff,SH}$ + (7.6 ± 2.0) $\mu_{ep}/\mu_{ep,SH}$ - (1.03 ± 0.42)$logD/logD_{SH}$, where R^2 = 0.8604, * and ** represent statistically significant parameters at $P < 0.05$ and $P < 0.001$, respectively. Overall, the average absolute error for the predictive model was 23% with a MSEC = 4.488 and normal error distribution (top inset). Analyte peak numbering corresponds to: 1-Cys, 2-Hcy, 3-CysGly, 4-GluCys, 5-GSH, whereas a-NMM, b-NEM, c-NPEM, d-NMBA, e-MHA, f-NAEM, g-NTAM.

thiol-maleimide adducts, respectively (**Figure 2.2 b**).[29, 36] This quantitative approach towards sensitivity enhancement in ESI-MS not only improves fundamental understanding of multifactorial ionization processes, but also provides a rational approach towards the design of new classes of thiol-selective labels.

2.4.2 Thiol-selective labeling with on-line sample preconcentration by CE-MS

Overall, NTAM was selected as the optimum cationic maleimide label since it provided an average 15-fold improvement in effective RRF (peak height) with better resolution and shorter analysis times for aminothiols, while also allowing simultaneous analysis of acidic thiols, such as *N*-acetyl-*L*-cysteine (NAC)[37] (**Figure 2.3**). An experimental design based on surface response modeling was also performed for optimization of ionization conditions for thiol-maleimide adducts in CE-ESI-MS when using a coaxial sheath liquid interface,[38] which increased sensitivity by a modest 2-fold relative to standard operating conditions (**Figure S2.9**). However, on-line sample preconcentration in CE-ESI-MS[35] provided an additional 15-fold boost in concentration sensitivity that was applicable to both NTAM-thiol adducts and oxidized disulfides simultaneously. Indeed, a linear increase in ion response for thiols was found when injecting sample plugs that filled over 6% of the total capillary length without significantly impacting resolution, separation efficiency or migration times (**Figure S2.10**). Altogether, about a 400-fold and 30-fold improvement in concentration sensitivity was achieved for NTAM-thiols and oxidized disulfides, respectively. Given

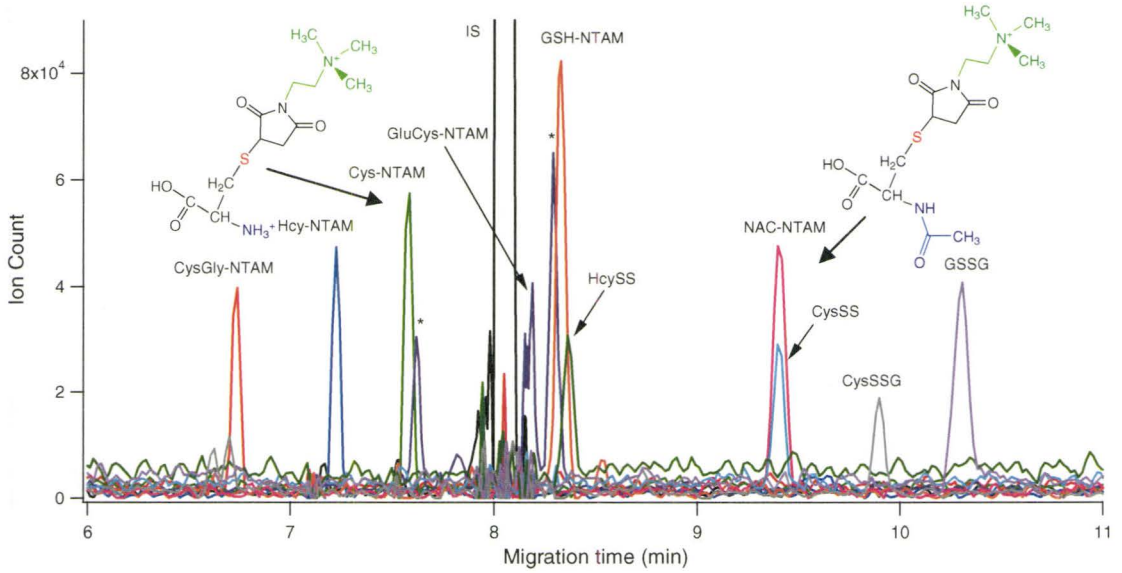

Figure 2.3: Thiol-selective maleimide labeling with non-specific on-line sample preconcentration for comprehensive thiol redox status determination by CE-ESI-MS. Series of extracted ion electropherograms for an equimolar standard mixture of 100 nM NTAM-labeled reduced aminothiols (including the acidic thiol, NAC) and oxidized thiols as their intact symmetric and mixed disulfides that demonstrate excellent sensitivity with low nanomolar detection limits. Note that two low abundance several isobaric ions (*) were found to migrate close to GluCys-NTAM, which were associated with minor methanolysis products of NTAM.

the greater intrinsic ionization efficiency of bulkier oxidized disulfides relative to reduced thiols (*e.g.*, larger *MV*), overall detection limits (*S/N* ≈ 3) were in fact similar in magnitude in CE-ESI-MS of about 8 nM for NTAM-thiol adducts compared to 30 nM for thiol disulfides (**Table 2.1**). This sensitivity is in fact superior to reported LODs for reduced thiols (≈ 50-100 nM) when using LC-FL.[16] Other sample enrichment strategies have been developed to improve concentration sensitivity for sulfhydryls,[20, 32, 39] however these procedures are time-consuming and/or not directly applicable to oxidized disulfides, which are involved in complex yet reversible thiol/disulfide reactions with protein and reduced thiols (**Figure S2.11**).

Table 2.1: Validation criteria of optimized assay for simultaneous analysis of free reduced and oxidized thiols derived from filtered human plasma using CE-ESI-MS in conjunction with pre-column NTAM derivatization.

Thiol	Linear Range (μM)	Linearity (R^2)	Sensitivity[a] (μM^{-1})	LOD S/N ≈ 3 (nM)	RMT[b] Intra-day (%RSD)	RMT[b] Inter-day (%RSD)	RPA[b] Intra-day (%RSD)	RPA[b] Inter-day (%RSD)	Plasma Conc.[c] (μM)	Recovery[d] (%)
Cys-NTAM	0.05-10	0.9878	0.145	8	0.09	0.36	6.6	7.1	1.90 ± 0.24	82 ± 4
Hcy-NTAM	0.025-1.5	0.9971	0.183	10	0.16	0.62	15	18	0.052 ± 0.018	110 ± 11
NAC-NTAM	0.03-1.5	0.9980	0.374	8	*nd*	*nd*	*nd*	*nd*	*nd*	--
CysGly-NTAM	0.04-4.0	0.9823	0.170	10	0.30	1.0	11	13	0.278 ± 0.044	--
GluCys-NTAM	0.1-4.0	0.9999	0.112	10	*nd*	*nd*	*nd*	*nd*	*nd*	--
GSH-NTAM	0.02-2.0	0.9976	0.253	6	0.10	0.20	5.6	6.3	1.98 ± 0.13	110 ± 6
CysSS	0.2-50	0.9955	0.0813	30	0.34	0.94	6.0	7.1	38.8 ± 3.0	68 ± 5
HcySS	0.2-10	0.9985	0.108	30	*nd*	*nd*	*nd*	*nd*	*nd*	84 ± 6
CysSSG	0.13-4.0	0.9984	0.0712	30	0.47	1.3	5.4	6.4	3.73 ± 0.23	--
GSSG	0.04-1.0	0.999	0.242	10	0.57	1.6	8.8	16	0.314 ± 0.053	112 ± 9

a. Slope of calibration curve based on measured normalized peak area of thiol relative to the internal standard, 20 μM diAla.
b. RMT and RPA of thiols normalized to the internal standard was performed on filtered plasma samples in a single day (intra-day, n=3) and over three days (inter-day, n=9). No significant changes in thiol responses were measured when performing three consecutive freeze-thaw cycles on plasma samples.
c. Filtered plasma samples from a healthy male volunteer were diluted three-fold prior to NTAM labeling/quenching and CE-ESI-MS analysis.
d. Spike and recovery studies were performed to assess method accuracy for thiol-NTAM adducts and oxidized thiols detected in filtered plasma samples at 50% calibration level.

2.4.3 Comprehensive thiol speciation in human plasma

The optimized method was next applied to the analysis of plasma thiols by CE-MS. Briefly, pre-chilled EDTA-coated tubes were used to collect microliter amounts of whole blood (≈ 300 μL) using a convenient fingerpricking method with disposable lancets adopted from our recently validated procedure.[33] Prompt fractionation of anti-coagulated blood at 4°C was then performed to minimize thiol oxidation and thiol exchange processes without hemolysis.[13] Plasma samples were deproteinized by ultrafiltration and then diluted with pre-chilled reaction buffer at pH ≈ 5 that included an IS with excess NTAM, where the reaction was carried out on ice for 3 min until quenching. Only about 25 min was required to process the original finger-prick blood specimen prior to CE-MS analysis. A series of extracted ion electropherograms depict the thiol redox status in a filtered plasma sample derived from a healthy male volunteer (**Figure 2.4**). Plasma thiol species were quantified using external calibration with an IS over a 100-fold dynamic range, including reduced thiols (*e.g.*, Cys-NTAM), as well as various symmetric (*e.g.*, CysGlySS) and mixed (*e.g.*, CysSSG) oxidized disulfides. Method validation was performed in this work, which demonstrated excellent linearity (R^2 ≈ 0.995), RMT precision (RSD ≈ 0.86% for endogenous plasma thiols, n=9) with acceptable quantification (RSD ≈ 10.6% for endogenous plasma thiols, n=9) and a good average recovery (≈ 94%) when using a single non-isotopic IS (**Table 2.1**). Moreover, plasma derived NTAM-thiols were found to form stable thioether adducts with no significant changes in responses (P = 0.05) measured over 3 days after two consecutive

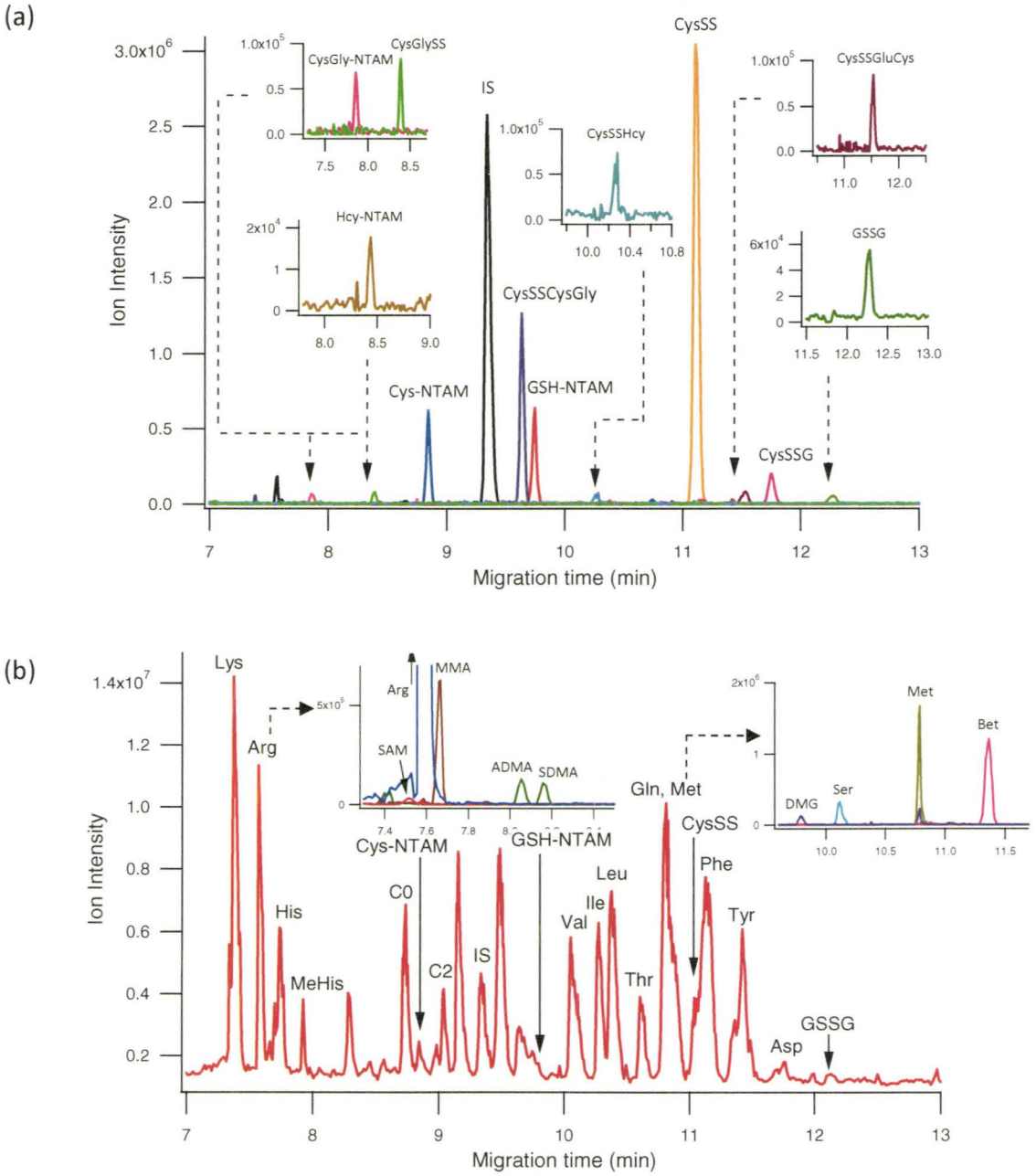

Figure 2.4: **(a)** Series of extracted ion electropherograms (EIEs) demonstrating comprehensive assessment of plasma thiol redox status by CE-ESI-MS. Filtered plasma samples were diluted three-fold prior to NTAM derivatization in conjunction with on-line sample preconcentration by CE-MS for simultaneous analysis of low abundance thiols (*e.g.*, Hcy, GSH), as well as intact symmetric (*e.g.*, CysSS, GSSG) and mixed oxidized disulfides (*e.g.*, CysSSCysGly, CysSSG) over a wide dynamic range. **(b)** Overlay of the total ion electropherogram for the same plasma specimen that highlights integration of untargeted metabolite profiling for deeper insight into metabolic pathways modulated by thiol dysregulation, including of various classes of polar metabolites/cofactors related to thiol metabolism, including methionine (Met), betaine (Bet), dimethylglycine (DMG), *S*-adenosylmethionine (SAM) and asymmetric dimethylarginine (ADMA).

freeze-thaw cycles. This is an important feature as it allows for long-term storage and re-analysis of filtered plasma samples.

There was no evidence of auto-oxidation during sample processing with consistent plasma glutathione concentration levels[6, 26] measured for free GSH (1.98 ± 0.13) μM and GSSG (0.314 ± 0.053) μM (**Table 2.1**), which is equivalent to a GSH/GSSG redox potential of –(119 ± 2) mV at pH 7.4 using the Nernst equation.[40] Among plasma thiols, glutathione is unusual due to its low fraction of oxidation (≈ 24%) since intra-cellular GSH is present at low mM levels, which is required to maintain a intra-cellular redox potential of about -260 mV for healthy young subjects.[33, 37] Plasma reduced Hcy concentrations are rarely directly measured due to sensitivity limitations in quantifying trace levels present in the sulfhydryl form (≈ 2%) since the majority is protein-bound (70-80%) or present as free oxidized disulfides (20-30%).[14] Both reduced Hcy (as Hcy-NTAM) and CysSSHcy (*m/z* 255 as MH^+) as its mixed disulfide with Cys were detected in filtered plasma samples (**Figure 2.4 a**). Hcy was quantified near the LOQ of our method with a concentration of (52 ± 18) nM that is near the normal low-end range (≈ 0.07-0.44 μM) reported for healthy males. [41] Although commercial standards for CysSSHcy were not available, we estimated its concentration to be approximately 0.8 μM based on a response factor predicted from its physicochemical properties using CE-ESI-MS,[29] which is consistent with its free reduced:oxidized distribution ratio.[14] Similar to Hcy, Cys (1.90 ± 0.24) μM and CysSS (38.8 ± 3.0) μM were found to have plasma concentrations at the lower-end range for healthy male subjects.[41] Although plasma thiol levels vary according to diet, gender and diurnal cycle,[42] plasma Cys, CysSS and Hcy

levels tend to have much larger inter-subject variations[43] as compared to GSH whose concentration levels are tightly regulated by cells. Two of the major mixed disulfides detected in filtered plasma (**Figure 2.4 a**) were CysSSCysGly (*m/z* 298 as MH^+) and CysSSG (*m/z* 214 as MH_2^{2+}), the latter with a concentration of (3.73 ± 0.23) μM. CysSSG has been reported previously as a novel intermediate of Cys and GSH metabolism that can serve as a biomarker of endothelial function.[44] To the best of our knowledge, this is the first reported detection of several mixed disulfides of Cys in human plasma, including CysSSHcy and CysSSGluCys (*m/z* 370 as MH^+).

2.4.4 Untargeted metabolite profiling and qualitative identification

Several other plasma metabolites relevant to thiol metabolism were also measured simultaneously by CE-MS (**Figure 2.4 b**), including methionine (Met), *S*-adenosylmethionine (SAM), betaine (Bet), dimethylglycine (DMG), serine (Ser) and asymmetric dimethylarginine (ADMA). SAM (*m/z* 200 as MH_2^{2+}) is a key intermediate of the Met and Hcy metabolic pathways that functions as a methyl donor modulating the activity of various substrates, including neurotransmitters, DNA/RNA and protein.[45] Indeed, the latter process results in the generation of monomethylarginine (MMA) and two dimethylarginine positional isomers (*i.e.,* symmetric and asymmetric isobars, SDMA and ADMA) during post-translational modification of arginine (Arg) residues on protein that are resolved by CE.[46] Bet plays a key role in Hcy regulation that is catalyzed by betaine-homocysteine methyltransferase to generate Met and DMG as products (**Figure S2.11**). In addition to characterization of coupled metabolic pathways directly associated with Hcy, Cys and GSH biosynthesis, a representative total ion electropherogram also

demonstrates that untargeted profiling of hundreds of other cationic metabolites can be readily integrated with this method, including various amino acids, amines, nucleosides and acylcarnitines (**Figure 2.4 b**).[29]

One of the most significant challenges in metabolomics research is *de novo* identification of unknown metabolites when using ESI-MS in cases when commercial standards are lacking and/or MS databases are incomplete.[35] Low level signals associated with biologically-relevant metabolites limit the efficacy of MS/MS experiments and the precision of isotopic pattern recognition when using high resolution MS for structural elucidation (**Figure 2.5 a,b**). In this work, reduced thiols and oxidized disulfides were identified by their *m/z* and comparing mobility and MS or MS/MS spectra with authentic standards. In addition, RMT was also used a qualitative parameter to support or reject putative thiols detected in filtered plasma samples. An excellent correlation (R^2 = 0.9903) was found between RMT and three intrinsic electrohydrodynamic properties of an ion when using MLR, namely μ_{ep}, z_{eff} *and MV* (**Figure 2.5 c**). In this case, a comparison of RMTs derived from standards, plasma and predicted from the MLR model confirmed the identity of all thiols detected in plasma except for a putative low abundance ion initially ascribed to HcySS (*m/z* 269). This ion was subsequently determined to be an unknown isobaric interference given its significantly higher RMT compared to the predicted/standard value (rejected at P =0.002) for HcySS (**Figure 2.5 d**). In fact, even if experimental values for μ_{ep} cannot be directly measured due to lack of authentic standards, only three intrinsic properties of an ion (*i.e.,*

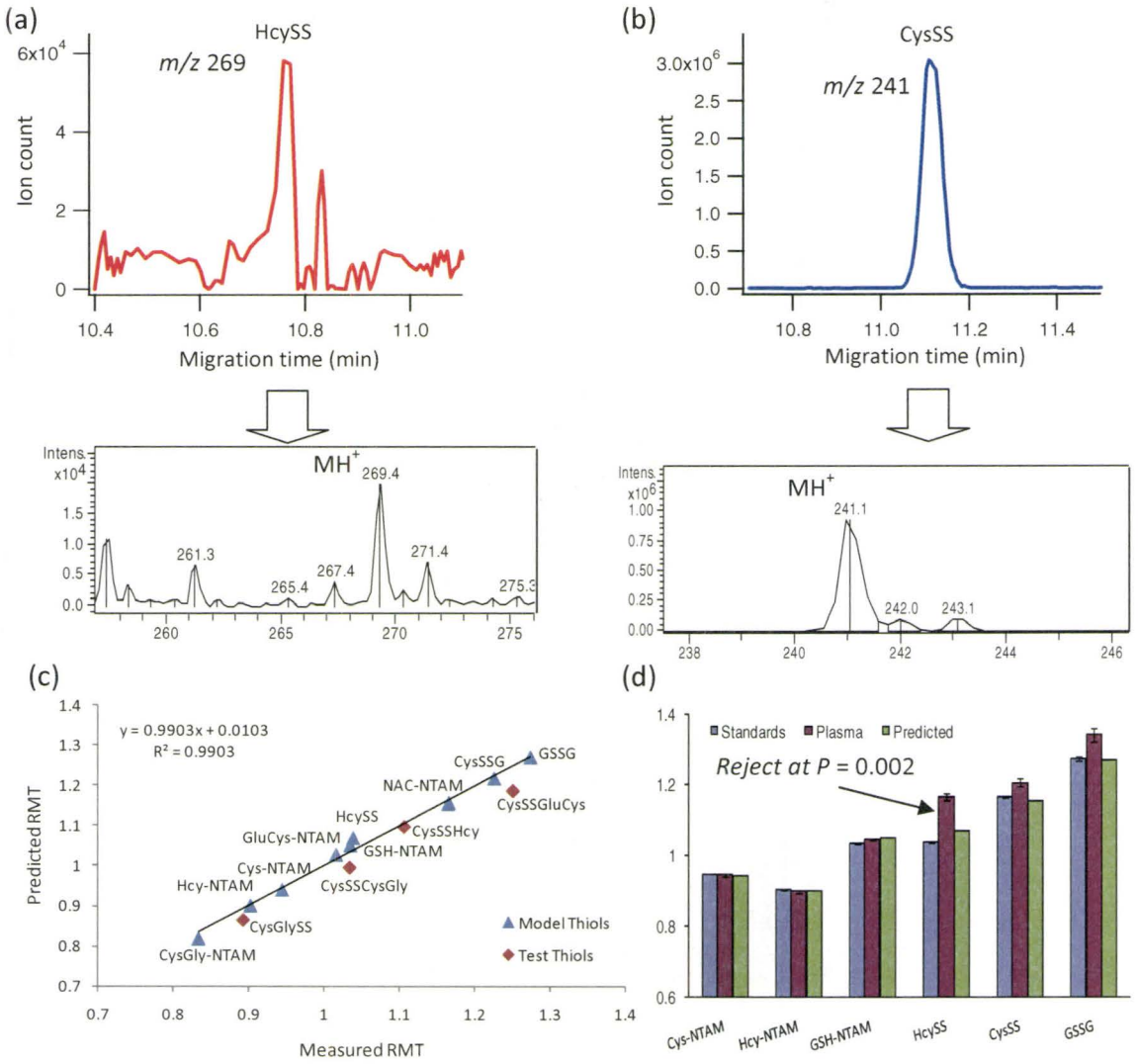

Figure 2.5: Qualitative identification of putative thiols supported by CE based on comparison of RMTs notably for low abundance and/or isobaric ions in complex biological samples that do not provide diagnostic ESI-MS spectra, such as a feature tentatively identified as **(a)** HcySS in plasma in contrast to the major thiol **(b)** CysSS. **(c)** Predicted RMTs in CE were estimated by MLR based on measured RMT of model thiol standards using three intrinsic chemical parameters (μ_{ep}, z_{eff} and MV), where the empirical equation was RMT = (1.447 ± 0.048) - (1550 ± 220)μ_{ep} - (6.5 ± 2.8) x $10^{-2}z_{eff}$ + (2.11 ± 0.095) x $10^{-3}MV$ with R^2 = 0.9903 and an average absolute error = 0.67 %. **(d)** Given the good precision of measured RMTs (*i.e.*, RSD < 2%) in CE, the isobaric ion attributed to HcySS was subsequently rejected at $P < 0.002$ using a Welch's t-test due to the major discrepancy in RMTs measured between standard (n = 30) and plasma (n = 3) samples, where error bars represent ± 1σ. This strategy also allowed for tentative assignment of other mixed disulfides (*i.e.*, test thiols) detected in plasma samples based on comparison of their predicted versus experimental RMTs in cases when ESI-MS spectra were ambiguous and/or commercial standards are unavailable.

Table 2.2: De novo prediction of RMTs for plasma metabolites based on intrinsic physicochemical properties to support their qualitative identification by CE-ESI-MS.

Plasma Metabolites	Measured RMT[a]	m/z (MH^+; $^*MH_2^{2+}$)	z_{eff}[b] (pH 1.8)	MV[c] ($Å^3$)	Pred. RMT[d]	Bias (%)
SAM	0.7934 ± 0.0097	200*	2.60	323	0.7711	-2.8
Arg	0.8017 ± 0.0092	175	1.83	143	0.8390	+4.6
MMA	0.8106 ± 0.0090	189	1.83	165	0.8306	+2.4
CysGly-NTAM	0.8327 ± 0.0084	361	1.95	314	0.8753	+5.1
MeHis	0.8401 ± 0.0080	170	1.49	145	0.9093	+8.2
ADMA	0.8543 ± 0.0076	203	1.83	193	0.8146	-4.6
SDMA	0.8663 ± 0.0072	203	1.84	187	0.8221	-5.1
CysGlySS	0.8924 ± 0.0059	355	1.91	259	0.9508	+6.5
Hcy-NTAM	0.8971 ± 0.0056	318	1.72	284	0.9020	+0.54
C0	0.9305 ± 0.0041	162	1.00	155	1.002	+7.6
Cys-NTAM	0.9438 ± 0.0034	304	1.72	266	0.9908	-4.2
C2	0.9753 ± 0.0092	204	1.00	197	1.001	+3.5
CysSSCysGly	1.034 ± 0.0016	298	1.61	215	0.9908	-4.2
GSH-NTAM	1.046 ± 0.0020	246*	1.72	416	1.001	-4.3
DMG	1.0511 ± 0.0024	104	0.59	94.1	1.088	+3.5
Bet	1.0823 ± 0.0041	118	0.50	116	1.101	+1.7
Ser	1.0882 ± 0.0045	106	0.70	75.0	1.091	+0.29
CysSSHcy	1.1064 ± 0.0055	255	0.67	189	1.181	+6.7
Met	1.1657 ± 0.0091	150	0.73	126	1.084	-7.0
Gln	1.1686 ± 0.0091	147	0.75	113	1.092	-6.5
Glu	1.196 ± 0.0011	148	0.70	112	1.107	-7.4
CysSS	1.204 ± 0.0011	241	0.62	171	1.195	-0.74
CysSSGluCys	1.251 ± 0.014	370	0.67	258	1.272	+1.6
CysSSG	1.278 ± 0.016	214*	0.67	328	1.269	-0.72
GSSG	1.339 ± 0.021	307*	0.72	481	1.346	+0.51

a. Measured RMTs for metabolites were measured in human plasma (n=9), where error represents ±1σ.
b. Calculated from predicted pK_a using ACD/pKa8.03 at pH1.8, where $z_{eff} = 1/(10^{[pH-pK_a]}+1)$.
c. Chem3D Ultra 8.0 after MM2 energy minimization as Connelly Solvent-Excluded Volume.
d. Predicted RRFs (y) determined by MLR using three physicochemical properties (z_{eff}, MV, m/z), where model equation was $y=(1.189 \pm 0.029) -(0.238 \pm 0.020)z_{eff} - (0.00138 \pm 0.00058)MV + (0.00161 \pm 0.00044)m/z$ and $R^2 = 0.9150$ for the full model. A five-fold cross-validation was performed which showed good predictive accuracy with an average $R^2 = 0.9170$ and $Q^2 = 0.9050$ for the training and test sets, respectively.

z_{eff}, *MV* and *m/z*) derived *in silico* are required for prediction of RMTs that is applicable to a wide variety of polar metabolites (**Table 2-2**). In this case, MLR with a five-fold cross-validation demonstrated good predictive accuracy for RMTs (R^2 = 0.9150 for

complete model and Q^2 = 0.9050 ± 0.035 for average test sets) of plasma metabolites (n=25, selected over a wide range of RMT from 0.8-1.4 min) with an average absolute bias of about 4.0%. This approach allows for improved confirmation of low abundance thiols and other plasma metabolites based on their characteristic RMTs by CE that supports ESI-MS in uses when isobaric/isomeric ions have weak signals that preclude MS/MS or isotopic ratio measurements.

2.5 Discussion

Plasma thiol redox status analysis plays an important role in clinical research for assessing the deleterious impact of altered thiol metabolism in human health.[47] Large-scale population studies have shown that modestly raised total Hcy levels (> 15 μM) in adults are correlated with higher incidences of mortality, cardiovascular disease, depression, cognitive deficiency, osteoporosis among other negative health outcomes.[48] Acquired or inherited glutathione deficiency is also widely documented as a significant risk factor in disease given its critical functions in cell detoxification, redox regulation and apoptosis.[2] Regrettably, conventional methodologies based on total reduced thiol determination achieve good assay robustness at the expense of biological context since reduced thiols, free oxidized disulfides and other plasma metabolites are not directly measured.[14] Few methods have reported simultaneous analysis of free plasma thiols without time-consuming or complicated sample pretreatment.[6, 20, 26] In this work, NTAM-labeling in conjunction with on-line sample preconcentration by CE-ESI-MS was developed for quantification of nanomolar levels of reduced thiols, while allowing for simultaneous analysis of free symmetric/mixed disulfides and other classes of polar

metabolites. Although tandem MS is a more selective mass analyzer to lower detection limits for specific thiols[20], it is not applicable for untargeted metabolomic studies requiring exploratory data analysis with full-scan monitoring. Hence, our protocol offers a promising approach to reveal the molecular mechanisms underlying thiol dysregulation in specific disease processes since plasma thiol redox status is assessed in the context of global metabolism (*i.e.,* metabotype).

Ultrafiltration of plasma followed by maleimide labeling was performed at 4°C under weakly acidic conditions as a way to minimize oxidation of reduced thiols while avoiding thiol/disulfide exchange reactions with protein. For instance, deproteinization by acid or organic solvent can induce *ex vivo* oxidation artifacts upon denaturation of redox-active protein.[33] Although methods for plasma thiol analysis typically perform thiol-selective labeling immediately upon blood collection to quench oxidation,[26, 41] this procedure can perturb other metabolic pathways via alkylation of protein with accessible Cys residues at room temperature. In our case, plasma filtration was performed prior to thiol-selective labeling using buffer conditions that were compatible with on-line sample preconcentration in CE. Bulky maleimide analogs with strongly basic moieties (*e.g.,* NTAM) were found to provide the greatest enhancement in RRF notably for low molecular weight/hydrophilic thiols that have poor ionization efficiency in ESI-MS, such as Cys and Hcy. An increase in effective surface activity and ion desorption rate for thiols upon maleimide labeling were determined to be primarily responsible for the boost in sensitivity as reflected by relative changes in MV, z_{eff} and μ_{ep} (**Figure 2.2 b**). Comprehensive profiling of a wide variety of polar metabolites in filtered plasma was

also achieved by CE-MS, including several key species associated with thiol metabolism. For example, Bet serves as an endogenous cofactor for methylation of Hcy to Met, which also represents a promising therapeutic strategy to lower elevated plasma Hcy levels to reduce the risk of cardiovascular disease among healthy adults.[49] Similarly, ADMA has been shown to play an important role in cardiovascular endothelial function since it acts as a natural inhibitor of nitric oxide (NO) synthase that is modulated by thiol metabolism.[50] Although this protocol is currently not applicable to the analysis of hydrophobic metabolites that are neutral, weakly responsive in ESI-MS and/or predominately protein-bound (*e.g.,* steroids), comprehensive thiol redox status determination together with untargeted profiling of polar metabolites offers an improved strategy for early detection, treatment and prevention of human disorders associated with oxidative stress.

In summary, a new strategy for comprehensive thiol speciation using finger-prick blood microsampling was developed that relies on thiol-selective maleimide labeling in conjunction with on-line sample preconcentration by CE-ESI-MS. Since the distribution of free thiols and oxidized disulfides are analyzed simultaneously by this method with low nanomolar detection limits (≈ 8-30 nM), reduction potentials for multiple thiol redox couples can be deduced as a way to reduce inter-subject variability confounded by thiol/disulfide exchange reactions. For instance, the high plasma concentration levels of CysSS results in the generation of various mixed oxidized disulfide species present at different concentration levels (*e.g.,* CysSSCysGly, CysSSHcy, CysSSGluCys and CysSSG) that are not routinely measured by methods that target only Cys/CysSS or

GSH/GSSG redox couples.[6] Indeed, a large fraction of low abundance reduced thiols exist primarily as their mixed disulfides (*e.g.*, CysSSHcy) in plasma, whereas higher abundance sulfhydryls can also form significant levels of symmetric disulfides (*e.g.*, CysGlySS) as revealed in our work (**Figure 2.4 a**). This represents a major source of biological variation in clinical investigations that can be improved with protocols amenable to comprehensive plasma thiol speciation. Given the versatile therapeutic properties of non-specific thiol agents (*e.g.*, NAC) in the treatment of human disorders,[51] it is anticipated that this methodology will also prove useful for optimizing the efficacy of nutritional intervention for attenuation of oxidative stress with improved health outcomes.[37] Our protocol also provides a simple yet integrated strategy for qualitative identification of low abundance metabolites based on characteristic electrohydrodynamic properties of an ion (*e.g.*, *m/z* and RMT). Future work is aimed at clinical validation of this method involving a larger cohort, which will offer a systemic approach for elucidation of the causal relationship of altered thiol metabolism in disease pathogenesis among individual subjects.

Acknowledgement. This work was funded by a grant by the National Science and Engineering Research Council of Canada (NSERC) and the Canada Foundation for Innovation. P.B.M. thanks support from the Japan Society for Promotion of Science – Invited Fellowship, whereas L.A.D. acknowledges a NSERC-Canada Graduate Scholarship.

2.6 References

1. Jones, D. P., Redefining oxidative stress. *Antioxid. Redox Signal.* **2006,** 8, 1865-1879.
2. Wu, G.; Fang, Y.-Z.; Yang, S.; Lupton, J. R.; Turner, N. D., Glutathione metabolism and its implications for health. *J. Nutri.* **2004,** 134, 489-492.
3. Dalle-Donne, I.; Rossi, R.; Giustarini, D.; Colombo, R.; Mizani, A., S-glutationylation in protein redox regulation. *Free Radic. Biol. Med.* **2007,** 43, 883-898.
4. Dalle-Donne, I.; Rossi, R.; Colombo, R.; Giustarini, D.; Milzani, A., Biomarkers of oxidative damage in human disease. *Clin. Chem.* **2006,** 52, 601-623.
5. Ueland, P. M.; Mansoor, M. A.; Guttormsen, A. B.; Muller, F.; Aukrust, P.; Refsum, H.; Svardal, A. M., Reduced, oxidized and protein-bound forms of homocysteine and other aminothiols in plasma comprise the redox thiol status - A possible element of the extracellular antioxidant system. *J. Nutr.* **1996,** 126, 1281S-1284S.
6. Jones, D. P.; Liang, Y., Measuring the poise of thiol/disulfide couples in vivo. *Free Radic. Biol. Med.* **2009,** 47, 1329-1338.
7. Droge, W., Aging-related changes in the thiol/disulfide redox state: implications for the use of thiol antioxidants. *Exper. Gerontol.* **2002,** 37, 1333-1345.
8. Jones, D. P.; Mody, V. C. J.; Carlson, J. L.; Lynn, M. J.; Sternberg, P. J., Redox analysis of human plasma allows separation of pro-oxidant events of aging from decline in antioxidant defenses. *Free Radic. Biol. Med.* **2002,** 33, 1290-1300.
9. Giustarini, D.; Dalle-Donne, I.; S.Lorenzini; Milzani, A.; Rossi, R., Age-related influence on thiol, disulfide, and protein-mixed disulfide levels in human plasma. *J. Gerontol. A Biol. Sci. Med. Sci.* **2006,** 61, 1030-1038.
10. Ashfaq, S.; Abramson, J. L.; Jones, D. P.; Rhodes, S. D.; Weintraub, W. S.; Hooper, W. C.; Vaccarino, V.; Harrison, D. G.; Quyyumi, A. A., The relationship between plasma levels of oxidized and reduced thiols and early atherslerosis in healthy adults. *J. Am. College Cardiol.* **2006,** 47, 1005-1011.
11. Wlodek, P. J.; Smolenski, O. B.; Chwatko, G.; Iciek, M. B.; Milkowski, A.; Bald, E.; Wlodek, L., Disruption of thiol homeostasis in plasma of terminal renal failure patients. *Clin. Chim. Acta* **2006,** 366, 137-145.
12. Raijmakers, M. T. M.; Peters, W. H. M.; Steegers, E. A. P.; Poston, L., Amino thiols, detoxification and oxidative stress in pre-eclampsia and other disorders of pregnancy. *Curr. Pharma. Design* **2005,** 11, 711-734.
13. Andersson, A.; Lindgren, A.; Hultberg, B., Effect of thiol oxidation and thiol export from erythrocytes on determination of redox status of homocysteine and other thiols in plasma from healthy subjects and patients with cerbral infarction. *Clin. Chem.* **1995,** 41, 361-366.
14. Ueland, P. M., Importance of chemical reduction in plasma and serum homocysteine analysis. *Clin. Chem.* **2008,** 54, 1085-1086.
15. Toyo'oka, T., Recent advances in separation and detection methods for thiol compounds in biological samples. *J. Chromatogr. B* **2009,** 877, 3318-3330.

16. McMenamin, M. E.; Himmelfarb, J.; Nolin, T. D., Simultaneous analysis of multiple aminothiols in human plasma by high performance liquid chromatography with fluorescence detection. *J. Chromatogr. B* **2009,** 877, 3274-3281.
17. Rafii, M.; Elango, R.; House, J. D.; Courtney-Martin, G.; Darling, P.; Fisher, L.; Pencharz, P. B., Measurement of homocysteine and related metabolites in human plasma and urine by liquid chromatography electrospray tandem mass spectrometry. *J. Chromatogr. B* **2009,** 877, 3282-3291.
18. Steghens, J.-P.; Fluorie, F.; Arab, K.; Collombel, C., Fast liquid chromatography-mass spectrometry glutathione measurements in whole blood: micromolar GSSG is a sample preparation artifact. *J. Chromatogr. B* **2003,** 798, 343-349.
19. Zhu, P.; Oe, T.; Blair, I. A., Determination of cellular redox status by stable isotope dilution liquid chromatography/mass spectrometry analysis of glutathione and glutathione disulfide. *Rapid Comm. Mass Spec.* **2008,** 22, 432-440.
20. Suh, J. H.; Kim, R.; Yavuz, B.; Lee, D.; Lal, A.; Ames, B. N.; Shigenaga, M. K., Clinical assay of four thiol amino acid redox couples by LC-MS/MS: Utility in thalassemia. *J. Chromatogr. B* **2009,** 877, 3418-3427.
21. Seiwert, B.; Karst, U., Simultaneous LC/MS/MS determination of thiols and disulfides in urine samples based on differential labeling with ferrocene-based maleimides. *Anal. Chem.* **2007,** 79, 7131-7138.
22. Rellan-Alvarez, R.; Hernandez, L. E.; Abadia, J.; Alvarez-Fernandez, A., Direct and simultaneous determination of reduced and oxidized glutathione and homoglutathione by liquid chromatography–electrospray/mass spectrometry in plant tissue extracts *Anal. Biochem.* **2006,** 356, 254-264.
23. Guan, X.; Hoffman, B.; Dwivedi, C.; Matthees, D. P., A simultaneous liquid chromatography/mass spectrometric assay of glutathione, cysteine, homocysteine and thier disulfides in biological samples. *J. Pharma. Biomed. Anal.* **2003,** 31, 251-261.
24. Iwasaki, Y.; Hoshi, M.; Saito, K.; Nakazawa, H., Analysis of glutathione and glutathione disulfide in human saliva using hydrophilic interaction chromatography with mass spectrometry. *J. Chromatogr. B* **2003,** 839, 74-79.
25. Bouligand, J.; Deroussent, A.; Paci, A.; Morizet, J.; Vassal, G., Liquid chromatography-tandem mass spectrometry assay of reduced and oxidized glutathione and main precursors in mice liver. *J. Chromatogr. B* **2006,** 832, 67-74.
26. Johnson, J. M.; Strobel, F. H.; Reed, M.; Pohl, J.; Jones, D. P., A rapid LC-FTMS method for the analysis of cysteine, cystine and cysteine/cystine steady-state redox potential in human plasma. *Clin. Chim. Acta* **2008,** 396, 43-48.
27. Lanza, I. R.; Zhang, S. C.; Ward, L. E.; Karakelides, H.; Raftery, D.; Nair, K. S., Quantitative metabolomics by ^{1}H-NMR and LC-MS/MS confirms altered metabolic pathways in diabetes. *Plos One* **2010,** 5, e10538.
28. Sreekumar, A.; Poisson, L. M.; Rajendiran, T. M.; Khan, A. P.; Cao, Q.; Yu, J.; Laxman, B.; Mehra, R.; Lonigro, R. J.; Li, Y.; Nyati, M. K.; Ahsan, A.; Kalyana-Sundaram, S.; Han, B.; Cao, X.; Byun, J.; Omenn, G. S.; Ghosh, D.; Pennathur, S.; Alexander, D. C.; Berger, A.; Shuster, J. R.; Wei, J. T.; Varambally, S.; Beecher, C.; Chinnaiyan, A. M., Metabolomic profiles delineate potential role for sarcosine in prostate cancer progression. *Nature* **2009,** 457, 910-914.

29. Chalcraft, K. R.; Lee, R.; Mills, C.; Britz-McKibbin, P., Virtual quantification of metabolites by capillary electrophoresis-electrospray ionization-mass spectrometry: Predicting ionization efficiency without chemical standards. *Anal. Chem.* **2009,** 81, 2506-2515.
30. Yang, W.-C.; Adamec, J.; Regnier, F. E., Enhancement of the LC/MS analysis of fatty acids through derivatization and stable isotope coding. *Anal. Chem.* **2007,** 70, 5150-5157.
31. Williams, D. K.; Meadows, C. W.; Bori, I. D.; Hawkridge, A. M.; Comins, D. L.; Muddiman, D. C., Synthesis, characterization and application of iodoacetamide derivatives utilized for the ALIPHAT strategy. *J. Am. Soc. Chem.* **2008,** 130, 2122-2123.
32. Carlson, E. E.; Cravatt, B. F., Chemoselective probes or metabolite enrichment and profiling. *Nat. Met.* **2007,** 4, 429-435.
33. Lee, R.; Britz-McKibbin, P., Differential Rates of Glutathione Oxidation for Assessment of Cellular Redox Status and Antioxidant Capacity by Capillary Electrophoresis-Mass Spectrometry: An Elusive Biomarker of Oxidative Stress. *Anal. Chem.* **2009,** 81, (16), 7047-7056.
34. Chalcraft, K. R.; Britz-McKibbin, P., Newborn Screening of Inborn Errors of Metabolism by Capillary Electrophoresis-Electrospray Ionization-Mass Spectrometry: A Second-Tier Method with Improved Specificity and Sensitivity. *Anal. Chem.* **2009,** 81, (1), 307-314.
35. Lee, R.; Ptolemy, A. S.; Niewczas, L.; Britz-McKibbin, P., Integrative metabolomics for characterizing unknown low-abundance metabolites by capillary electrophoresis-mass spectrometry with computer simulations. *Anal. Chem.* **2007,** 79, 403-415.
36. Oss, M.; Kruve, A.; Herodes, K.; Leito, I., Electrospray ionization effieincy scale of organic compounds. *Anal. Chem.* **2010,** 82, 2865-2872.
37. Lee, R.; West, D.; Phillips, S. M.; Britz-McKibbin, P., Differential metabolomics for quantitative assessment of oxidative stress with strenuous exercise and nutritional intervention: Thiol-specific regulation of cellular metabolism with N-acetyl-L-cysteine pretreatment. *Anal. Chem.* **2010,** 82, 2959-2968.
38. Maxwell, E. J.; Chen, D. D. Y., Twenty years of interface development for capillary electorphoresis-electrospray ionization-mass spectrometry. *Anal. Chim. Acta* **2008,** 627, 25-33.
39. Chang, C.-W.; Tseng, W.-L., Gold nanoparticle extraction followed by capillary electrophoresis to determine the total, free, and protein-bound aminothiols in plasma. *Anal. Chem.* **2010,** 82, 2696-2702.
40. Schafer, F. Q.; Buettner, G. R., Redox environment of the cell as viewed through the redox state of the glutathione disulfide/glutathione couple. *Free Radic. Biol. Med.* **2001,** 30, 1191-1212.
41. Mansoor, M. A.; Svardal, A. M.; Ueland, P. M., Determination of the in vivo redox status of cysteine, cysteinylglycine, homocysteine and glutathione in human plasma. *Anal. Biochem.* **1992,** 200, 218-229.

42. Blanco, R. A.; Ziegler, T. R.; Carlson, B. A.; Cheng, P. Y.; Park, Y.; Cotsonis, G. A.; Accardi, C. J.; Jones, D. P., Diurnal variation in glutathione and cysteine redox states in human plasma. *Am. J. Clin. Nutr.* **2007,** 86, 1016-1023.
43. Garg, U. C.; Zheng, Z.-J.; Folsom, A. R.; Moyer, Y. S.; Tsai, M. Y.; McGovern, P.; Eckfeldt, J. H., Short-term and long-term variability of plasma homocysteine measurement. *Clin. Chem.* **1997,** 43, 141-145.
44. Ashfaq, S.; Abramson, J. L.; Jones, D. P.; Rhodes, S. D.; Weintraub, W. S.; Hooper, W. C.; Vaccarino, V.; Alexander, R. W.; Harrison, D. G.; Quyyumi, A. A., Endothelial function and aminothiol biomarkers of oxidative stress in healthy adults. *Hypertension* **2008,** 52, 80-85.
45. Struys, E. A.; Jansen, E. E. W.; Meer, K. d.; Jakobs, C., Determination of S-adenosylmethionine and S-adenosylhomocysteine in plasma and cerebrospinal fluid by stable-isotope dilution mass spectrometry. *Clin. Chem.* **2000,** 46, 1650-1656.
46. Desiderio, C.; Rossetti, D. V.; Messana, I.; Giardina, B.; Castagnola, M., Analysis of arginine and methylated metabolites in human plasma by field amplified sample injection capillary electrophoresis tandem mass spectrometry. *Electrophoresis* **2010,** 31, 1894-1902.
47. Elshorbagy, A. K.; Nurk, E.; Gjesdal, C. G.; Tell, G. S.; Ueland, P. M.; Nygard, O.; Tverdal, A.; Vollset, S. E.; Refsum, H., Homocysteine, cysteine, and body composition in the Hordaland Homocysteine Study: Does cysteine link amino acid and lipid metabolism? *Am. J. Clin. Nutr.* **2008,** 88, 738-746.
48. Refsum, H.; Nurk, E.; Smith, A. D.; Ueland, P. M.; Gjesdal, C. G.; Bjelland, I.; Tverdal, A.; Tell, G. S.; Nygard, O.; Vollset, S. E., The Hordaland Homocysteine Study: A community-based study of homocysteine, its determinants and associations with disease. *J. Nutri.* **2006,** 136, 1731S-1740S.
49. Steenge, G. R.; Verhoef, P.; Katan, M. B., Betaine supplementation lowers plasma homocysteine in healthy men and women. *J. Nutr.* **2003,** 133, 1291-1295.
50. Smith, C. L.; Anthony, S.; Hubank, M.; Leiper, J. M.; Vallance, P., Effects of ADMA upon gene expression: An insight into the pathophysiological significance of raised plasma ADMA. *Plos Medicine* **2005,** 2, e264.
51. Atkuri, K. R.; Mantovani, J. J.; Herzenberg, L. A.; Herzenberg, L. A., N-acetylcysteine-A safe antidote for cysteine/glutathione deficiency. *Curr. Opin. Pharmacol.* **2007,** 7, 355-359.

2.7 Supplementary Figures and Tables

Table S2.3: Summary of fundamental physicochemical parameters for predicting the enhancement of ionization efficiency for thiols labeled with various maleimide derivatives by CE-ESI-MS.

Thiol	MV ($Å^3$)[a]	$\mu_{ep} \times 10^{-4}$ (cm^2/Vs)[b]	z_{eff}[c]	logD[d]	Meas. RRF[e]	Pred. RRF[e]	m/z (MH^+; $^TMH_2^{2+}$)
Cys	87.4	1.75	0.62	-2.3	--	--	122
Hcy	105	2.05	0.72	-2.3	--	--	136
CysGly	130	2.62	0.95	-3.5	--	--	179
GluCys	192	1.32	0.72	-4.2	--	--	251
GSH	235	1.22	0.72	-4.4	--	--	308
Cys-NMM	179	1.14	0.62	-3.1	9.54	7.81	233
Hcy-NMM	196	1.54	0.72	-3.4	5.01	6.82	247
CysGly-NMM	222	2.03	0.95	-4.4	4.97	4.95	290
GluCys-NMM	286	1.10	0.72	-5.2	3.31	3.06	362
GSH-NMM	331	1.05	0.72	-5.4	2.68	2.61	419
Cys-NEM	198	1.10	0.62	-2.5	11.8	10.6	247
Hcy-NEM	216	1.49	0.72	-2.9	6.56	9.19	261
CysGly-NEM	240	1.96	0.95	-3.8	5.73	6.72	304
GluCys-NEM	301	1.07	0.72	-4.6	4.72	4.21	376
GSH-NEM	348	1.03	0.72	-4.8	4.05	3.71	433
Cys-NMBA	220	0.972	0.62	-4.3	11.6	11.2	291
Hcy-NMBA	239	1.33	0.72	-4.6	6.25	9.24	305
CysGly-NMBA	263	1.78	0.95	-5.7	6.03	6.40	348
GluCys-NMBA	324	0.981	0.72	-6.4	4.41	3.22	420
GSH-NMBA	369	0.953	0.72	-6.5	4.23	2.53	477
Cys-NPEM	270	0.989	0.62	-0.9	25.8	21.0	323
Hcy-NPEM	289	1.34	0.72	-1.2	14.3	17.8	337
CysGly-NPEM	315	1.77	0.95	-2.2	11.8	13.9	380
GluCys-NPEM	387	1.00	0.72	-3.0	8.16	10.0	452
GSH-NPEM	423	0.968	0.72	-3.2	9.60	8.49	509
Cys-MHA	274	0.887	0.62	-3.5	23.3	18.7	333
Hcy-MHA	294	1.230	0.72	-3.8	12.4	15.6	347
CysGly-MHA	321	1.630	0.95	-4.9	9.07	11.6	390
GluCys-MHA	391	0.924	0.72	-5.6	6.88	7.46	462
GSH-MHA	426	0.903	0.72	-5.8	7.56	5.40	519
Cys-NAEM	203	3.00	1.62	-4.4	8.44	8.13	262
Hcy-NAEM	220	3.30	1.72	-4.7	2.30	2.30	276
CysGly-NAEM	245	3.77	1.95	-4.5	1.60	1.64	319
GluCys-NAEM	311	2.54	1.72	-4.8	3.00	3.28	$196^{\dagger}$
GSH-NAEM	352	2.45	1.72	-4.9	4.86	3.35	$224^{\dagger}$
Cys-NTAM	266	2.91	1.62	-4.2	22.8	16.4	304
Hcy-NTAM	284	3.19	1.72	-4.9	7.68	9.79	318
CysGly-NTAM	314	3.66	1.95	-4.3	4.68	4.46	361
GluCys-NTAM	370	2.49	1.72	-4.5	5.77	6.72	$217^{\dagger}$
GSH-NTAM	416	2.41	1.72	-4.7	7.53	6.32	$245.5^{\dagger}$

a. Chem3D Ultra 8.0 after MM2 energy minimization as Connelly Solvent-Excluded Volume.

b. Apparent μ_{ep} measured in 1.0 M formic acid, pH 1.8 (n=5).

c. Calculated using ACD/logD 8.02 at pH 7.

d. Calculated from predicted pK_a using ACD/pKa8.03 at pH1.8, where $z_{eff} = 1/(10^{[pH-pK_a]}+1)$.

e. Measured RRF assessed by the ratio in the slope of calibration curve (i.e., sensitivity based on measured peak area) for thiol maleimide adduct relative to free thiol, whereas predicted RRF determined by MLR using four intrinsic physicochemical properties with 7-fold cross-validation.

Table S2.4: Summary of 7-fold cross-validation method for assessing the performance of the MLR model and significance of variables to predict RRF of thiol-maleimide adducts by CE-ESI-MS.

#Training; #Test; #Variables[a]	R^2[b] ***(Training)***	***MSEC***[b] ***(Training)***	Q^2[b] ***(Test)***	***MSEP***[b] ***(Test)***
30; 5; 4	0.863 ± 0.015	4.35 ± 0.54	0.86 ± 0.10	6.4 ± 3.8
30; 5; 3 (without *logD*)	0.835 ± 0.011	5.28 ± 0.79	0.84 ± 0.14	6.7 ± 5.5
30; 5; 2 (without *logD;0* μ_{ep})	0.738 ± 0.017	8.36 ± 0.98	0.73 ± 0.16	10.8 ± 6.5
30; 5; 1 (only *MV*)	0.704 ± 0.019	9.5 ± 1.2	0.72 ± 0.18	10.7 ± 7.4

a. Cross-validation of MLR model performed by randomly holding out 5 thiol maleimide adducts as a test set seven times with the remaining 30 thiols serving as the training set using either four, three or two intrinsic solute parameters.

b. MSEC and MSEP are the average mean square error of calibration and mean square error of prediction, whereas R^2 and Q^2 represent the average coefficient of determination (linearity) for the training and test sets, respectively from the 7-fold cross validation

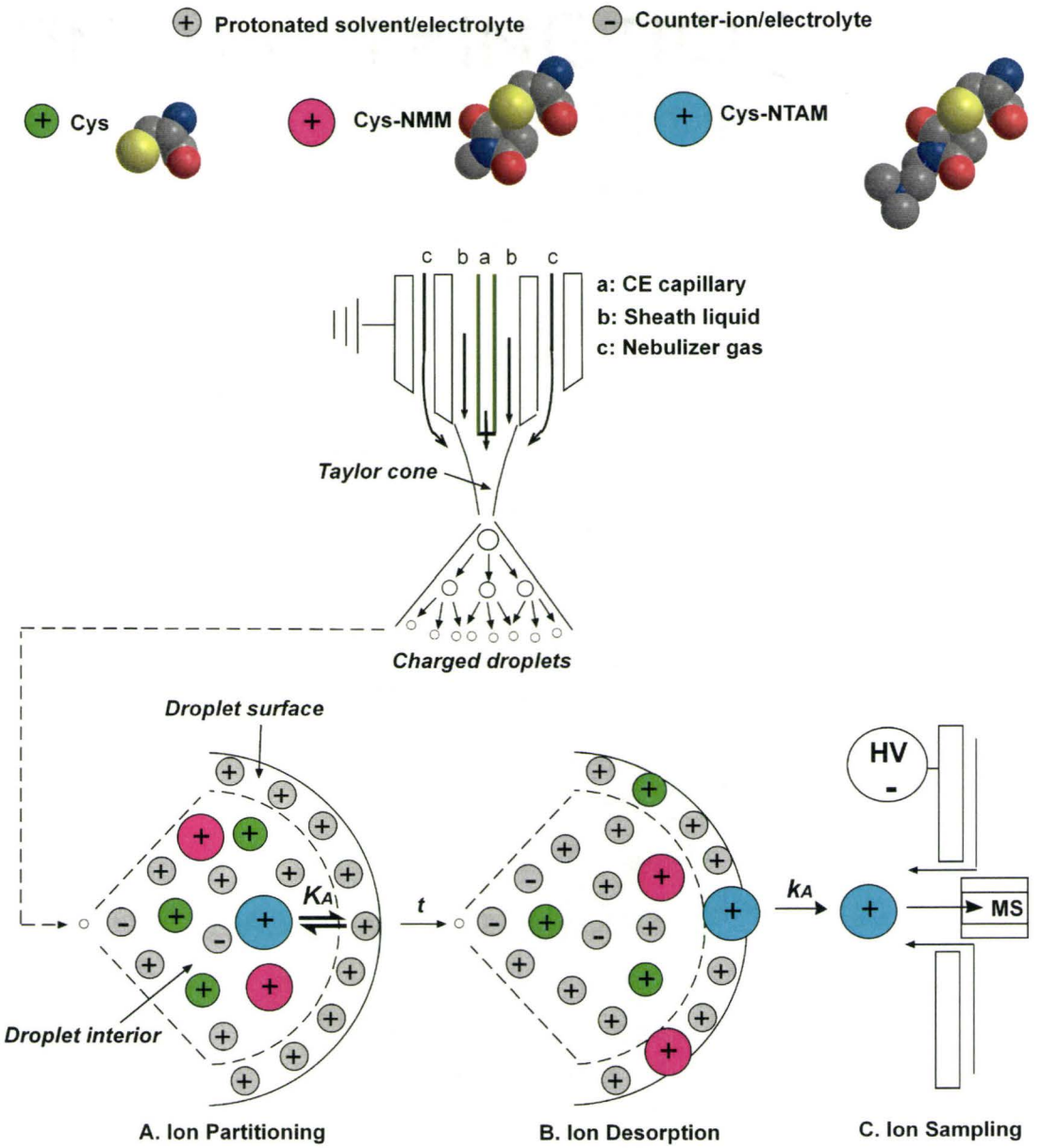

Figure S2.6: Multivariate ionization model for describing the enhancement in ionization efficiency for thiols with maleimide derivatization (*e.g.*, Cys, Cys-NMM and Cys-NTAM) when using a grounded coaxial sheath liquid interface in CE-ESI-MS. The overall ion response in ESI-MS is dependent on the magnitude of equilibrium partitioning (K_A) of ions at the liquid-gas interface of the droplet surface, the rate of ion desorption into the gas-phase (k_A) and the fraction of ions collected/transferred into the mass analyzer. Overall, maleimide derivatization of cationic thiols improves ionization efficiency by enhancing their surface activity as reflected by increases in *MV* and lower charge density that is associated with reduced energy requirements for desolvation needed for ion desorption. In addition, electrokinetic factors that favor faster ion desorption from the droplet surface into the gas phase also improve ionization efficiency, such as larger μ_{ep}. With the exception of NPEM-thiol derivatives, most maleimide adducts were more hydrophilic relative to their native free thiols in this study, thus *logD* was a less significant parameter influencing ionization response in this work.

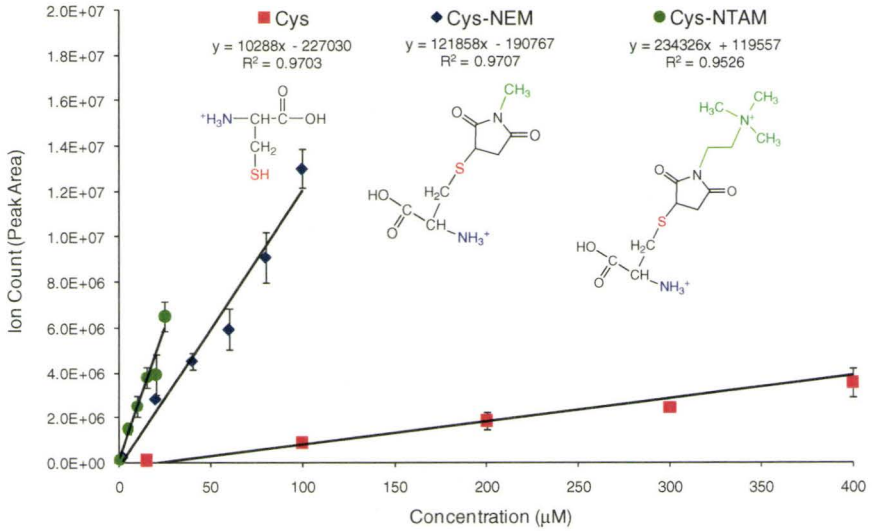

Figure S2.7: Impact of maleimide derivatization on enhancing thiol ionization efficiency based on the apparent increase in concentration sensitivity (*i.e.*, slope) when using CE-ESI-MS as highlighted by a series of calibration curves for Cys conjugated to various maleimides with different substituent groups, such as NEM (neutral) and NTAM (cationic). In order to correct for changes in trapping efficiency for thiol-maleimide conjugates with different *m/z* when using a 3D ion trap mass analyzer, absolute peak areas were quantified without normalization to an internal standard, while adjusting target mass (*i.e.*, average *m/z*) among model thiols derivatized to a specific maleimide analog.

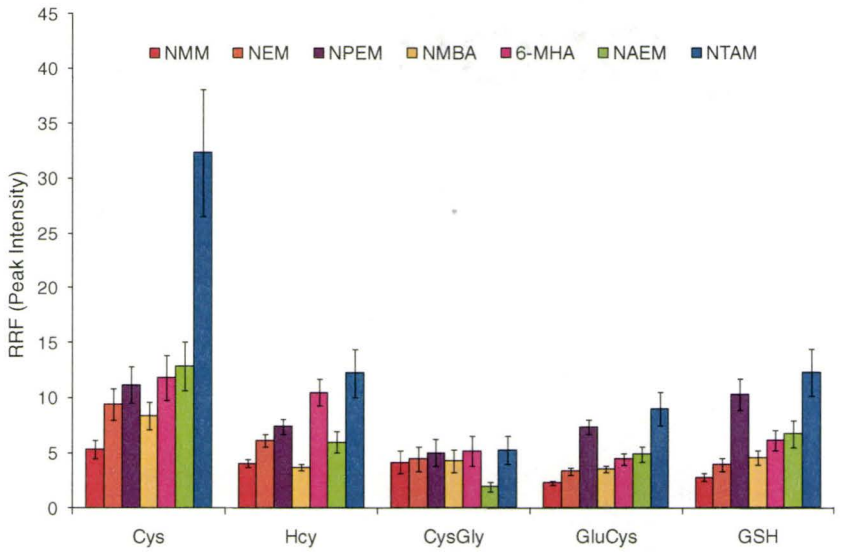

Figure S2.8: Comparison of apparent RRF for thiol-maleimides derived from measured peak height of ion responses in CE-ESI-MS. Peak height derived RRFs provide a more reliable indicator of sensitivity enhancement since it also takes into account the extent of band broadening and *S/N* increase despite resulting in poorer model fitting (R^2 = 0.6737) when using MLR as compared to peak area (R^2 = 0.8604). NTAM was selected as the optimum maleimide label for thiols in this study due to their faster mobility/shorter migration times and reduced band dispersion for greater concentration sensitivity in CE-ESI-MS relative to bulky yet neutral maleimides (*e.g.*, MHA, NPEM).

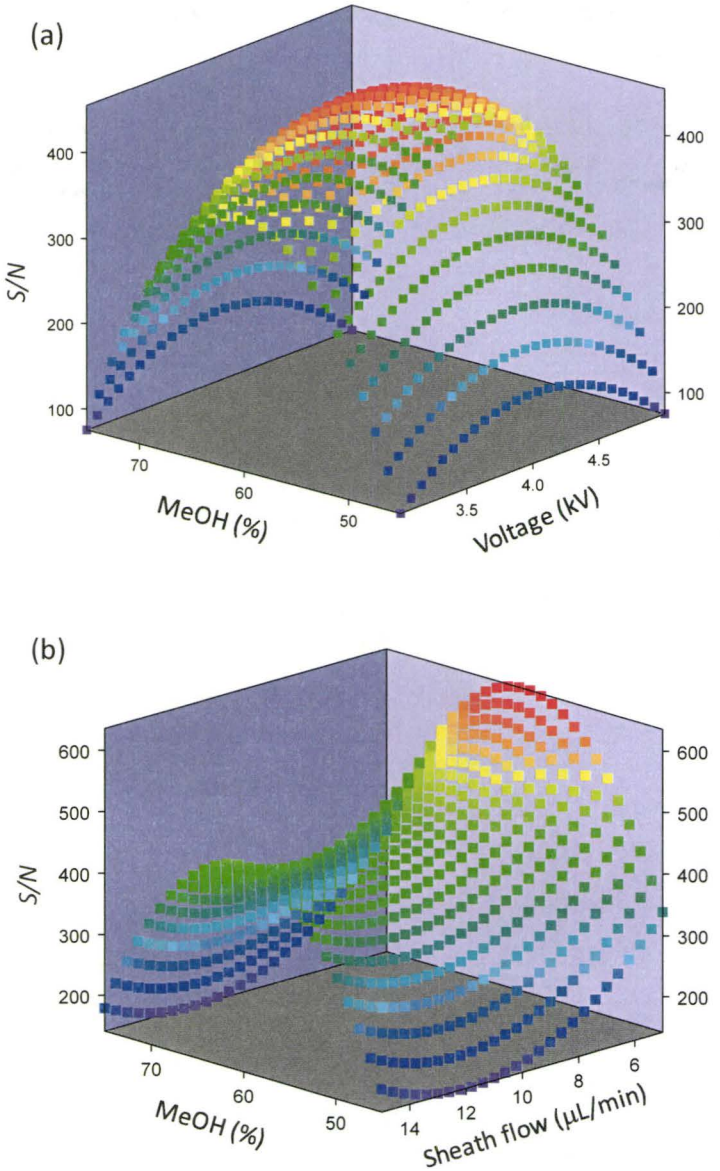

Figure S2.9: Representative 3D surface response models based on a 3-factor/2-level face-centred central composite experimental design for optimization of thiol maleimide ionization efficiency based on three variables in the coaxial sheath liquid ESI interface for CE-MS, namely cone voltage (V: 3-5 kV), MeOH% (MeOH: 45-75%) and sheath flow (SF: 5-15 µL/min). MLR model (R^2 = 0.8131) was used for determination of coefficients and significance of key variables (*e.g.,* SF and MeOH) involving 30 µM Hcy-MHA when using a 5 s hydrodynamic injection. In the case of Hcy-MHA, the refined empirical equation was determined to be $S/N = (455 \pm 30) + (-80 \pm 28)SF + (-298 \pm 53)MeOH^2 + (101 \pm 53)SF^2 + (-82 \pm 53)V^2$ Overall, optimal conditions for maximizing detection of thiol-maleimide adducts by CE-ESI-MS in this study while ensuring long-term stability was found to be 4 kV, 10 µL/min and 60% MeOH for cone voltage, sheath flow and %MeOH, respectively.

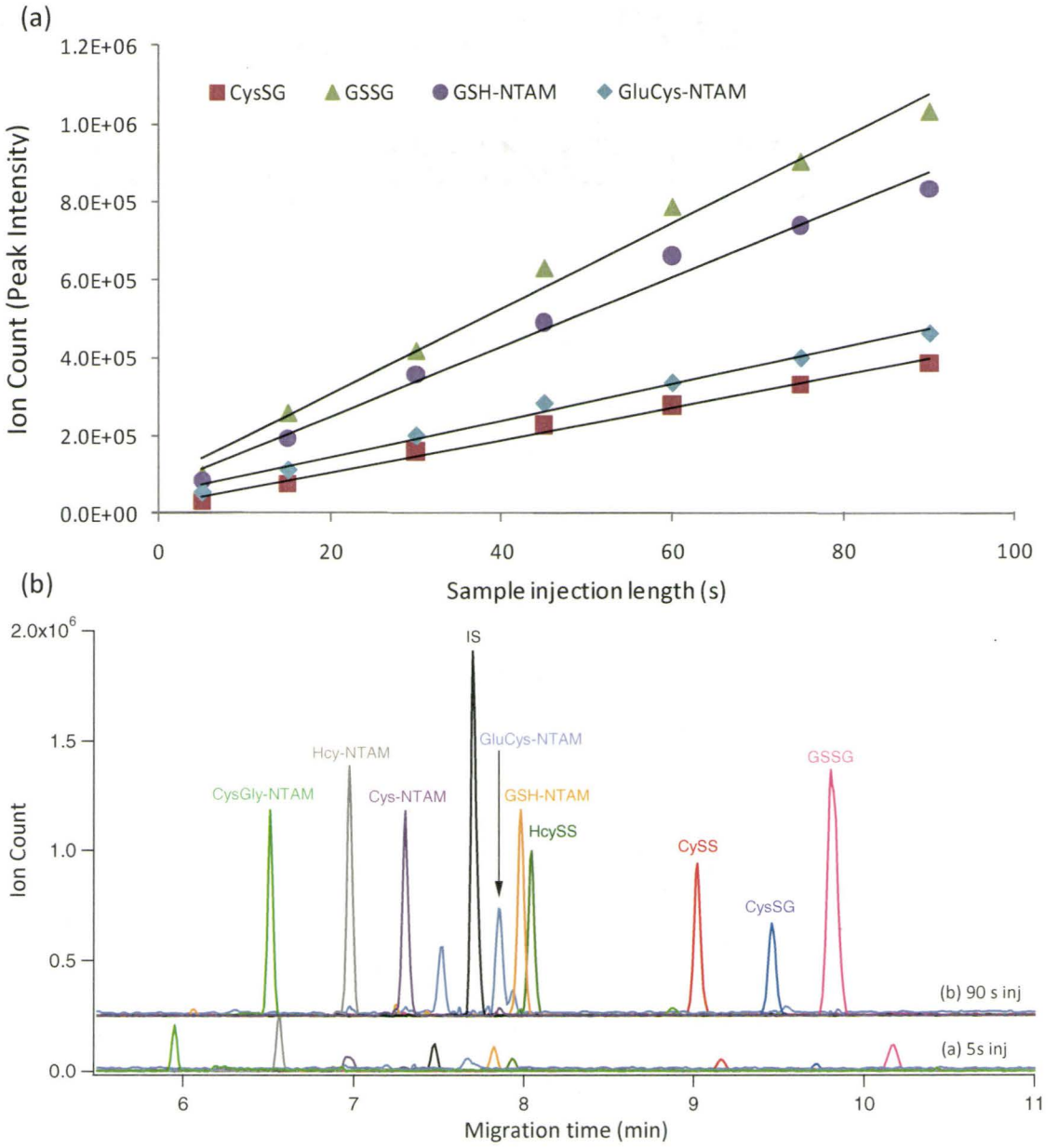

Figure S2.10: CE-ESI-MS in conjunction with on-line sample preconcentration for enhancement of concentration sensitivity for thiol-maleimide adducts and oxidized thiols when using longer injection plug lengths. **(a)** Graphs demonstrating the linear increase in sensitivity for representative NTAM-thiols and oxidized thiols with longer sample injections without band broadening and **(b)** electropherogram overlay highlighting about a 15-fold enhancement in concentration sensitivity that allows for sub-micromolar detection of thiols when using a 90 s relative to a conventional 5 s sample injection length without significant detrimental effects on resolution, migration time and separation efficiency.

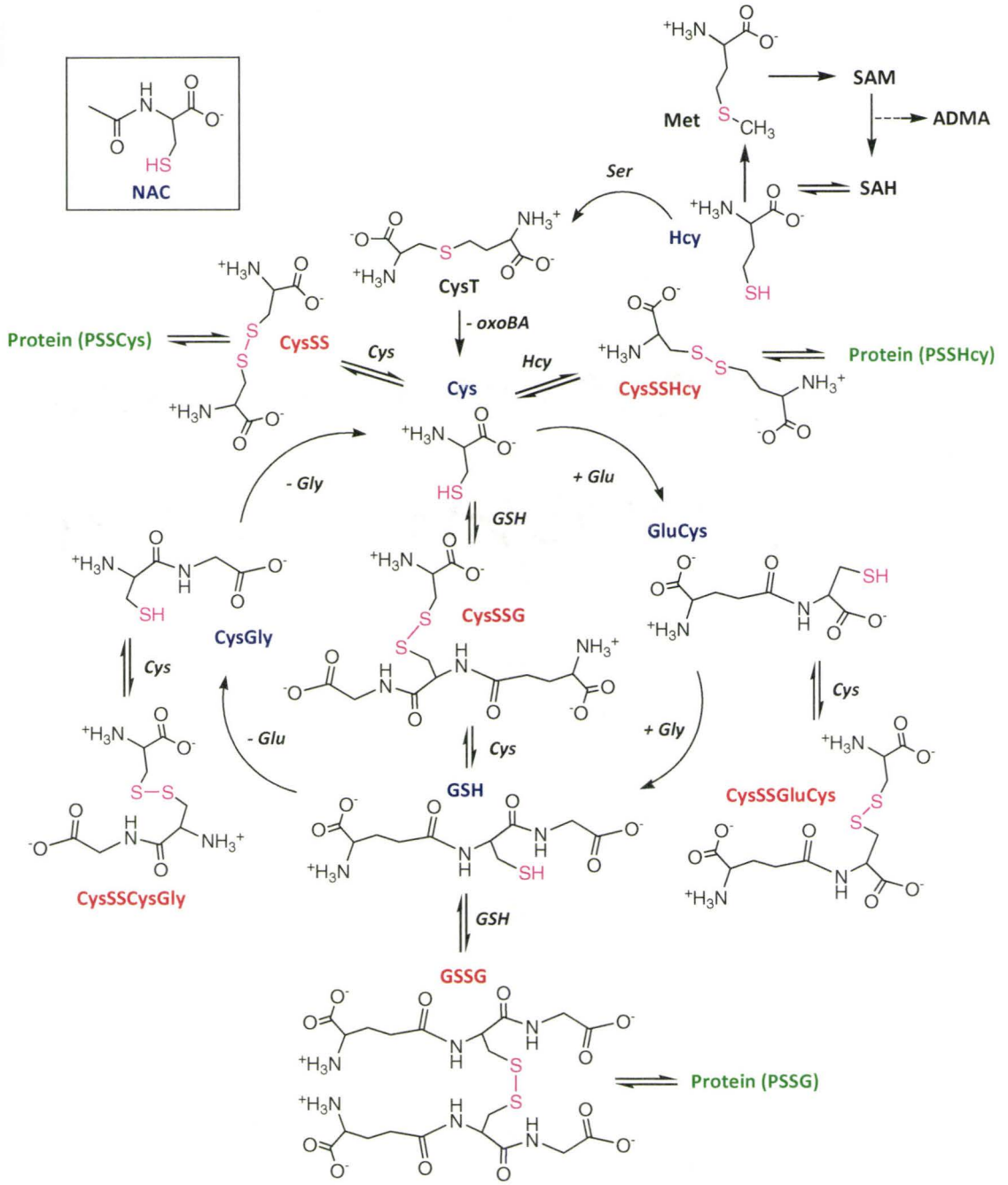

Figure S2.11: Schematic of coupled thiol reactions associated with homocysteine (Hcy), cysteine (Cys) and glutathione (GSH) metabolism. Three major classes of thiols exist in plasma, including free reduced thiols, free oxidized disulfides (*i.e.*, homodimer and mixed disulfides) and protein-bound thiol disulfide fractions. Reliable analysis of biological-active free reduced thiols in plasma is challenging given their low concentration levels, poor ionization efficiency and lability. CysT, SAM, SAH, ADMA and oxoBA represent cystathionine, *S*-adenosylmethionine, *S*-adenosylhomocysteine, asymmetric dimethylarginine and 2-oxobutyric acid, respectively.

Chapter 3:

Successes, Challenges, and Future Work in Thiol Redox Status Analysis by CE-ESI-MS

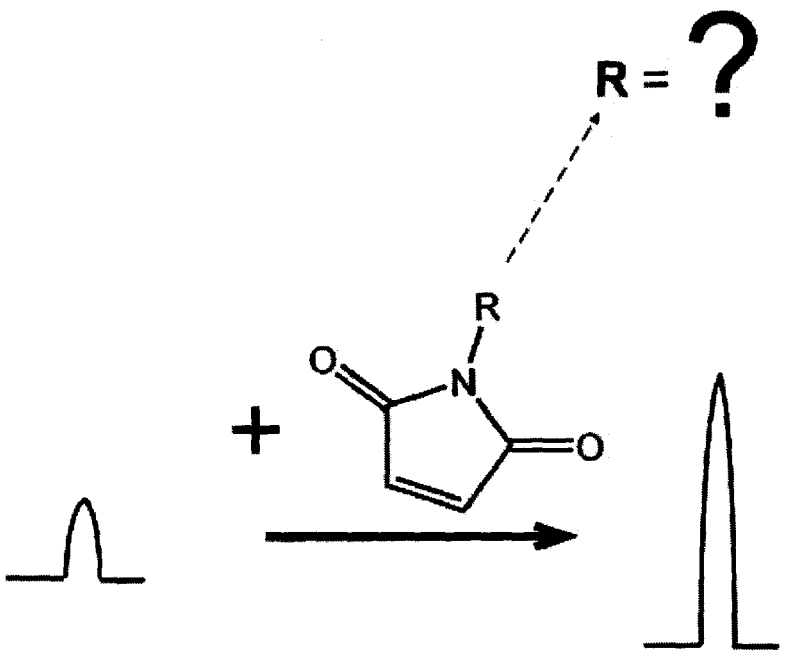

3: Successes, Challenges, and Future Work in Thiol Redox Status Analysis by CE-ESI-MS

3.1 Performance of Thiol Redox Status Method

The CE-ESI-MS method for plasma thiol analysis presented in **Chapter 2** has a number of significant advantages. By resolving intact symmetric and mixed disulfides, it measures plasma reduced thiols and intact oxidized disulfides simultaneously using a minimally-invasive finger-prick blood micro-sampling technique. Analyzing intact disulfides reveals the precise chemical context of free oxidized disulfides so that their biological significance can be interpreted. This may be important in differentiating various reduced and oxidized thiols when specific disulfides are associated with disease. For instance, elevated CySSG and CySS have been found to correlate with diminished endothelial function, an early sign of atherosclerosis.[1] In addition, concentrations of specific symmetric disulfides in biological samples are needed for accurate determination of the redox potentials (E_h) of important thiol redox couples, such as Cys/CysSS and GSH/GSSG and as a way to derive more reliable measures of thiol redox potential. Importantly, several redox potentials associated with thiol reactivity can be determined using the developed CE-ESI-MS method. Since analyses are performed using full-scan mass spectrometry, the method is also amenable to untargeted metabolite profiling, which could reveal metabolic pathways associated with alterations in thiol metabolism and disease pathogenesis.[2] The potential for untargeted metabolite profiling with this method is evident in the detection of several mixed disulfides in plasma whose detection has not previously been reported, such as CysSSHcys, CysSSCysGly, and CysSSGluCys. It is

also notable that the plasma sample was stable over two consecutive freeze-thaw cycles indicating that the maleimide derivatization procedure successfully stabilizes reduced thiols as thioether adducts for future analysis, while avoiding thiol-disulfide cross-reactivity.

Despite its advantages, the CE-ESI-MS method for thiol redox status analysis has several limitations that should be addressed in future studies before the method is suitable for clinical application. Although the method had sub-nanomolar sensitivity to detect many reduced thiols in plasma including Cys, Hcy, CysGly, and GSH; GluCys was not detected and Hcy was measured near the detection limit. The poor sensitivity for GluCys is in part due to isobaric interferences in the *N*-[2-(trimethylammonium)ethyl]maleimide (NTAM) derivatization solution. Therefore, it would be beneficial to further improve the sensitivity of the method in order to detect low nanomolar levels of reduced thiols with low background noise.

It was observed that hydrolysis and methanolysis occurred in concentrated NTAM stock solutions prepared in aqueous and methanolic solution, respectively. The increase in the NTAM methanolysis peak at *m/z* 215 for 5 mM NTAM derivatized samples prepared with a methanolic NTAM solution on the day the NTAM solution was prepared and two days later from the same NTAM solution is shown in the extracted ion electropherograms (EIEs) in **Figure 3.1**. Hydrolysis of aqueous stock solutions was also evident in NTAM hydrolysis product peaks at *m/z* 201 that were increasingly abundant the longer NTAM was kept in aqueous solution. After 3 days in 0.1% formic acid aqueous solution, the NTAM hydrolysis peaks increased in intensity by 20-50%.

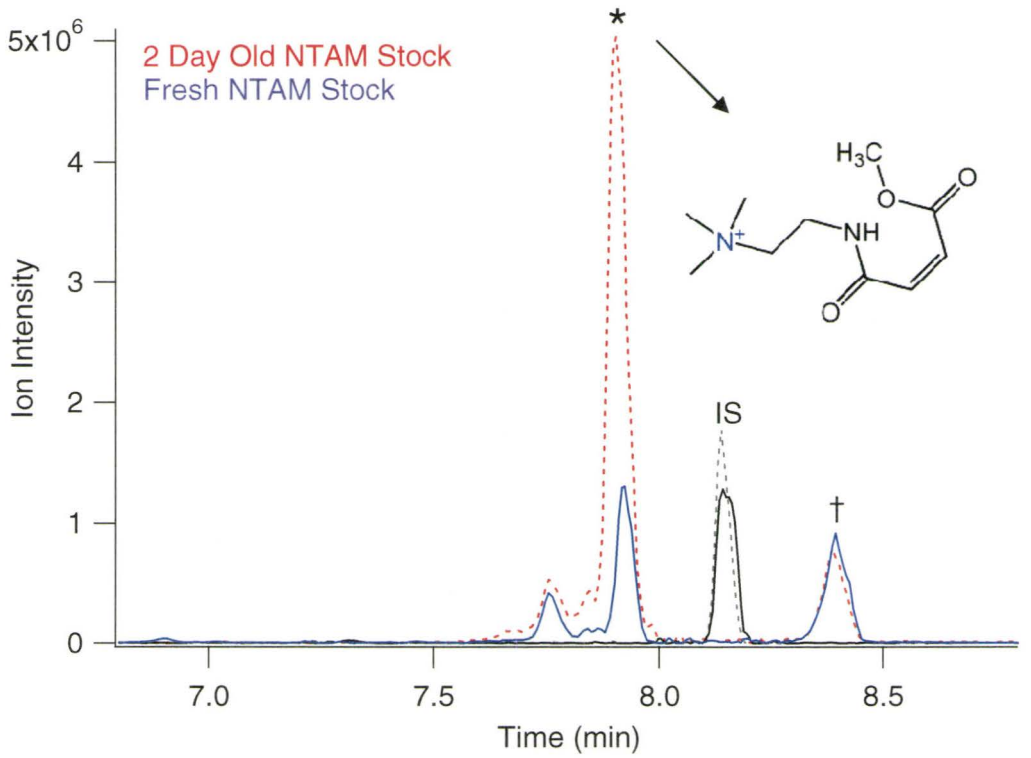

Figure 3.1: Extracted ion electropherograms (EIEs) for 90 sec injections of 5 mM NTAM quenched with 6.25 mM MESNA and 2 mM NMM prepared with a methanolic NTAM stock the day the stock was prepared (blue and black traces) and two days after the stock was prepared (red and grey dashed traces). The red and blue traces are the NTAM methanolysis products (*m/z* 215). The black and grey traces are 20 µM dialanine IS. Traces are normalized to the IS peak area. The proposed structure of the methanolysis product of NTAM (*) that increases in abundance is also shown. Another isobaric impurity is also present (†).

Because of this hydrolysis, stock solutions of NTAM in 0.1% formic acid aqueous solution for the method presented in Chapter 2 were used within 24 hours. Acidic solution was used to slow hydrolysis because maleimide is hydrolyzed faster by base-catalysis under alkaline conditions.[3] Preparing derivatization solutions daily for an in-depth study of thiol redox status would waste large amounts of reagent. Stock solutions of other maleimide analogues in acetonitrile have been stable over longer time periods

without methanolysis or hydrolysis, but NTAM is insoluble in acetonitrile. The significant baseline level of the hydrolysis product peaks seen in **Figure 3.2** for freshly prepared NTAM stocks indicates that the hydrolysis products are likely present as trace impurities in the commercial NTAM standard that was purchased.

The NTAM derivatization method required quenching with MESNA followed by NMM. The MESNA quench was necessary to displace the interfering peak from excess NTAM to the EOF through its reaction with MESNA by forming a neutral thioether adduct. However, excess MESNA was found to undergo thiol-disulfide exchange with the disulfides in samples gradually depleting the concentrations of CysSS and CysSSG. Therefore, NMM was added to react with the residual MESNA in filtered plasma samples to prevent thiol exchange. The impact of MESNA quenching in displacing the excess NTAM peak is shown in **Figure 3.2**. Importantly, quenching excess NTAM prevents it from hydrolyzing in the sample and increasing the intensity of the hydrolysis product peaks over time. Excess NTAM co-migrates with CysGly-NTAM and Hcy-NTAM, while the hydrolyzed NTAM co-migrates with GluCys-NTAM and dialanine IS. Thus, excess NTAM and hydrolyzed NTAM may contribute to ionization suppression of these analytes. This emphasizes the necessity of the quench step to prevent ionization suppression in ESI-MS.

Because the CE-ESI-MS method for plasma thiol analysis using NTAM has lower sensitivity than would be ideal for biological concentrations of some thiols and is subject to hydrolysis of the NTAM stock solutions, an improved method is required for further validation and clinical application. This method would utilize a maleimide that is soluble

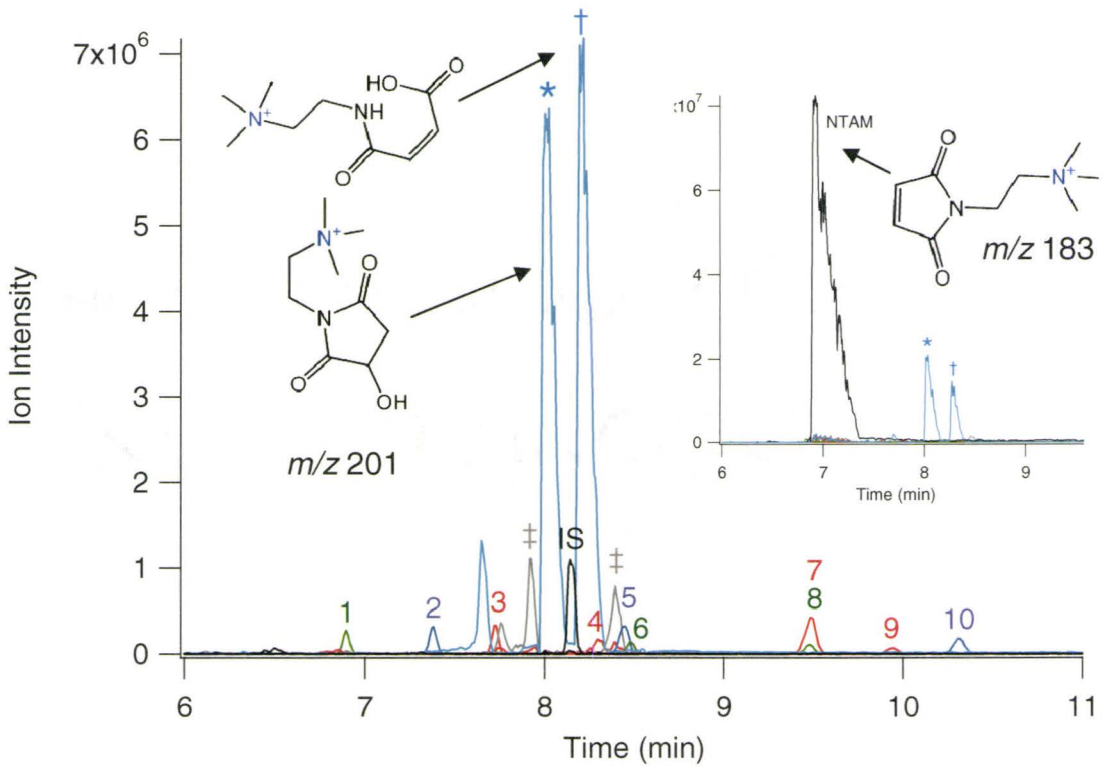

Figure 3.2: EIEs of 1 µM thiols and disulfides and 20 µM dialanine IS derivatized with 5 mM NTAM injected for 90 seconds either after quenching with 6.25 mM MESNA and 2 mM NMM. Insets show the high intensity of the excess NTAM peak (*m/z* 183) without quenching, the structure of NTAM and proposed structures for the hydrolysis products of NTAM (*, †, *m/z* 201). Peaks are numbered: 1 – CysGly-NTAM, 2 – Hcy-NTAM, 3 – Cys-NTAM, 4 – GluCys-NTAM, 5 – GSH-NTAM, 6 – HcySS, 7 – NAC-NTAM, 8 – CysSS, 9 – CysSSG, 10 – GSSG. Impurities that are probable methanolysis products of NTAM (*m/z* 215) are marked with ‡.

in acetonitrile thereby reducing hydrolysis effects with a non-aqueous stock solution and does not contain isobaric impurities that interfere with thiol adducts. This method may involve negative ion mode CE-ESI-MS rather than positive ion mode in order to investigate the use of long chain carboxylic acid maleimide analogs, such as MHA. It was found that cationic maleimides improve sensitivity and enable the analysis of acidic thiols in positive ion mode. Anionic maleimides may provide similar advantages in negative ion mode and stable stock solutions can be prepared in acetonitrile.

3.2 Negative Ion Mode Thiol Analysis with Maleimide Derivatization

Negative ion mode CE-ESI-MS differs from the positive ion mode CE-ESI-MS used so far in two key ways. First, instead of a highly acidic BGE it uses a neutral or alkaline BGE prepared with ammonium acetate or ammonium bicarbonate for ESI compatibility. This encourages the formation of deprotonated, negatively charged forms of solutes that can be separated in normal polarity CE due to the strong EOF at a higher BGE pH. Second, the polarity of the ESI source is reversed and the MS inlet is at a positive potential relative to the CE-ESI-MS sprayer. Thus, negative gas phase ions are produced in the electrospray rather than positive ions.

To complement the predictive model for changes in the ionization efficiency of thiols with maleimide derivatization in positive ion mode presented in **Chapter 2**, preliminary studies were performed in negative ion mode, which has been reported to have different ionization mechanisms than positive ion mode.[4] This would allow a comparison of the physicochemical factors affecting ionization efficiency with maleimide derivatization in both ionization modes. Previous studies have suggested that pK_a and octanol-water partition coefficient (*logP*) may be predictive of ionization efficiency in negative ion mode ESI-MS.[5] However, increasing *logP* was found to have the greatest influence in increasing ionization efficiency in negative ion mode in a study of 30 organic acids, while pK_a was not predictive of ionization efficiency overall.[5] The impact of *logP* is explained by the role of increasing hydrophobicity in increasing surface activity and thereby increasing ionization efficiency in an ion evaporation mechanism. It can be hypothesized that the factors influencing ionization efficiency in negative ion mode CE-

ESI-MS will be similar to those found in **Chapter 2** for positive ion mode. It is likely that increasing *MV* will increase surface activity and ionization efficiency in negative ion mode. To ionize in negative ion mode solutes will require acidic functional groups that can be deprotonated to impart a negative charge, whereas in positive ion mode basic functional groups that could be protonated to impart a positive charge were required. Increasing the charge beyond a single negative charge would increase polarity and decrease surface activity. Therefore, a decrease in ionization efficiency with increasing charge, as was observed in positive ion mode, would be expected.

Despite the propensity for corona discharge and resulting higher background signals in negative ion mode ESI-MS,[4, 6] preliminary studies were performed to assess the feasibility of negative ion mode CE-ESI-MS for plasma thiol redox analysis. Such a method would be able to circumvent the hydrolysis issues encountered with NTAM by using MHA in acetonitrile solution for derivatization. Anionic MHA may also provide advantages for analysis in negative ion mode similar to those of cationic derivatization in positive ion mode.

3.2.1 Instability of Thiol-Maleimide Adducts Under Alkaline Conditions

Initially, negative ion mode analysis of thiol-maleimide adducts was explored using alkaline BGE solutions with buffer pH above 8. Unusual results were observed that can be attributed to instability of the thiol-maleimide adducts in the alkaline BGE. Adducts of maleimides with thiols are known to undergo two reactions subsequent to the initial Michael addition of the thiol to the double bond of maleimide forming a

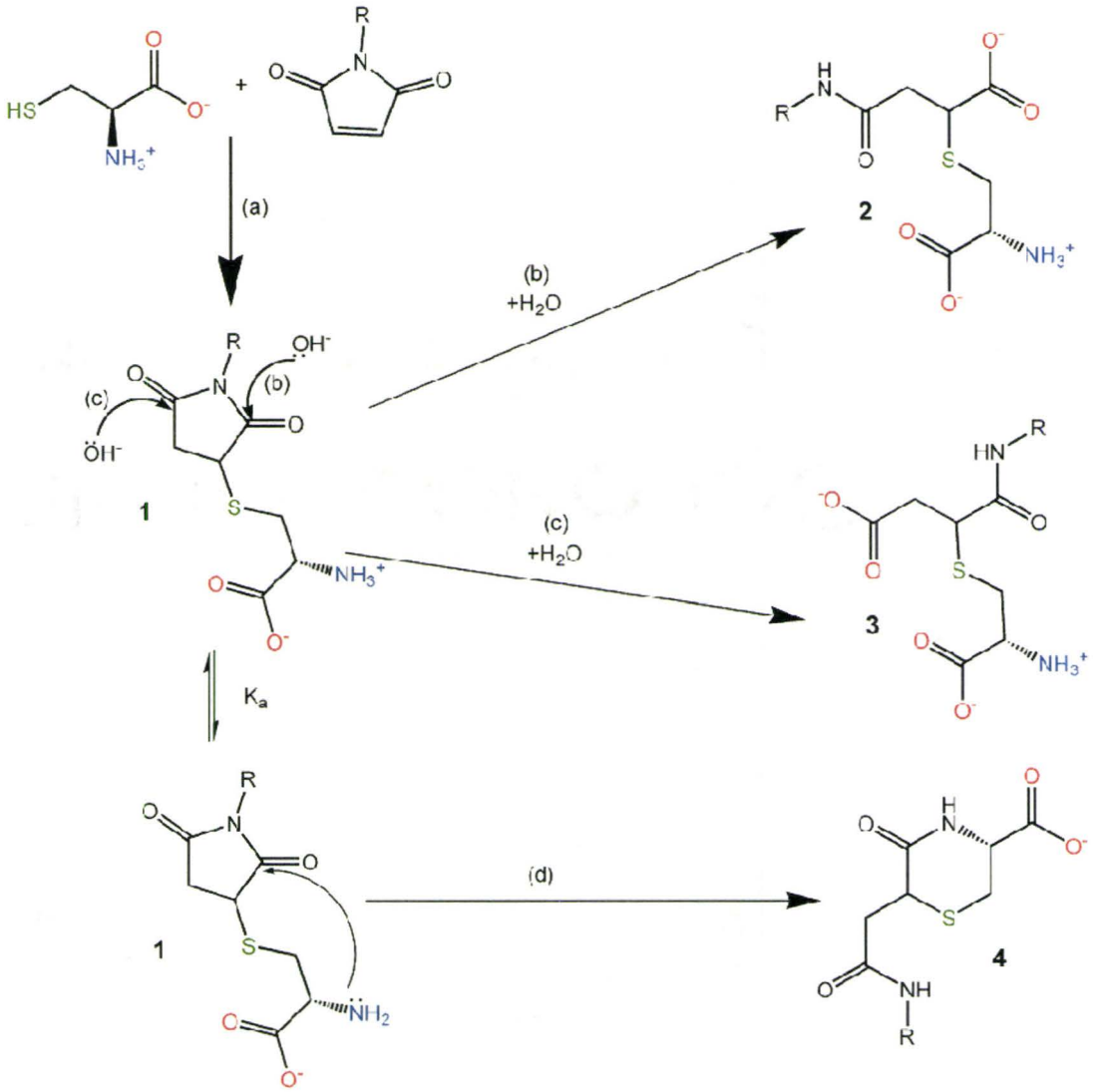

Figure 3.3: Schematic of reactions of Cys with a general maleimide showing **(a)** Michael addition of Cys to a maleimide forming a succinimide-type product (1), **(b)** and **(c)** hydrolysis of the succinimide-type product forming isomeric open-type products (2 & 3) **(d)** intramolecular nucleophilic attack of the amine group forming a thiazine-type product (4).

succinimide-type product. These reactions are intra-molecular nucleophilic attack of an amine group forming a six-membered ring in a thiazine-type product and hydrolysis of the five-membered ring forming an open-type product.[7] These reactions are illustrated in **Figure 3.3** for Cys and a general maleimide.

Both reactions of the succinimide-type product occur more rapidly with increasingly basic pH.[7] To prevent these reactions, samples of maleimide derivatized thiols were prepared at pH 5. Intramolecular nucleophilic attack forming a thiazine-type product occurs for thiol maleimide adducts where a six-membered ring is formed by the intramolecular nucleophilic attack of an amine group. For example, it may occur with Cys-maleimide adducts but not with GSH-maleimide adducts or NAC-maleimide adducts.[7] This is because while Cys-maleimide adducts can form a thermodynamically favorable six-membered ring through intramolecular nucleophilic attack, GSH-maleimide adducts would form a thermodynamically unfavorable, strained 11-membered ring and NAC-maleimide adducts do not have an amine available to attack.

Samples of maleimide derivatized thiols for negative ion mode analysis were prepared in 50 mM ammonium acetate, pH 5 to prevent hydrolysis and nucleophilic attack from occurring in the sample. However, these reactions may still occur during a CE separation performed in an alkaline BGE. Evidence that intramolecular nucleophilic attack of amine groups was occurring during separations was observed in the form of band broadening for maleimide adducts of Cys, CysGly, and penicillamine (Pna), which can form a six-membered ring by intra-molecular nucleophilic attack. This band broadening was not observed for Hcy, GluCys, GSH, and MESNA adducts, which cannot form a six-membered ring by intramolecular nucleophilic attack. **Figure 3.4** highlights that for Cys-NMM, there is no band broadening at pH 8.0. However, band broadening increases significantly above pH 8.5 due to intramolecular nucleophilic attack catalyzed under more alkaline conditions. With many of the maleimide analogs, including MHA,

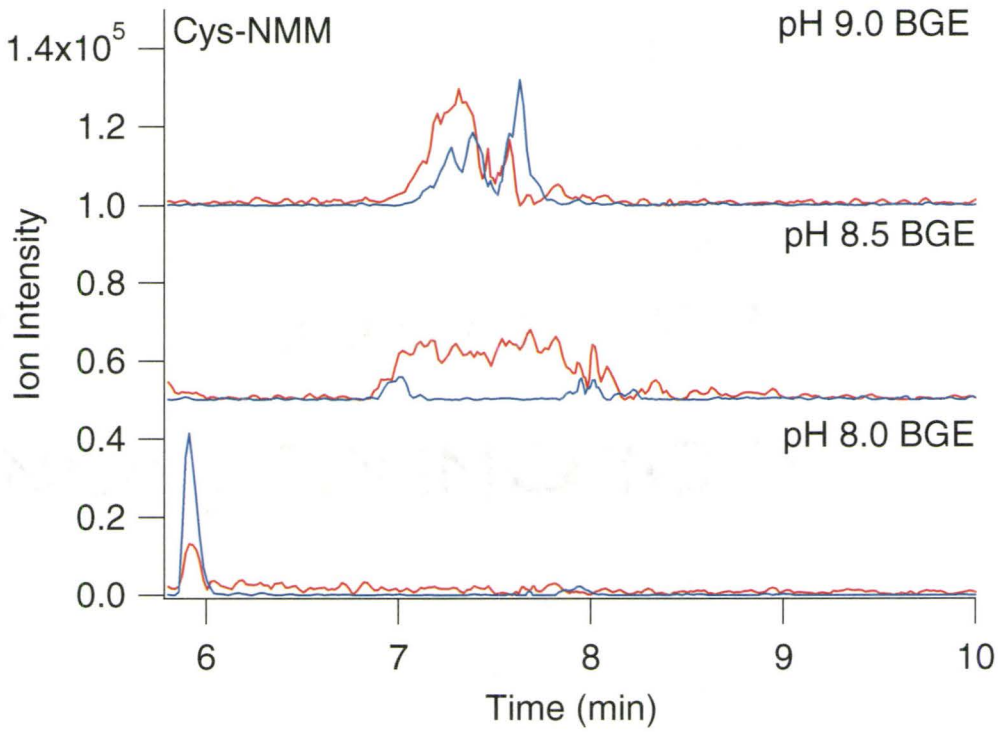

Figure 3.4: EIEs for 5 sec injections of 200 µM Cys-NMM separated with pH 8.0, pH 8.5, and pH 9.0 50 mM ammonium bicarbonate BGEs showing increasing nucleophilic attack with increasing BGE pH. Band broadening due to intramolecular nucleophilic attack is evident at pH 8.5 and pH 9.0. The red trace is for the $[M\text{-}H]^-$ ion (*m/z* 231) and the blue trace is for a $[2M\text{-}H]^-$ ion cluster (*m/z* 463).

the band broadening was observed even when using pH 8.0 ammonium bicarbonate BGE. Evidence of hydrolysis during CE separation was not observed for most of the maleimides examined. Given the instability of thiol-maleimide adducts in alkaline BGE conditions, they are unsuitable for further investigations. Therefore, neutral BGE conditions were investigated for negative ion mode CE-ESI-MS analysis of thiol-maleimide adducts and disulfides.

3.2.2 Electrophoretic Mobilities of Thiol-Maleimide Adducts and Disulfides in Negative Ion Mode

While BGE conditions approaching neutral pH can prevent intramolecular nucleophilic attack during separations of thiol maleimide adducts in CE-ESI-MS, some analytes of interest tend to co-migrate with the EOF under such conditions. When using 50 mM ammonium acetate BGE with pH from 6.5 to 8.0, derivatives of Cys, Hcy, CysGly,and Pna with the neutral maleimides—NMM, NEM, and NPEM—co-migrate with the EOF. These thiols contain one amine functional group and one carboxylic functional group and form zwitterionic adducts with neutral maleimides at neutral pH. Other thiols, including GSH, GluCys, NAC, and MESNA that have more acidic functional groups than amines form negatively charged adducts with neutral maleimides at neutral pH. Anionic maleimides (*e.g.*, MHA or NMBA) enable analysis of Cys, Hcy, CysGly, and Pna with a BGE pH between 6.5 and 8.0. Unfortunately, certain native oxidized disulfides (*e.g.*, CysSS and HcySS) are zwitterionic and co-migrate with the EOF in a neutral BGE as shown in **Figure 3.5**. This signifies that in negative ion mode with a BGE pH less than 8, quantitation of CysSS and determination of the predominant plasma Cys/CysSS redox potential is not feasible by CE-ESI-MS. Thus, due to both the instability of thiol-maleimide adducts at alkaline pH and the co-migration of key oxidized disulfides with the EOF under neutral conditions, negative ion mode CE-ESI-MS does not offer practical opportunities thiol redox status analysis unlike the strongly acidic, positive ion mode conditions described in **Chapter 2**.

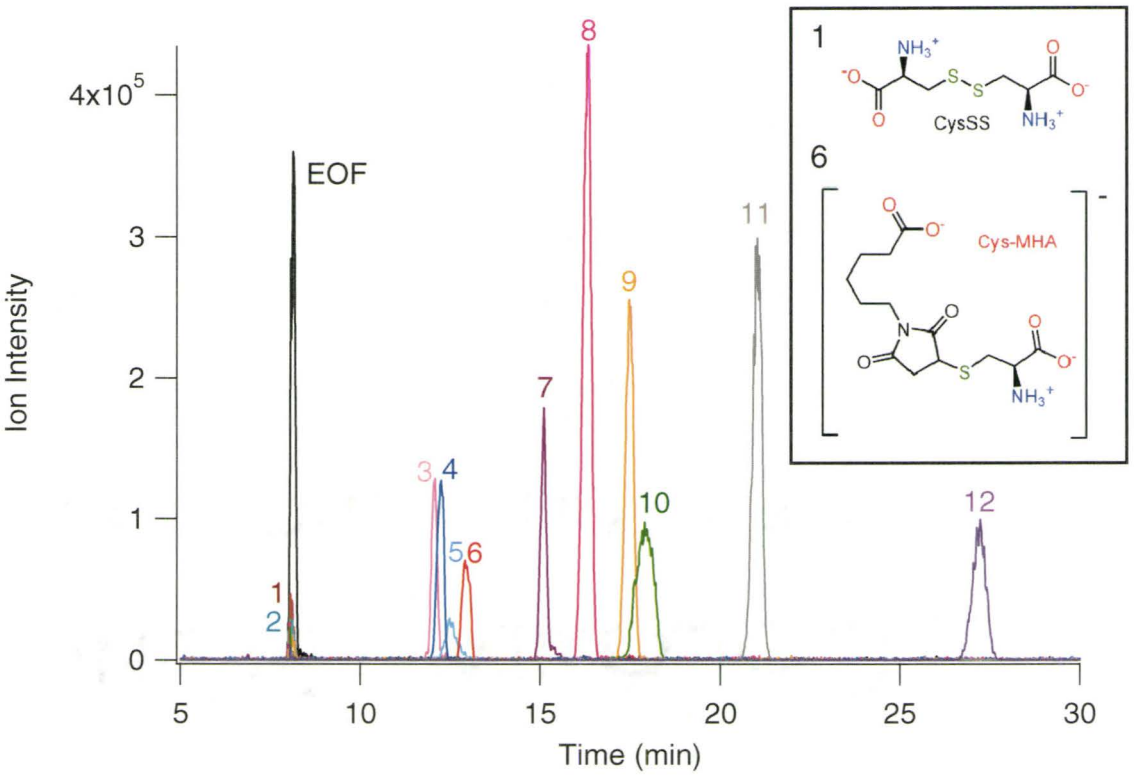

Figure 3.5: EIEs of a mixture of 100 µM MHA derivatized thiols and 50 µM disulfides injected for 5 sec and separated with pH 7.9, 50 mM ammonium acetate BGE at 25 kV. CysSS and HcySS co-migrate with the 100 µM melatonin EOF marker. Structures of negatively charged Cys-MHA and zwitterionic CysSS are also shown. Peaks are labeled: 1 – CysSS, 2 – HcySS, 3 – CysSSG, 4 – Hcy-MHA, 5 – Pna-MHA, 6 – Cys-MHA, 7 – GSSG, 8 – GSH-MHA, 9 – GluCys-MHA, 10 – CysGly-MHA, 11 – NAC-MHA, 12 – MESNA-MHA

3.3 NAM—A Better Maleimide Label for Thiol Redox Status Analysis?

Given the lack of promising results in negative ion mode CE-ESI-MS, positive ion mode appears to be ideal for thiol redox status analysis using maleimide derivatization. However, for broader clinical application of the method, improvements in sensitivity for thiol analysis and maleimide stock solution stability are required. Since ionization efficiency is augmented by maleimide derivatization and the instability of the

NTAM stock solution is a result of its insolubility in acetonitrile, the use of a more non-polar maleimide will likely improve method performance.

N-(9-Acridinyl)maleimide (NAM) appears to be a promising alternative to NTAM for labeling thiols. Like NTAM, it is cationic because its heterocyclic nitrogen atom ($pK_a \approx 3.8$) that is protonated in acidic BGE. This should give NAM similar advantages to NTAM in terms of faster migration times for adducts, reduced band broadening, and greater sensitivity. In addition, NAM has a greater *MV* than NTAM, which is predictive of greater ionization efficiency in ESI. NAM is expected to improve ionization efficiency since using calculated parameters and the mobility of Hcy-NAM in the model developed in **Chapter 2**, its RRF is predicted to be 17, which is greater than the predicted RRF for Hcy-NTAM of 11. In addition, 5 mM NAM is soluble in acetonitrile allowing for the preparation of a stable NAM stock solution.

3.3.1 Instability of NAM-Thiol Adducts

When NAM derivatization of thiols was carried out, multiple peaks for a single thiol were immediately apparent in the EIEs. **Figure 3.6 (a)** shows that multiple peaks can be seen for the NAM derivatives of cysteamine (Cyst), CysGly, Cys, and Pna immediately after sample preparation. After approximately two hours at room temperature, the early migrating peaks for these adducts disappear and the later migrating peaks become larger as shown in **Figure 3.6 (b)**. The NAM-thiol adducts that form multiple peaks are those that can form a thiazine-type product with a six-membered ring, if an intramolecular nucleophilic attack by the amine group occurs as illustrated in reaction (c) of **Figure 3.3**. The multiple peaks all have the *m/z* that is expected for the

initial succinimide-type adduct, which is as expected for intramolecular nucleophilic attack forming a thiazine-type product. Where possible, this reaction occurs readily in a pH 5 sample and is complete after more than 2 hours at room temperature. Lowering the pH of the sample to prevent the intramolecular reaction is not a viable option, as the reaction still occurs in pH 3.9 samples and lower pH samples are not compatible with the on-line preconcentration.

CE-ESI-MS provides data that supports the characterization of the early-migrating peaks for adducts of NAM with Cys, CysGly, Pna, and Cyst as succinimide-type products and the late migrating peaks as thiazine-type products. The early-migrating peaks include an $[M+2H]^{2+}$ ion peak in addition to the main $[M+H]^{+}$ peak consistent with protonation of one or both of the two amine groups of the succinimide-type product, while the late migrating peaks have only the $[M+H]^{+}$ ion peak consistent with protonation of the single amine group of the thiazine-type product. In addition, MS/MS experiments provide support for the characterization of the succinimide-type and thiazine-type products. An *m/z* 275 fragment occurs in the MS/MS spectra of all the peaks assigned to succinimide-type products but in none of the spectra assigned to thiazine-type products. The *m/z* 275 fragment is consistent with the formula $[C_{17}N_2O_2H_{11}]^{+}$ corresponding to the intact NAM moiety. The five-membered ring portion of NAM is rearranged in the thiazine-type product. Thus, thiazine-type products cannot lose the *m/z* 275 fragment, which contains the five-membered ring portion of the NAM moiety and this fragment is characteristic of the succinimide-type products.

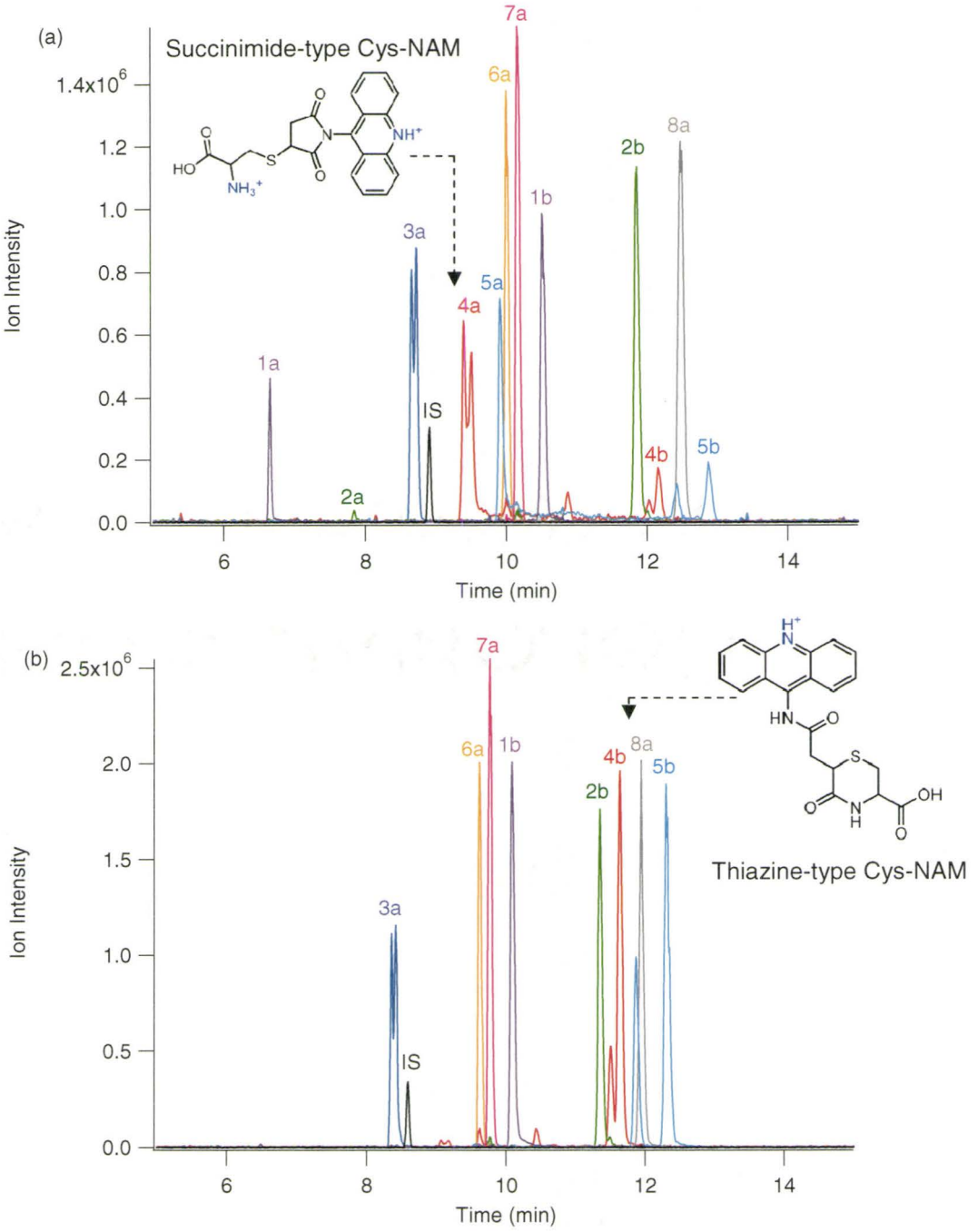

Figure 3.6: EIEs of a sample containing a mixture of 50 µM thiols derivatized with 1 mM NAM, quenched with 1.5 mM MESNA and 1 mM NMM, and injected for 5 sec **(a)** immediately after sample preparation was complete and **(b)** after the sample was at room temperature for approximately 2 hours. The structures of NAM, succinimide-type Cys-NAM (4a) and thiazine-type Cys-NAM (4b) are also shown. Peaks are numbered: 1 – Cyst-NAM, 2 – CysGly-NAM, 3 – Hcy-NAM, 4 – Cys-NAM, 5 – Pna-NAM, 6 – GluCys-NAM, 7 – GSH-NAM, 8 – NAC-NAM, a – succinimide-type product, b – thiazine-type product.

The changes in μ_{ep} going from the putative succinimide-type products to the thiazine-type products also are consistent with an intra-molecular reaction forming the thiazine-type product. For the same thiol, the thiazine type product has one less amine group and therefore decreases in z_{eff} compared to the succinimide-type product due to the participation of an amine in a nucleophilic attack to form an amide. *MV* is largely unchanged with the intramolecular reaction. Therefore, the decrease in charge to size ratio results in a decrease in μ_{ep}, which was observed in CE-ESI-MS. Using *m/z* and calculated *MV* and z_{eff}, an MLR predictive model for the μ_{ep} of the proposed succinimide-type and thiazine-type thiol-NAM adducts and four disulfides with an R^2 of 0.8385 was prepared that supports the proposed structures of the succinimide-type and thiazine-type NAM adducts.

3.3.2 NAM Derivatization and Analytical Sensitivity

NAM derivatization was expected to improve sensitivity relative to NTAM derivatization. To determine if this occurs, a 1 μM mixture of NTAM derivatized thiols quenched with MESNA and NMM was left at room temperature for 3 hours to complete the reaction to form the thiazine-type products for the Cys and CysGly adducts. Using a 90 second injection, CE-ESI-MS responses for this sample were compared to those for three 1 μM mixtures of thiols each derivatized with either NEM, NAEM, or MHA. The results did not show increased sensitivity with NAM derivatization, with peak intensity and *S/N* generally similar to or less than those obtained with NAEM or MHA. This lack of improvement in sensitivity using NAM, compared to using maleimides previously found to offer inferior sensitivity to NTAM, indicates that NAM is not a promising label

for thiol redox status analysis. Furthermore, the time required at room temperature to complete conversion to the thiazine-type products with NAM might degrade other sample components, which would interfere with untargeted metabolite profiling applications.

Several factors could have contributed to the lack of markedly improved sensitivity with NAM derivatization. Firstly, as can be seen in **Figure 3.6** there is some splitting of the CE peaks for certain NAM-thiol adducts, particularly Cys-NAM and Hcy-NAM due to partial separation of diastereomers produced by maleimide derivatization that contributes to band broadening, reducing peak intensities and overall sensitivity. Such splitting has been observed for succinimide-type products separated by LC.[7] Secondly, there may be a limit beyond which increasing *MV* does not increase ionization efficiency and actually decreases it. Muddiman *et al.* have shown that there is a non-polar surface area range for peptides alkylated with various alkylating reagents that produces the greatest ionization efficiency, while smaller and larger non-polar surface areas produce poorer ionization efficiency.[8, 9] When using NAM, the non-polar surface area of some thiols may be increased beyond that which provides the greatest ionization efficiency and the derivatives are too hydrophobic for maximum ionization efficiency. Poorer ionization efficiency may occur because of the diminished solubility of hydrophobic species and the tendency of surfactants to form desolvated films on the surface of droplets, which are a significant barrier to solvent evaporation and inhibit ion formation.[10]

3.4 Optimum Design of Maleimide for Thiol Derivatization

3.4.1 Characteristics of an Ideal Maleimide for Thiol Derivatization

One limitation of the NTAM derivatization method was the inability to prepare a stable stock solution of NTAM in acetonitrile due to its poor solubility. Thus, the ideal maleimide for thiol redox status analysis should be soluble in acetonitrile in order to reduce hydrolysis and improve maleimide stock solution stability. Of all the maleimides examined, only cationic maleimides obtained as salt, NTAM and NAEM, were poorly soluble in acetonitrile.

The divalent thiol-maleimide adducts with NTAM and NAEM have shorter migration times due to increased z_{eff}, which decreases band broadening while enhancing sensitivity. The additional positive charge also enables the simultaneous analysis of acidic thiols, such as NAC, under acidic conditions in positive ion mode. Therefore, the ideal maleimide should contain an amine group that adds a positive charge to derivatized thiols.

The NTAM purchased contained impurities that resulted in additional high intensity peaks in CE-ESI-MS from hydrolysis products and methanolysis products that interfered with analysis of GluCys-NTAM below concentrations of 100 nM. The ideal maleimide should be free of interfering impurities.

NAM derivatization revealed that the formation of unstable succinimide-type thiol-maleimide adducts is undesirable since a wait time is necessary to complete conversion to the thiazine-type products and migration times are increased, which leads to band-broadening. NAM-thiol adducts may be especially prone to intra-molecular

nucleophilic attack because the bond between the nitrogen of the five-membered ring and an unsaturated carbon in the aromatic heterocycle allows the maleimide nitrogen to donate electron density into the π-system of the aromatic heterocycle. This makes the nitrogen and the carbonyl groups in the five-membered ring more electron deficient and thus more susceptible toward intra-molecular nucleophilic attack. Another maleimide with an unsaturated carbon in an aromatic ring bound to the nitrogen atom, eosin-5-maleimide (EMA), has been shown to be less stable towards hydrolysis than NEM by a factor of 100 at a neutral pH.[7, 11] Relatively unstable EMA is electronically similar to NAM suggesting that a bond between the maleimido nitrogen atom and an unsaturated carbon atom destabilizes such thiol-maleimide adducts compared to adducts of maleimides with a bond between nitrogen and a saturated carbon, such as NEM. Therefore, in the ideal maleimide, the maleimido nitrogen atom should be bound to a saturated carbon atom.

Peak splitting due to partial separation of diastereomeric thiol-maleimide adducts is undesirable because it causes band broadening and diminishes sensitivity. Diastereomers are formed in all maleimide derivatizations of chiral thiols because biological thiols have at least one chiral center and a new stereogenic center is formed where the sulfhydryl adds to the maleimide. Peak splitting was observed with several NAM-thiol adducts and with Cys-NPEM, but was not observed with any of the other maleimides examined. NAM and NPEM are the only maleimides utilized that contain aromatic rings, which suggests that aromatic rings contribute to conformational rigidity

that facilitates the separation of diastereomeric thiol-maleimide adducts by CE-ESI-MS. Therefore, the ideal maleimide should not contain aromatic substituents.

NTAM derivatization resulted in lower sensitivity than is ideal for analysis of reduced Hcy and GluCys in plasma. The results of the predictive model for ionization efficiency enhancement show that an increase in *MV* enhances ionization efficiency and improves sensitivity. Therefore, the ideal maleimide should have a greater *MV* than NTAM in hopes of enhancing ionization efficiency by increasing surface activity to improve sensitivity.

3.4.2 Proposed Maleimide for Thiol Derivatization

Incorporating all of the characteristics for the ideal maleimide—being soluble in acetonitrile, containing a nitrogen atom that can be protonated, being of high purity, lacking a bond between the maleimide nitrogen and an unsaturated carbon, lacking an aromatic ring, and being larger than NTAM—one arrives at a proposal for the ideal maleimide for thiol redox status analysis. The structure of this proposed maleimide, *N*-[2-(di-*n*-butylamino)ethyl]maleimide, is given in **Figure 3.7**. Its calculated *MV* is 264 $Å^3$ and its predicted *logD* is 1.4 at pH 7. This makes it larger and more hydrophobic than NTAM, which has a calculated *MV* of 174 $Å^3$ and a predicted *logD* at pH 7 of -3.5. Using calculated μ_{ep}, *MV*, *logD*, and z_{eff} the RRF for thiols labeled with the ideal maleimide can be predicted. These calculations predict that the ideal maleimide will provide 2.6-fold greater sensitivity than NTAM for Hcy, a thiol that is present at particularly low concentrations in plasma.

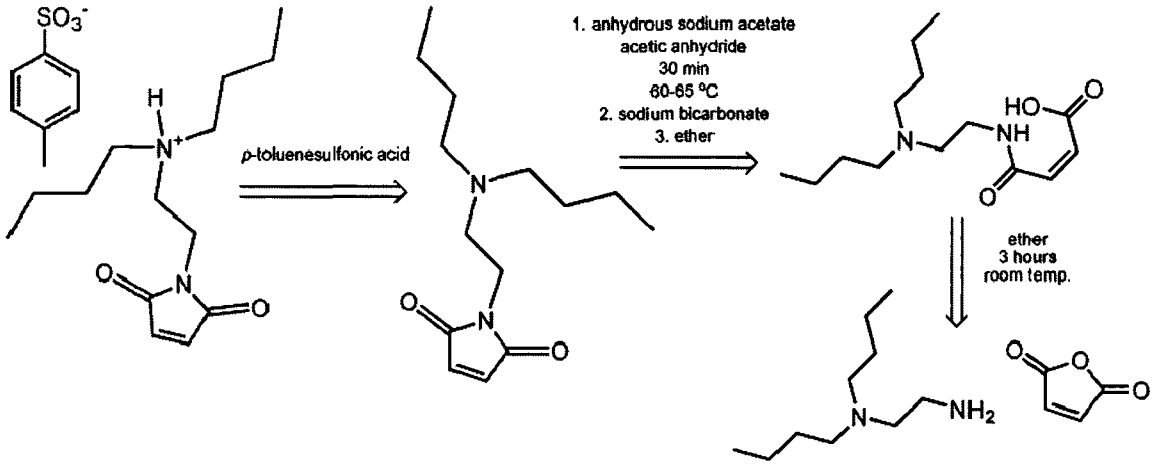

Figure 3.7: Structure and retrosynthetic scheme for proposed ideal maleimide, *N*-[2-(di-*n*-butylamino)ethyl]maleimide

N-[2-(di-*n*-butylamino)ethyl]maleimide could be synthesized from commercially available *N,N*-Di-*n*-butylethylenediamine and maleic anhydride using the general method of El-Merzabani *et al.*[12] First, the maleamic acid is prepared by reacting the amine and maleic anhydride at room temperature in ether. The maleamic acid is recovered by filtration and washed to remove excess starting materials. The maleamic acid and acetic anhydride react in the presence of sodium acetate at 60-65°C to cyclize the maleamic acid into the maleimide. After neutralizing the reaction mixture with sodium bicarbonate, the maleimide is extracted into ether, dried and evaporated to yield the maleimide.[12] If the amine cannot be recovered and purified in the amine form, it may be precipitated as a salt with a bulky acetonitrile-soluble acid counter-ion, such as *p*-toluenesulfonic acid.

3.5 Future Studies Utilizing Thiol Redox Status Analysis by CE-ESI-MS

Using an improved maleimide for sub-nanomolar detection of thiols by CE-ESI-MS, methods for determination of thiol redox status will be developed and validated. These methods will provide a comprehensive analysis of the thiol fractions in biological samples including reduced thiols, free oxidized thiols as the intact mixed and symmetric disulfides, and protein-bound thiols. Analysis of reduced thiols and intact disulfides will be accomplished in a manner similar to the method in **Chapter 2** with sample deproteinization by ultrafiltration at 4°C followed by dilution with pH 5 ammonium acetate and maleimide derivatization. Most methods derivatize upon blood collection to prevent artifactual oxidation of labile sulfhydryl groups, but this can perturb metabolism by alkylating protein thiols and can be avoided by derivatizing after deproteinization. To analyze protein-bound thiols, they will be recovered from the protein pellet after ultrafiltration with a 3 kDa filter by reconstituting and washing the protein, reducing the protein-bound thiols with TCEP, performing maleimide derivatization, and then acid deproteinizing the sample.[13] The protein-bound fraction will then be injected for analysis by CE-ESI-MS. Together, the methods for free thiol and protein-bound thiol determination will provide a comprehensive assessment of thiol redox status in biological samples with just two sample preparations. If excess TCEP in the protein-bound sample can be quenched to prevent reduction of intact disulfides and if sensitivity is adequate, then the protein-bound sample could be combined with the free thiol sample for comprehensive thiol redox status analysis in a single analytical run. The CE-ESI-MS

method could be applied to analysis of both plasma and erythrocytes to gain an understanding of both extracellular and intracellular redox status.

Once the methods for comprehensive thiol redox status analysis in plasma and erythrocytes have been developed and validated in terms of reproducibility, linearity, and recovery, they can be applied to studies of how thiol metabolism and redox status are related to aging and disease. For instance, the relationship between thiol redox status and the development of cardiovascular disease is an area for further investigation. The plasma GSH/GSSG redox potential and plasma levels of CysSS and CysSSG have been associated with early stages of atherosclerosis.[1, 14] Elevated total Hcy in plasma has also been correlated with increased risk of cardiovascular disease.[15] Heart disease and cerebrovascular disease are the number two and three causes of death in Canada, respectively.[16] Therefore, studying how altered thiol levels or redox status is related to the development of cardiovascular disease as either a cause or an epiphenomenon, would be important research that could lead to new therapies to prevent or treat heart disease or to the discovery of relevant biomarkers. For instance, Hcy is hypothesized to cause atherosclerosis. However, Hcy levels have been lowered without significantly reducing subsequent cardiovascular events or improving measures of atherosclerosis in clinical trials of Hcy lowering vitamin B_{12}, vitamin B_6, and folic acid therapy in patients with pre-existing cardiovascular disease.[17-20] These results may be caused by complex metabolic interactions of the vitamin supplements that counteract the benefits of lowered plasma Hcy. For example, folic acid and vitamin B_{12} may increase the methylation potential, increasing concentrations of methylated metabolites such as ADMA. ADMA inhibits

nitric oxide synthase and increases risk of cardiovascular disease due to inhibition of the production of NO, which is an important signaling molecule for vasodilation.[1, 17] By applying CE-ESI-MS with untargeted metabolite profiling, the impact of vitamin supplementation on levels of Hcy and other polar metabolites, such as ADMA, could be assessed in a more holistic approach. It may be found that ADMA levels increase with vitamin supplementation counteracting the expected benefit of Hcy in lowering in reducing cardiovascular risk. Alternatively, comprehensive analysis of thiol and polar metabolite profiles may reveal other alterations in metabolism that could be hypothesized to increase cardiovascular risk counteracting any benefit of Hcy lowering. In addition, the correlation between Hcy and cardiovascular risk does not prove that Hcy causes atherosclerosis because both increased Hcy and cardiovascular disease may be caused by another confounding factor. Therefore, more research is needed to elucidate by what, if any, mechanism Hcy causes cardiovascular disease. Profiling thiol and other polar metabolite levels could assist in such research by revealing other metabolites that are altered with elevated Hcy and identifying those that may play a role in the pathogenesis of cardiovascular disease. In addition to investigations of cardiovascular disease, CE-ESI-MS analysis of thiol redox status and untargeted profiling of polar metabolites could also be used to examine the role of thiol redox status in numerous other diseases in which altered thiol metabolite levels and/or oxidative stress have been implicated.

3.6 References

(1) Ashfaq, S.; Abramson, J. L.; Jones, D. P.; Rhodes, S. D.; Weintraub, W. S.; Hooper, W. C.; Vaccarino, V.; Alexander, R. W.; Harrison, D. G.; Quyyumi, A. A. *Hypertension* **2008**, *52*, 80-85.

(2) Soga, T.; Baran, R.; Suematsu, M.; Ueno, Y.; Ikeda, S.; Sakurakawa, T.; Kakazu, Y.; Ishikawa, T.; Robert, M.; Nishioka, T.; Tomita, M. *J. Biol. Chem.* **2006**, *281*, 16768-16776.

(3) Khan, M. N. *J. Pharm. Sci.* **1984**, *73*, 1767-1771.

(4) Cole, R. B.; Harrata, A. K. *J. Am. Soc. Mass Spectrom.* **1993**, *4*, 546-556.

(5) Henriksen, T.; Juhler, R. K.; Svensmark, B.; Cech, N. B. *J. Am. Soc. Mass Spectrom.* **2005**, *16*, 446-455.

(6) Soukup-Hein, R. J.; Remsburg, J. W.; Dasgupta, P. K.; Armstrong, D. W. *Anal. Chem.* **2007**, *79*, 7346-7352.

(7) Majima, E.; Goto, S.; Hori, H.; Shinohara, Y.; Hong, Y. M.; Terada, H. *Biochim. Biophys. Acta-Gen. Subj.* **1995**, *1243*, 336-342.

(8) Williams Jr, D. K.; Comins, D. L.; Whitten, J. L.; Muddiman, D. C. *J. Am. Soc. Mass Spectrom.* **2009**, *20*, 2006-2012.

(9) Shuford, C. M.; Comins, D. L.; Whitten, J. L.; Burnett, J. C.; Muddiman, D. C. *Analyst* **2010**, *135*, 36-41.

(10) Fenn, J. B. *J. Am. Soc. Mass Spectrom.* **1993**, *4*, 524-535.

(11) Gregory, J. D. *J. Am. Chem. Soc.* **1955**, *77*, 3922-3923.

(12) El-Merzabani, M.; Sakurai, Y. *Chem. Pharm. Bull.* **1972**, *20*, 2459-2462.

(13) Lee, R.; Britz-McKibbin, P. *Anal. Chem.* **2009**, *81*, 7047-7056.

(14) Ashfaq, S.; Abramson, J. L.; Jones, D. P.; Rhodes, S. D.; Weintraub, W. S.; Hooper, W. C.; Vaccarino, V.; Harrison, D. G.; Quyyumi, A. A. *J. Am. College Cardiol.* **2006**, *47*, 1005-1011.

(15) Refsum, H.; Nurk, E.; Smith, A. D.; Ueland, P. M.; Gjesdal, C. G.; Bjelland, I.; Tverdal, A.; Tell, G. S.; Nygard, O.; Vollset, S. E. *J. Nutr.* **2006**, *136*, 1731S-1740.

(16) Statistics Canada: Ottawa ON, 2006; Vol. 84-215-X.

(17) Loscalzo, J. *N. Engl. J. Med.* **2006**, *354*, 1629-1632.

(18) Wald, D. S.; Wald, N. J.; Morris, J. K.; Law, M. *BMJ* **2006**, *333*, 1114-1117.

(19) Potter, K.; Hankey, G. J.; Green, D. J.; Eikelboom, J.; Jamrozik, K.; Arnolda, L. F. *BMC Cardiovasc. Disord.* **2008**, *8*, 14.

(20) Potter, K.; Lenzo, N.; Eikelboom, J. W.; Arnolda, L. F.; Beer, C.; Hankey, G. J. *Cerebrovasc. Dis.* **2009**, *27*, 259-265.